Surface Structure Modification of ZnO and the Impact on Electronic Properties

*Robert M. Hewlett, Martyn A. McLachlan**

Dr Martyn A. McLachlan
Department of Materials & Centre for Plastic Electronics, Royal School of Mines, Imperial College London, Prince Consort Road, London, SW7 2BP, United Kingdom
Email: martyn.mclachlan@imperial.ac.uk

Keywords: zinc oxide, defects, surface chemistry, interface modification, organic photovoltaics

Zinc oxide (ZnO) is a widely utilized, versatile material implemented in a diverse range of technological applications, particularly in optoelectronic devices where its inherent transparency, tunable electronic properties, and accessible nanostructures can be combined to confer superior device properties. ZnO is a complex material with a rich and intricate defect chemistry, and its properties can be extremely sensitive to processing methods and conditions; consequently, surface modification of ZnO using both inorganic and organic species has been explored to control and regulate its surface properties, particularly at heterointerfaces in electronic devices. Here, we describe in detail the properties of ZnO, particularly its surface chemistry and the role of defects in governing its electronic properties, and describe methods employed to modulate the behavior of as-grown ZnO and outline how the native and modified oxide interact with molecular materials. To illustrate the diverse range of surface modification methods and their subsequent influence on electronic properties, a comprehensive review of modification of ZnO surfaces at molecular interfaces in hybrid photovoltaic (hPV) and organic photovoltaic (OPV) devices is presented. This is a case study rather than a progress report, aiming to highlight the progress made towards controlling and altering the surface properties of ZnO, and to bring attention to the ways in which this may be achieved by using various interfacial modifiers (IMs).

1. Introduction

ZnO has emerged as a workhorse semiconducting metal oxide material in recent years, owing to its high optical transparency, tuneable electronic properties, ease of preparation, low cost, and low toxicity. This is evident from the large number of reports of ZnO being employed as an acceptor material in hybrid photovoltaics (hPVs),[1,2] as a charge transport layer in organic photovoltaics (OPVs),[3,4] as a semiconducting scaffold in dye-sensitised solar cells (DSSCs),[5,6] as a charge injection material in hybrid light-emitting diodes (HyLEDs),[7,8] and as the active channel layer in thin-film transistors (TFTs).[9–11] Additionally, ZnO possesses other properties including a large free-exciton binding energy which may be exploited in a number of optoelectronic applications, piezoelectric properties arising from its non-centrosymmetric crystal structure (useful in transducers and actuators), high surface sensitivity appropriate for sensing applications, high thermal conductivity, and hardness to radiation.[12,13] Underpinning the continued interest in ZnO is the relative ease of thin-film preparation which may be achieved by a diverse range of solution and vacuum-based techniques, including those compatible with existing industrial processes.

Three polymorphs of ZnO have been identified: *i)* the predominant hexagonal wurtzite phase ($P6_3mc$, **Figure 2**); *ii)* zinc blende (sphalerite, $F\bar{4}3m$); *iii)* cubic (rock salt, $Fm\bar{3}m$), the latter two being metastable. A diverse range of ZnO nanostructures (some of which are highlighted in **Figure 3**) may be prepared, owing to the crystallographic anisotropy of the material: these have been widely employed in sensing and optoelectronic applications owing to their relative ease of deposition *via* comparatively simple, often solution-based, processes which generally employ simple ionic precursors. Reported ZnO nanostructures include (but are not limited to) nanoparticles (NPs);[14,15] nanorods (NRs), **Figure 3 (b)**;[16,17] nanowires (NWs**), Figure 3 (c)**;[18] 3-dimensional ordered macroporous (3-DOM) structures, **Figure 3 (d)**;[19–21] nanotubes;[22] nanohelices, **Figure 3 (e)**;[23] nanoflowers;[24,25] tetrapods;[26,27] nanosheets.[28,29] Nanostructuring of materials predominantly increases the surface area of the material, considered advantageous in applications

such as OPVs, hPVs and sensing.[1,30] Additionally, periodically ordered nanostructures may also lead to light trapping effects,[31,32] although this has not been studied in depth in OPV or organic light-emitting diodes (OLED) applications to date. Nanostructures are employed in a number of the works cited here, especially in solar cell applications where structures such as NRs and NWs have been used successfully to enhance device performance.[33]

The n-type semiconductivity of ZnO arises from its rich defect chemistry and is exploited in various applications. The bulk conductivity of ZnO is highly variable, with maximum carrier concentrations on the order of 10^{21} cm^{-3} having been reported,[12] compared to a 'typical' bulk value of 10^{17} cm^{-3}.[34] Whilst this variation was originally attributed to the presence of oxygen vacancies (V_O), more recent research has identified these as deep-level defects as opposed to shallow donors.[35,36] Research led by van der Walle *et al.* has suggested that the n-type conductivity of ZnO arises from extrinsic rather than intrinsic defects, namely through the incorporation of hydrogen into the material[13,37] (other impurity species have also been put forward as potential sources of this n-type behaviour, such as formation of Zn_i–N_O complexes).[38] H can act as both an interstitial[39] and substitutional (for O) donor,[13] forming strong bonds with neighbouring oxygen atoms. Moreover, hydrogen plays an important role in the electronic behaviour of the ZnO surface, as discussed in the following section. As such, it can be difficult to assume direct control of the conductivity of ZnO, especially when deposited from environments with plentiful sources of hydrogen — as is the case with solution-processing — thus ZnO is often doped in order to control the conductivity more effectively.

2.1 ZnO Surfaces and Interfaces

Several studies into the properties of the ZnO surface have been carried out in recent years, helping to provide an insight into the various factors which govern its behaviour at heterointerfaces. ZnO possesses both non-polar and polar crystal faces, shown in **Figure 2**, which arise from the

anisotropy of the wurtzite crystal structure.[40] Non-polar faces, *e.g.* ($10\bar{1}0$), contain equal numbers of Zn and O, whereas the polar crystal faces are either nominally Zn-terminated, *e.g.* (*0001*), or O-terminated, *e.g.* ($000\bar{1}$) — it should be noted that these surfaces reconstruct to lower the surface energy,[41] as well as adsorbing –OH groups at the Zn-terminated face and –H at the O-terminated face.[42,43] Consequently, different ZnO faces will interact differently with organic species.[44,45] Additionally, variations in the defect structure of each individual crystal face can lead to differences in their electronic properties.[46,47] The defect structure of the ZnO surface has been probed in a number of studies, particularly focussing on the incorporation of the material into organic electronic devices: in such systems, ZnO is often deposited at relatively low temperatures (typically < 400 °C, and in many cases < 150 °C) when solution-based techniques are employed — as such, these films are exposed to plentiful sources of hydrogen and often contain significant traces of residual carbon.

Reported values of the work function of ZnO have been shown to vary substantially and appear to be extremely sensitive to processing conditions either during deposition of in post-processing — for example, Heinhold *et al.* recorded a range of values spanning 0.8 eV on the O-terminated polar ZnO face.[42] The work function of ZnO has been found to depend on a multitude of factors, most significantly the surface termination and defect chemistry, both of which can contribute to changes in the surface carrier concentration and band-bending.[48] It has been proposed that metallisation of polar ZnO surfaces may occur through bonding with hydrogen[49] as ZnO has been reported to interact strongly with water.[50] The termination of O-polar faces with –H has been measured to donate ~0.5 electrons per hydrogen atom to the electronic structure of the surface[51] and may contribute to the surface conduction layers which have been observed in ZnO.[46,52,53] Heinhold *et al*. studied the surface electronic properties of ZnO at different coverages of hydrogen on polar faces using X-ray photoelectron spectroscopy (XPS): at ~0.9 monolayer (ML) hydrogen coverage on the O-terminated face, a flat-band condition was observed, *i.e.* no band-bending; in comparison, a reduction in hydrogen coverage (to ~0.4 ML) resulted in upward band-bending giving the surface greater semiconductor character, whilst increasing hydrogen coverage to over 1 ML led to

downward band-bending and more metallic behaviour. However, on Zn-terminated faces, reduction of H coverage below 0.8 ML was not achieved and the surfaces exhibited downward band-bending, with slight increases in magnitude with increasing –OH coverage (in the range 0.8–1.3 ML, a variation of ~0.25 eV was observed). Using density functional theory (DFT), Li *et al.* modelled the polar Zn-terminated (*0002*) face in terms of V_O, Zn vacancies (V_{Zn}), Zn interstitials (Zn_i), and hydroxylation and compared these to experimental photoelectron spectroscopy (PES) data.[54] From this computational work, it was determined that V_{Zn}, V_O, and surface hydroxylation would lead to increases in the work function, with V_{Zn} producing the biggest impact (these defects are also known to act as electron traps and can be detrimental to device performance, particularly at interfaces). Additionally, two distinct –OH groups were identified, one filling V_O at the surface (V_O have previously been noted to play a role in dissociation of H_2O at the ZnO surface)[55] and a bridging –OH group. **Table 1** presents a summary of data from the study by Schulz *et al.* which compares the work function of ZnO surfaces which have been subjected to different sputtering post-treatments (thus altering the defect populations of the ZnO near-surface region), and calculated surfaces containing V_O, V_{Zn}, or Zn_i defects ZnO defects, showing how these can affect the surface's measured properties.[56]

Given this variability in the surface properties of ZnO, interface modification (IM) of the material has become a popular method for regulating its functional properties.[57] Modification of ZnO interfaces is usually carried out by three distinct routes:

i) **Doping**: doping of the ZnO bulk will also change the surface characteristics of the material; alternatively, surface doping may be carried out by depositing a thin layer of doped ZnO material on top of an undoped ZnO thin-film, or by surface treatments such as UV–ozone[58] or plasma exposure.[59] A comprehensive overview of ZnO doping is given in the excellent review by Özgür *et al.*.[12] Nominally, elements such such as Al, Ga, In, and Cl may be used for n-type doping, whereas Li, Na, N, P, and As are used for

p-type doping; however, the actual behaviour of dopants can be highly variable and is discussed in more detail in the relevant sections in this review. Additionally, alloying ZnO with elements such 2+ ions Cd[60] and Mg[61] can be carried out to modulate the band gap.

ii) **Inorganic modification**: the surface of ZnO can be modified by growing a thin layer of another species on it or through chemical treatment. This may have a substantial impact on the electronic properties of the ZnO and change behaviour at this interface: for example, modification with Al_2O_3 has been observed to modulate the PL emission of NR arrays.[62] Recently, structures such as ZnO-based core-shell structures such as NWs have been researched for a number of different applications: for example, ZnO–TiO_2 NWs have been used in hPVs,[63] and ZnO–MgO and ZnO–ZrO_2 structures for DSSCs,[64] whilst ZnO–PZT (lead zirconate titanate) NWs may be employed in piezoelectric devices.[65,66] Notably, ZnO layers have been modified with ZnO, for example, coating of sol-gel-derived films with thin overlayers of ALD-deposited ZnO was shown to improve the performance of OPV devices, highlighting how processing conditions may affect the properties of ZnO.[67]

iii) **Organic modification**: molecular modification of ZnO has been employed in many applications to alter the material's surface properties. Generally, polar groups on the modifying species such as carboxyl (–COOH),[68] phosphonic acid (–P(O)$(OH)_2$),[69] amine (–NH_2),[70] and thiol (–SH)[71,72] anchor the molecule to the oxide surface. Bonding to the surface can occur through different modes: for example, carboxyl and thiol linkers favour dissociative absorption, whereas groups such as amines and hydroxyl tend to bind non-dissociatively.[73]

The effects of such modifications are wide-ranging and can considerably alter properties such as the surface energy, surface defects and chemistry, electronic structure and transport properties, all of which are important in governing the behaviour at heterointerfaces. Given the complexity of ZnO, it can be difficult to isolate the specific effects of a modification on the performance of devices fabricated with such layers. In the following sections, the interaction between modifying species and ZnO is outlined, followed by an extensive review of modification in ZnO-based organic and hybrid photovoltaic devices.

2.2 Molecular Interaction with ZnO

Considering IM, the bonding and conformation of molecules on ZnO surfaces can have a significant effect on the resulting functional properties of the interface, *e.g.* electron transfer and dipole moments.[74] Although interaction between ZnO and organic species has been well documented — for example, in the formation of self-assembled monolayers (SAMs) in electronic devices,[57] and the absorption of molecular species on ZnO in sensing and catalysis applications[75] — reports on the nature of bonding on the ZnO surface, whether by chemical bonding or physisorption, and layer coverage have been somewhat variable.[73] This is partially due to the nature of the individual ZnO faces, each of which exhibit differing degrees of reactivity in the order: polar O-terminated < apolar neutral < polar Zn-terminated.[76] As an illustration of this, alkanethiols are frequently used as surface modifiers for NPs by binding to the inorganic surface through the –SH group (for bonding to ZnO, this is expected to occur through dissociation of the thiol head-group): one study found no evidence for adsorption of hexanethiol to ZnO,[77] whereas in others alkanethiols have been observed to form S–O–Zn linkages on polar O-terminated ZnO surfaces (albeit with low surface coverage and uniformity),[71,78] and strong Zn–S linkages shown to be dominant for polar Zn-terminated face, with a bond enthalpy calculated to be 430 kJ mol^{-1} by DFT in one study.[72,79] Functionalisation of ZnO is most frequently carried out using organic species containing carboxylic acid groups, a notable example being in the case of sensitisation of ZnO arrays with Ru-based complexes for DSSCs.[68] Typically, –COOH groups are expected to bind to the oxide surface

through the deprotonated species[1], with the dissociated hydrogen atom binding to surface oxygen and interacting with the modifier through H-bonding.[80,81] The three main modes of chemical bonding to the ZnO surface are *i)* monodentate ester linkage, which leaves the carbonyl group unaffected by the bonding; *ii)* bidentate chelation to a single Zn centre through both oxygen atoms; *iii)* bidentate bridging between both oxygen atoms and two Zn centres.[82,83] For a ($10\bar{1}0$) non-polar ZnO surface, simple carboxylic acids (formic and acetic acid) have been calculated to form bidentate bridging linkages at half-monolayer coverage, and bidentate chelates at full coverage, the latter being the most thermodynamically stable.[73,80,82] Carboxylic acid linkages tend to be quite stable: Moreira *et al.* calculated that under dry conditions, pressures of 10^{-12} atm are require to reduce a full monolayer to half coverage, and 10^{-36} atm to remove the monolayer, and that these linkages tend to be more stable under wet conditions than $–NH_2$ and –OH bonds.[73] Phosphonic acid modifiers have also been researched extensively, although their acidity makes SAM formation on ZnO challenging.[84,85] Zhang *et al.* proposed that phosphonic acid groups chemisorb on ZnO through condensation with surface Zn–OH groups in tridentate bridging, tridentate chelating (through migration of an H atom to the surface),[86] or bidentate binding modes (with the P=O group not involved in chemical bonding with the surface): the various possible binding modes are presented in **Figure 4 (a)**.[69] Bidentate linkages may be preferred in some cases due to the greater surface coverage that may be achieved with this configuration: this has been demonstrated for phenylphosphonic acid derivatives with lesser degrees of flexibility between the phenyl and phosphonic acid moiety (in *p*-(trifluoromethyl)phenylphosphonic acid).[87] Li *et al.* calculated that the tilt angle of benzylphosphonic acids increased by ~12° for bonding on a gallium-doped ZnO (GZO) surface compared to undoped ZnO, attributed to a difference in surface electrostatic potentials. With the different binding modes, different degrees of electron transfer at the material interface have been measured: this will be covered further in this section. Amine-based interface

[1] Surface modifiers are often acidic and may alter the surface chemistry[71] or etch the oxide[68,232] and is often observed for modifiers thiol, carboxyl, and phosphonate linkers.[77,84] Taratula *et al.* mollified this by using the more acid-resistant ZnMgO alloy;[77] additionally, careful choice of solvent and SAM deposition conditions can reduce the degree of material etching.

modifiers have been of interest in ZnO surface engineering: for example, dodecylamine ligands have been shown to passivate surface hydroxide-related defects in ZnO nanocrystals;[70] additionally, simple species such as polyethylenimine ethoxylated (PEIE) have been shown to produce low work-function surfaces on oxide (including ZnO), metal, and polymer semiconductor materials.[88] These species are generally calculated to bond non-dissociatively with the surface (by physisorption),[89] and the preferred geometry enabling hydrogen-bonds to form.[73,90] Acetylacetone and acetylacetonate have been considered as alternative anchoring groups to carboxylic acids due to their reasonably high absorption energies[83] and lower acidity which may reduce chemical etching of the ZnO surface.[91] As with carboxyl groups, optimised bonding structures for acetylacetone include bidentate chelating and bidentate bridging modes through the two oxygen atoms. Alkoxysilanes form Si–O–Zn linkages with ZnO: modification with these species is often undertaken to tune the surface energy of the oxide. Whilst successful functionalisation has been reported simply mixing ZnO with the silane in solution,[92] Taratula *et al.* found that binding was only achieved on MgZnO after acid pre-treatment.[77] Recent studies have successfully carried out IM with this class of molecules using *n*-butylamine as a catalyst.[93,94]

The interaction between the oxide and organic species is immensely important in governing the surface electronic properties and interfacial energy level alignment. Although studies often present work-function measurements to evaluate the electronic properties of modified surfaces, there are several factors which govern these values, and the precise effect of a given modifier on an interface's properties can be hard to identify. Greiner *et al.* present a generally applicable model for energy level alignment of organics on metal oxide (although the study did not include ZnO), asserting that this is governed by the equilibration of the electron chemical potential of the oxide with the redox potentials of the modifying species. As such, when the Fermi level (E_F) of the oxide is higher lying than the ionisation potential of the organic, the molecule binds as a neutral species, whereas ionisation of the molecules tends to occur in the opposite case.[95] A number of computational and experimental studies by Li *et al.* have developed a model to describe

modification-induced changes in work function ($\Delta\phi$) for surfaces which do not exhibit substantial band-bending. As per these studies, three main contributing factors have been identified: firstly, the change in electrostatic potential energy of an isolated SAM with the same geometry as that deposited on a surface (ΔV_{SAM}); secondly, the change in work function of the bare surface due to geometry relaxation on modification (ΔV_{ZnO}); thirdly, the potential energy step at the interface induced by charge redistribution, related to the formation of an interface dipole ($\Delta V_{interface}$).[89,96,97] As such, large changes in work function are often observed for modifiers in which the molecular and interface dipoles work in tandem, as has been observed in the case of pyridine[98] and PEIE[88] modification.

$\Delta V_{interface}$ is calculated from the electron density difference between the different interfacial components, thus depends strongly on the nature of bonding between the molecule and ZnO. The degree of electron transfer at the interface strongly influences this term and is very sensitive to the defect chemistry of the ZnO (and the carrier concentration), the organic modifier, and the bonding between the two species; additionally, the creation of hybrid interface states may have a substantial impact on the functional properties of the interface.[90] Several studies considering models of the ($10\bar{1}0$) interface have been carried out to investigate electronic interaction and transfer between the oxide and organic species: for example, carboxylic acid linkers have been calculated to transfer ~0.3 electrons per molecule to ZnO,[80,81] and pyridine to transfer ~0.25 electrons per molecule.[98] However, studies using the electron acceptor species PTCDI (3,4,9,10-perylenetetracarboxylicdiimide)[99] and F4TCNQ (2,3,5,6-tetrafluoro-7,7,8,8-tetracyanoquinodimethane),[100,101] **Figure 7**, have shown that a number of variables govern the electronic properties of these hybrid interfaces: F4TCNQ is calculated to lie parallel to the ZnO substrate, anchoring to the surface through interaction between its –CN groups and surface H atoms. F4TCNQ is expected to act as an electron acceptor in this system and has been measured to induce a $\Delta\phi$ of +1.4 eV on the O-terminated ($000\bar{1}$) surface and by +2.8 eV on the Zn-terminated (0001)

surface.[100] However, the contributions to the work functions were calculated to vary substantially with the doping concentration of ZnO: at low values of *n* (~10^{17} cm^{-3} in this experimental work), very little electron transfer was observed from ZnO to the molecule (0.03 electrons per molecule). In this regime, the low doping concentration leads to significant band-bending in ZnO (space-charge accumulation) which makes a substantial contribution to the work function change. On increasing *n* through the 10^{18} – 10^{21} cm^{-3} range, the degree of band-bending decreases which significantly lowers the barrier to electron transfer. Although the overall work function of the surface is calculated to vary by only a small amount, the electronic structure of the interface is extremely variable and would have a substantial impact on devices in which layers of these materials play an electrically active role. In the study with PTCDI, IM of the (*0002*) ZnO surface (possessing an estimated defect concentration of 10^{19} – 10^{20} cm^{-3}) was undertaken experimentally to investigate the influence of surface defects on the hybrid system, the authors noting that there was little difference in the PES data recorded for polar and non-polar face modification. PTCDI was measured to change the ZnO work function from 3.6 eV to 4.3 eV at 1 ML coverage, saturating at 4.5 eV for multilayer coverage.[99] Modelling for both polar and non-polar oxide surfaces, PTCDI was calculated to deviate slightly from cofacial conformation through tilting, and the interaction between the organic and the oxide was dependent on the defect population of ZnO: on stoichiometric and deep-level V_O-dominated surfaces, little charge transfer was calculated to occur from ZnO to PTCDI (< 0.1 electron per molecule); however, for ZnO surfaces containing significant populations of Zn_i defects, PTCDI was calculated to bind more closely to the surface and significantly enhanced electron transfer was predicted (~1 electron per molecule), yielding work-function values closely in agreement with the experimental results. Similar effects have been observed in studies on the ZnO/C_{60} system, which is discussed later in this review.[56] These studies highlight the importance of using detailed models for ZnO to adequately calculate the behaviour of hybrid interfaces.

A number of studies have aimed to tune the ZnO surface properties through control of the ΔV_{SAM} component. *para*-substitued benzene ring moieties have been particularly popular as the molecular dipole may be easily tuned through the *p*-substituent: for example, in the study by Kedem *et al.* on the ZnO/*p*-phenylphosphonic acid system, a ~1.1 eV difference was recorded between the work functions of the oxide modified with –OMe (–0.35 eV) and –CN (+0.72 eV) substituted interface modifiers on ZnO.[102] Wood *et al.* used benzylphosphonic and substituted fluorobenzylphosphonic acid species (**Figure 4 (c)**, from positive to negative dipole: *o*-difluoryl (*o*-2FBPA) > benzylphosphonic (BPA) > *p*-fluoro (*p*-FBPA) > pentafluoro (5FBPA)) to tune the work function: modifiers binding through bidentate and tridentate modes were found to exhibit a similar trend in work function change across the series, albeit with the energies for the bidentate modifiers shifted by approximately ~2.2 eV to more negative energy. The resulting $\Delta\phi$ ranges were calculated to fall between –1.38 eV and +0.03 eV for bidentate binding, and between +0.69 eV and +2.00 eV for tridentate. Work-function analysis revealed that the molecular dipole for each species was more negative for modifiers binding in the tridentate configuration, although this only partially accounted for the large discrepancy in work function between the two binding modes. As summarised in **Table 2**, $\Delta V_{interface}$ values were found to be roughly twice as large for tridentate case (between 2.10 eV and 2.5 eV) as for the bidentate (between 1.15 eV and 1.25 eV); conversely, the ΔV_{ZnO} values for the tridentate modifiers (around –0.85 eV) were calculated to be around half that of the bidentate (around –1.45 eV). These results highlight that the measured work function for these surfaces relies on the complex interplay between these different factors, and that care should be taken in the interpretation of such data. The study by Cornil *et al.* considers benzoic acid, BA, derivatives with the substituents –CN, –H, and –OMe in the *para* position on non-polar ZnO, tracking variation in ΔV_{SAM}, ΔV_{ZnO}, and $\Delta V_{interface}$ with different binding modes.[81] For bidentate binding, BA–CN was found to induce a work function change of around +1 eV, compared to around –0.3 eV and –0.6 eV for BA–H and BA–OMe respectively. The authors also noted that ΔV_{SAM} can vary with binding mode, due to the effects on the tilt angle of the molecules.

As described, IM is an immensely powerful tool for controlling the properties of hybrid oxide:organic interfaces. The following review presents an in-depth case study of IM in organic:ZnO hPVs and in OPVs: the purpose of this review is to illustrate the variety and effectiveness of modification strategies, rather than to highlight the progress of the field itself. IM has also been used extensively in hybrid oxide:polymer light emitting diodes,[7,103,104] as well as in ZnO-based thin-film transistors,[105] and there is plenty of scope for transferring this strategy to other applications which contain ZnO heterointerfaces. Despite the difficulties in controlling the properties of ZnO, these studies show that, with careful control of conditions and choice of modifying species, it is possible to tailor the properties of ZnO:organic interface to their applications and to minimise the impact of the oxide's rich defect chemistry.

3. Hybrid Photovoltaics

Both OPVs and hPVs operate in a fundamentally similar manner. Both device types are constructed around a mixed interface between donor (D) and acceptor (A) materials sandwiched between charge-selective electrodes, usually a transparent conducting oxide (TCO) such as indium tin oxide (ITO) as the bottom electrode, and metal at the top: the D species absorbs photons with energies equal to or greater than its band-gap, generating mobile excitons (bound electron–hole pairs) which may diffuse through the material: in general, excitons generated in conjugated polymers are short-lived species and thus will typically diffuse over lengths of only a few nanometres, *e.g.* for the widely studied "fruit-fly" polymer poly-3-(hexylthiophene), P3HT, diffusion lengths in the range 3–8.5 nm have been calculated.[106] When an exciton reaches a D–A, excitons may dissociate into free charge carriers, a process which has been observed to require an energy offset of at least 0.3 eV between the lowest unoccupied energy levels of the D (LUMO) and A (LUMO or conduction band, CB, for systems employing inorganic acceptors). Following separation, the free charge carriers diffuse to charge-selective electrodes with electrons moving through the A species and the holes moving through the D.

Fullerene-containing molecules, particularly phenyl-C_x-butyric acid methyl ester (PC_xBM, where x is typically 61 or 71), have been a mainstay in OPV device research over the past 10–15 years due to their role as high-performing acceptor species. However, inorganic acceptors have also attracted plenty of attention since the observation of electron transfer between photoactive polymers and NPs of the n-type II-VI semiconductors CdS and CdSe was reported in the mid-1990s[107,108] — this area grew substantially following the realisation of the first NP-CdS:P3HT active layer blend bulk-heterojunction (BHJ) hPV devices in 2002.[109] In subsequent years, several advances have been made, *e.g.* fabrication of devices employing nanostructured particles,[110] as well as the introduction of materials such as CdTe,[111] PbS,[112] and $CuInS_2$,[113] with power conversion efficiencies (*PCE*) exceeding 3 % being reported. In addition to as the superior charge transport of these materials compared to organic acceptors, their narrow band-gaps (*e.g.* 2.1 eV for CdSe) lead to the absorption of visible wavelength photons, thus contributing to the overall photocurrent output of the devices. Wide band-gap oxide acceptors – namely ZnO and TiO_2 (SnO_2 has also garnered some limited research interest) – have also been considered. These materials have been introduced to address a number of issues with the aforementioned narrow band-gap acceptors: firstly, ZnO and TiO_2 are non-toxic materials, unlike those based on elements such as Cd and Se; secondly, growth of planar films and nanostructured arrays of these materials is generally facile in comparison, particularly for ZnO.

In the following section, the behaviour of the ZnO:polymer interface and the ways in which it may determine hPV device performance is discussed. The subsequent discussion of IM divides the hPV field into two main branches based on the architecture active layer: *i)* planar, *i.e.* devices containing a solid, discrete layer of ZnO, and *ii)* distributed heterojunctions, *i.e.* BHJ-type NP-ZnO:polymer blend devices. Typically, the latter class has achieved superior performance in terms of both photocurrent and voltage output. However, there is still much interest in the production of devices with nanostructured arrays due to the ordered nature of the interface, whereas the creation of a

blend-type active layer affords a rather lesser degree of control over the morphology and the distribution of acceptor materials within the organic matrix.

3.1 hPV and OPV Device Principles

Typically, PV devices are evaluated by measuring their current density–voltage characteristics (*J–V*) under standard simulated illumination, *i.e.* irradiation under air mass 1.5 global (AM 1.5G) conditions at 100 mW cm^{-2}. Example *J–V* curves for an OPV device are presented in **Figure 5 (a)**. Solar cell performance is usually quoted in terms of four main quantities derived from these measurements: the short-circuit current density, J_{sc} (mA cm^{-2}); the open-circuit voltage, V_{oc} (V); the fill-factor, *FF*; and the power conversion efficiency, *PCE* (%). Resistance is also an important factor in device operation: the shunt resistance, R_{sh}, is a measure of resistance between anode and cathode in the device and is closely related to leakage current — this should typically be large for effective operation; the series resistance, R_s, is a parasitic parameter related to contact resistance and charge transport within the device and should be minimised. Lastly, the quantum efficiency of PV devices may be evaluated: the internal quantum efficiency, *IQE*, is a measure of the efficiency of photocurrent generation from the light absorbed by the device; in contrast, the external quantum efficiency *EQE* is a measure of photocurrent generation from the total irradiation of a device, *i.e.* it takes into account both the absorption of light by the solar cell as well as the *IQE* component.

Figure 5 (b) & (c) illustrate the difference between cells with 'normal' and 'inverted' architectures: in a normal device, the top metal electrode collects electrons (cathode) which generally requires a low work-function metal such as Ca/Al. In the inverted architecture, this is reversed: the top contact collects holes (anode) and requires metals with a higher work-function, *e.g.* Ag or Au. The inverted configuration has generally been found to be the more stable and has widely superseded normal cells.[114–116] The majority of hPV and ZnO-containing OPVs possess the inverted configuration; however, a few of the reports included in this review present devices with the normal architecture.

3.2 The Role of ZnO in Hybrid Photovoltaics and Rationale for Interface Engineering

ZnO-based hPV devices do not perform well compared to all-organic D–A systems and often lag behind devices employing a TiO_2 acceptor. For hPVs using unmodified ZnO, solid film acceptor devices have achieved 0.88 % efficiency (ZnO nanosheet structure with P3HT, J_{sc} = 3.85 mA cm^{-2}, V_{oc} = 0.42 V),[117] whereas BHJ-type devices have reached 2.0 % (1:1 w/w P3HT:NP-ZnO ratio, J_{sc} = 5.2 mA cm^{-2}, V_{oc} = 0.75 V).[118] For organic-based PV, a *PCE* value of 10 % is often considered as a benchmark for commercialisation and P3HT:PCBM devices have performed in the 5–6 % range (although values of 3–4 % are more common).[119]

Recently, research into the interfacial properties at the junction between oxide and organic materials has suggested that this area is one of the major reasons for the poor performance of hPV devices, particularly those reliant on ZnO. For example, the maximum V_{oc} attainable for a device is often estimated to be equivalent to the energy offset between the donor HOMO and the LUMO/CB of the acceptor: Noori *et al.* estimated that, for P3HT on the ZnO ($10\bar{1}0$) non-polar face, the maximum ideal V_{oc} attainable would be 2.07 V including contributions of about 0.5 V from an interfacial dipole although it should be noted that this model only considered the ideal case, neglecting ZnO defects and less favourable P3HT conformation.[120] In reality, a typical experimental V_{oc} value for a solid acceptor ZnO:P3HT device is 0.3–0.5 V,[1] with high rates of interfacial recombination cited as a likely mechanism for this loss in voltage. Experimental analysis of the energetic alignment of the ZnO:P3HT interface has been carried out by Nagata *et al.* using hard XPS depth-profiling techniques, finding the V_{oc} at the heterointerface to be around 1.5 V; in conclusion, the authors attributed the underperformance of hPV devices to the short depletion lengths observed in ZnO, which acts to increase charge recombination.[121]

The poor J_{sc} of ZnO-based hPV devices in part reflects losses in the charge generation processes. Tiwana *et al.* used optical pump terahertz spectroscopy to measure the relative charge injection

speeds between the Ru-based Z907 dye [cis-bis(isothiocyanato)(2,2'-bipyridyl-4,4'-dicarboxylato)(4,4'-di-nonyl-2'-bipyridyl)ruthenium(II)] and equivalent TiO_2, SnO_2, and ZnO structures, finding that charge injection from the dye to ZnO was much slower than for the corresponding dye-to-TiO_2 transfer[122] despite the similarity in band energies; further measurements showed that the charge injection efficiency for ZnO was only around half that observed for TiO_2. This was tentatively attributed to *i)* poor electronic overlap between the ZnO and the dye and *ii)* a multi-step electron transfer mechanism for ZnO not observed for TiO_2;[123] whilst this experiment relates to DSSC systems, given the similarity in the poor performance of ZnO-based devices relative to TiO_2 in both these and in hPVs, these findings may bear relevance in polymer:oxide systems. Time-resolved microwave conductivity measurements on the ZnMgO:P3HT system found little evidence to suggest that exciton dissociation occurs at the oxide:polymer interface — although this was not entirely discounted by the data — and the authors postulated that photocurrent derived from these devices originates predominantly from the auto-dissociation of excitons in P3HT.[124] Recently, papers investigating bound charge-pairs (BCP) in hPV systems have been published[2]. Such charge transfer (CT) states are well known in all-organic D–A systems, forming on initial separation of excitons into electrons and holes due to the Coulombic attraction between the opposite charges.[125] The BCP may either then separate into free charges or recombine, the latter being a not-insubstantial loss pathway in OPV systems. Measurements of BCPs in ZnO-based hPV devices have been conducted using an optical pump-push photocurrent probe technique, determining that 52 ± 5 % of photoinduced charges in the ZnO:P3HT system remain as BCPs rather than dissociating to free charges,[126] despite the high dielectric constant of the oxide which should assist in free charge generation. These substantial losses are an explanation as to the low photocurrents consistently observed in ZnO-based hPV devices. Whilst the authors posit that BCP persistence may be defect related, the study by Wu *et al.*

[2] Vaynzof *et al.* note that charge transfer (CT) states in hPVs, whilst analogous to those observed in OPVs, should be treated as distinct from each other given that the electron wavefunctions in inorganic and organic acceptors are substantially different.[126] As such, CT states in hPVs are referred to as bound charge pairs (BCPs) instead.

suggests that this is in fact due to the inherent properties of ZnO: here, a model of P3HT on the non-polar ($10\bar{1}0$) face of ZnO was analysed. In all-organic D–A systems, delocalisation of charge has been identified as a key step in dissociation of BCPs; however, in the hybrid model, BCPs were found to be highly localised at the ZnO surface which greatly favours charge recombination.[127] Moreover, the authors note that this is an intrinsic property of the ZnO surface, as opposed to being related to defects; whilst a similar treatment of polar ZnO faces was not conducted, the conclusions of the paper are clear – without removal of these surface states, efficient photocurrent generation cannot be achieved in the ZnO:P3HT system.

Despite these material limitations, IM of ZnO has proved to be a successful route in improving both the photocurrent and voltage outputs of hPV devices. Weickert *et al.* (working on interfacial modification of TiO_2-based hPVs) proposed four design rules for effective engineering of metal oxide–polymer interfaces in hPV devices:[128] *i)* modifier energy levels should facilitate polymer → oxide charge transfer, and the modifier should both completely cover the oxide and also be in intimate contact with the polymer; *ii)* physical spacers can be used to reduce charge recombination, although these should also not inhibit charge transfer; *iii)* surface modifiers should not create charge traps at the oxide surface and should promote crystallisation of the polymer; *iv)* combining sensitising interfacial layers (such as Sb_2S_3)[129] with hPVs would be desirable for improving charge generation, although these require well-matched energy levels.

The following sections outline hPV IM by doping, inorganic modification, and molecular modification. Lastly, reports detailing ligand modification of ZnO NPs in BHJ blend devices is reviewed.

3.3 Doped ZnO Layers in Hybrid Photovoltaics

Devices using doped ZnO generally outperform those based on undoped analogues. As different dopant species affect the behaviour of ZnO in a variety of ways, these observed improvements may arise from a number of factors. Firstly, we consider doping ZnO with Mg or Ca as a means to

widen the band gap (E_g) of the material. These studies aimed to improve device performance by increasing the CB_{ZnO}–$HOMO_D$ offset, thereby also increasing the maximum attainable V_{oc} of the system: as Mg and Ca doping was thought to increase the band-gap by pushing the CB level towards vacuum,[130] it was considered that these layers would improve the overall V_{oc} of the system. For Ca-doped ZnO, the V_{oc} was observed to change on doping from 0.5 V to 0.8 V for the composition x_{Ca} = 0.10, as well inducing a ~60 % increase in J_{sc}, attributed to changes in ZnO morphology induced by the Ca *i.e.* roughening of the surface increasing the interfacial area of the heterojunction.[131] The *PCE* thus doubled from 0.06 % to 0.12 %, although device performance was observed to decline for compositions with x_{Ca} > 0.10. For Mg doping, optimally performing devices were fabricated using sol-gel-derived acceptor layers with the composition x_{Mg} = 0.25, the devices producing similar increases in device performance as observed for Ca (V_{oc} increased from 0.5 V to ~0.8 V).[132] At a doping fraction x_{Mg} = 0.35, a V_{oc} of 0.9 V was achieved, although at this point the J_{sc} of the devices reduced due to the increasing resistivity of the doped oxide. Whilst these V_{oc} improvements were attributed to the shift in ZnO energy levels, it should be noted that more recent research into ZnMgO contests whether the changes in band gap arise through shifts in the CB towards vacuum or through shifts in the valence band away from it: whilst Olson *et al.* initially assumed the former,[132] this group's more recent work suggest that the conduction CB minima of ZnO and MgZnO are fairly similar, and as such these voltage improvements may arise from a different source, the origin of which remains unexplored to this point.[133] Doping with Li has been demonstrated in both bilayer and NR acceptor structures: whilst Li^+ should act as an acceptor species in the case of substitutional doping, in practice it is observed to occupy both substitutional and interstitial lattice sites in ZnO.[134] In the study by Lloyd *et al.*, bilayer devices employing sol-gel-derived Li-doped ZnO acceptor layers exhibited improved performance compared with reference cells: for the bulk composition x_{Li} = 0.15, the *PCE* increased from ~ 0.06 % to 0.44 %, with 90 % and 44 % increases in J_{sc} and V_{oc} respectively.[135] Although Li does not modify the E_g of the material, the authors posit that slight movement of the CB towards vacuum

may account for the increases in V_{oc}. Whilst a subtle increase in film roughness partially accounts for the J_{sc} increases, grazing-incidence X-ray diffraction (GI-XRD) data suggested an increase in polymer order and crystallinity on the Li-doped ZnO, which may also contribute to the enhanced photocurrent. Hydrothermally grown Li-doped ZnO NR arrays have also been incorporated into hPV devices: in this case, it was found that the Li was not distributed uniformly throughout ZnO, with Li-rich material being found closer to the nanorod surface. For NR arrays grown with a target composition x_{Li} = 0.05, the PL results suggested that Li predominantly substituted for Zn, whereas at x_{Li} = 0.10, evidence of interstitial lithium, i_{Li}, formation was found; additionally, the authors hypothesised that incorporation of Li into ZnO may enrich the surface with oxygen. Only modest gains in performance were attained in this case: for the target composition x_{Li} = 0.05, the *PCE* increased from 0.26 % to 0.37 % (an increase of 1.4×, compared to 7.3× for bilayer devices).[136] hPV devices based on Ga and Sr-doped ZnO have also been fabricated: for Ga-doped NRs, incorporating Ga for a target composition x_{Ga} = 0.01 improved device *PCE* from 0.15 % to 0.44 % with an observed doubling J_{sc} (to 1.98 mA cm^{-2}) and improvements in V_{oc} from 0.41 V to 0.53 V.[137] Sr-doped ZnO yielded modest gains in performance (50 % increase in *PCE* for the composition x_{Sr} = 0.06) due to improved V_{oc}, attributed to a reduction in dark current;[138] however, the J_{sc} was observed to decrease, attributed to increased BCP formation at the ZnSrO surface due to increased coverage by –OH terminating groups.

Doping of ZnO can also be used to control surface defects and may be achieved by using treatments which only affect the near-surface region of the oxide film: UV–ozone treatment, for example, has been thought to change the interfacial dipole at the ZnO surface, although this treatment was observed to reduce overall hPV device performance.[139,140] Surface doping with nitrogen has been undertaken by different methods: in the report by Oh *et al.*, this was achieved by using a near-atmospheric pressure nitrogen plasma treatment on a well-ordered ZnO NR array, leading to implantation of the N^{3-} ion in the surface.[59] This treatment created a more resistive ZnO surface and substantial gains in V_{oc} were realised (0.30 V to 0.71 V) which were attributed to a reduction in

leakage current through defect passivation; however, a this was accompanied by a 12 % reduction in J_{sc}. Musselman *et al.* used atmospheric atomic layer deposition to deposit ZnO:N layers (with the precursor solution containing 10 % NH_3) between 0 and 20 nm thick onto a 60 nm thick ZnO layer, leading to substantial gains in J_{sc} (from 0.17 mA cm^{-2} to 0.68 mA cm^{-2}) rather than in V_{oc} as observed in the aforementioned N-implantation study.[141] Surface photovoltage measurements suggested enhanced de-trapping of electrons in the N-doped ZnO films and, from transient absorption spectroscopy (TAS) results, the authors assert that the ZnO:N surface promotes enhanced exciton dissociation relative to undoped ZnO.

3.4 Inorganic Modification of ZnO Acceptor Arrays

A few studies have reported the successful incorporation of inorganic interlayers (typically < 20 nm thick) into ZnO-based hPV devices. Modification with titania-based species has been most widely reported: White *et al.* first reported the deposition of amorphous TiO_x layers (between 1 nm and 20 nm thick) on ZnO by pulsed laser deposition (PLD), finding that device performance improvements depended strongly on the conductivity of the ZnO layer.[142] For low-conductivity ZnO with an estimated carrier concentration estimated of 5×10^{14} cm^{-3}, TiO_x modification led to very slight increases in V_{oc}, but over 50 % decrease in J_{sc}; conversely, for high conductivity ZnO, optimal increases in device performance were achieved for a 10 nm interlayer, yielding a two-fold increase in *PCE* from 0.027 % to 0.053 % mainly accounted for by a V_{oc} increase from 0.217 V to 0.596 V (again, J_{sc} was observed to drop substantially). Modelling of the depletion (internal electric field) in the device stack was used as a means to investigate the effect of the modifier: for high conductivity ZnO, it was calculated that the electric field near the ZnO:P3HT interface (~5 nm) declines sharply, thus lowering the driving force for charge separation and extraction; subsequent incorporation of the TiO_x layer was shown to create a strong, sustained electric field in the device. In a similar study employing sol-gel-derived TiO_x layers, modified devices exhibited an increase in V_{oc} from 0.4 V to 0.8 V at an interlayer thickness of ~5 nm.[143] TAS measurements on this system revealed that charge recombination dynamics are relatively unchanged with the addition of TiO_x and thus the

interlayer does not improve performance by providing a recombination barrier; the authors instead propose that the V_{oc} improves through reduction in the saturation current under reverse bias, brought about by passivation of mid-gap ZnO surface defects. $TiCl_4$ has been used to introduce a thin TiO_2 layer on ZnO NRs, yielding increases in J_{sc} (0.24 mA cm^{-2} to 0.53 mA cm^{-2}), *FF* (0.36 to 0.41), and *PCE* (0.025 % to 0.070 %); unlike the aforementioned TiO_x work, no substantial V_{oc} increase was observed.[144] The hole polaron lifetime was observed to increase from 100 μs to 8 ms on coating the NRs with TiO_2, interpreted as TiO_2 providing a spatial barrier to charge recombination. However, the dark current in these devices was not observed to change substantially for modified devices (as was observed in TiO_x modified devices), suggesting that the $TiCl_4$ wash does not act to passivate defects: as such, this sets this report apart from other studies into inorganic modification. IM with CdS has been reported using layers between 10–20 nm thick, leading to a doubling of device *PCE* (0.055 % to 0.110 %) predominantly through a two-fold increase in the V_{oc} (0.309 V to 0.604 V).[145] Whilst CdS may contribute to photocurrent generation due to its narrow band-gap, the J_{sc} was not changed in the modified devices, possibly due to increased series resistance. The voltage enhancement was attributed to the CB band of CdS lying at a higher level than that of ZnO, leading to an increase in the maximum attainable V_{oc} of the device: the authors also recorded a suppression in reverse bias leakage which would also contribute to the voltage improvement. Recently, we employed the perovskite oxide lead zirconate titanate (PZT) as an IM in ZnO/P3HT bilayer devices (as presented in **Figure 8**): consequently, the hole polaron half-life was measured to increase from 16 μs to a maximum value of ~2 ms. The resulting devices exhibited much improved device performance with *PCE* improvements of up to six times (0.012 % to 0.073 %).[146] For thicker interlayers, although increased series resistance reduced the J_{sc} values from 0.233 mA cm^{-2} to 0.163 mA cm^{-2}, V_{oc} values of up to 0.73 V were obtained; prolonged illumination led to further increases in V_{oc}, reaching a maximum of 0.947 V. In contrast, prolonged exposure to UV light has previously been observed to completely degrade hPV device performance due to photoexcitation of the ZnO, giving it conducting characteristics.[147]

3.5 Molecular Modification of ZnO Acceptor Arrays

Oxide:polymer interfaces have been modified with a number of different molecules which may improve device performance through various pathways. The study by Goh *et al.* into modification of TiO_2/P3HT laid the foundations for IM in hPV devices: *para*-substituted benzoic acids (binding *via* the carboxyl group) possess a range of dipoles moments depending on the nature of the functional group, *i.e.* whether they are electron-donating (such as $–NH_2$) or electron-withdrawing (such as $–SO_2F$).[148] The former group of modifiers are expected to induce a dipole directed away from the oxide (δ^-), leading to a shift in the CB towards vacuum, whereas the latter group create a dipole directed towards the oxide (δ^+), lowering the CB edge; these changes in the surface properties are expected to yield increases in V_{oc} for the δ^- group and decreases for the δ^+ group. Whilst a good correlation between V_{oc} and dipole moment was observed in these experiments, the modifiers improving V_{oc} were also observed to lower the J_{sc} and vice-versa due to the changes in electron affinity (higher for the electron-withdrawing group-substituted modifiers and lower for electron-donating substituents). A similar study by Ruankham *et al.* was conducted on ZnO/P3HT systems using SAMs of substituted benzoic acids formed using either H_2O or ethanol as a solvent.[149] In this case, the trends in V_{oc} were similar to those found by Goh *et al.*; however, the authors noted that changes in the *J–V* curve profile suggested that the δ^- SAMs may play a role in reducing leakage current which would influence the V_{oc}, whereas the δ^+ SAMs appeared to increase it. Additionally, SAM formation was considered to be somewhat disrupted when performed from ethanol: considering that carboxylic acid linkages to ZnO are formed dissociatively, the ethanol could be expected to hinder chemisorption of the SAM.[77] NH_3 is a simple molecular modifier reported by Pradhan *et al.* to substantially improve hPV devices. The interaction of NH_3 with ZnO is two-fold: firstly, on immersion of NR arrays into solution, etching of the ZnO was observed owing to the basicity of the species; secondly, after removal of ZnO from solution, XPS measurements revealed the presence of nitrogen on the surface, suggesting that a thin overlayer of NH_3 had formed. In this study, NH_3 treatment (using a soaking time of 5 minutes to avoid over-

etching of the ZnO) appeared to increase the crystallinity of the ZnO nanorod array, and subsequent measurements of ZnO/MDMO-PPV (poly[2-methoxy-5-(3',7'-dimethyloctyloxy)-1,4-phenylenevinylene]) devices exhibited *EQE* improvements from 1.69 % to 5.87 %, along with substantial gains in both J_{sc} (0.11 mA cm^{-2} to 1.12 mA cm^{-2}) and V_{oc} (0.30 V to 0.82 V) albeit with reduced *FF*.[150] The authors accounted for these improvements by improved infiltration of the polymer into the NR array and by surface dipoles induced by the NH_3. The V_{oc} enhancement presented in this work is substantial (~0.5 V, far greater than for other dipolar modifiers) and it is unlikely that this can be fully accounted for by a dipole effect; additionally, the slope of the *J–V* curves under reverse bias suggest that the NH_3 treatment slightly increases the dark current, often associated with lowering V_{oc}. As such, further investigations on the electronic structure of NH_3-modified ZnO are required to fully explain the effects of this treatment. Chang *et al.* chose the small molecules tetraphenyldibenzoperiflanthene (DBP), also used as a small molecule donor species in OPV devices,[151] and 3,4,9,10-perylenetetracarboxylic bisbenzimidazole (PTCBI), reported as an acceptor in copper phthalocyanine (CuPc)-based OPV devices,[152] to modify ZnO NWs: as the LUMOs of these molecules have been measured to lie between the LUMO of P3HT and the CB of ZnO, it was thought that they would facilitate charge transfer from organic to oxide.[153] Whereas DBP yielded little in terms of device performance improvement, modification with a 30 nm thick layer of PTCBI was found to generate a substantial J_{sc} enhancement (2.32 mA cm^{-2} to 5.52 mA cm^{-2}) attributed to extended absorption of light over the visible range, although the V_{oc} fell from 0.40 V to 0.34 V.

Dye molecules have been used extensively as IMs in hPV devices: this interfacial engineering strategy was first reported by Ravirajan *et al.* who modified ZnO-NR/P3HT devices with the Ru-based complex Z907, shown in **Figure 9**.[154] Compounds in this class absorb light in the visible range and are often used as sensitisers in DSSCs; however, as the dye-loading in oxide:polymer hPVs tends to be much lower than in DSSCs (due to the substantially smaller active layer thickness and overall oxide surface area) the dye molecules are not expected to make substantial contributions

to photocurrent, instead influencing the surface electronic properties of the oxide or changing its wetting properties. The investigation by Goh *et al.* into modification of TiO_2/P3HT devices selected the Ru-based dyes N3 (cis-bis(isothiocyanato) bis[2,2'-bipyridyl-4,4'-dicarboxylato] ruthenium(II)), N719 (di-tetrabutylammonium cis-bis(isothiocyanato)bis(2,2'-bipyridyl-4,4'-dicarboxylato) ruthenium(II)), and Z907 (all shown in **Figure 9**), predominantly to facilitate rapid electron transfer to the oxide.[148] Additionally, dye LUMOs were measured to lie between the TiO_2 CB and the LUMO of the polymer, creating a cascade-type energy level structure in the device.[155,156] Modification of ZnO NRs with Z907 led to an increase in *EQE* from 7 % to 14 %, reflected in a noticeable reduction in dark current and improvements in both J_{sc} (roughly two-fold to 2 mA cm^{-2}) and V_{oc}.[154] Moreover, the dye modification led to an increase in hole polaron lifetime as measured by TAS: the Z907-modified rods exhibited a hole half-life approximately 4 to 5 times longer than for the unmodified case. The authors alluded to the improved wetting of the modified rods by the P3HT solution, although no measurements of polymer filling or morphology were undertaken in this work. The Hg-based dye mercurochrome (2',7'-dibromo-5'-(hydroxymercurio)fluorescein) has also been used in a similar fashion, yielding a four-fold increase in device *PCE* through improvements to both J_{sc} (0.30 mA cm^{-2} to 0.87 mA cm^{-2}) and V_{oc} (0.34 V to 0.45 V).[157] Phthalocyanines have been widely used as donor species in both OPVs[158] and hPVs.[159] Zinc phthalocyanine (ZnPc) has been used to modify normal hPV architecture cells with the structure ITO/PEDOT:PSS/P3HT/ZnPc/ZnO/Al (where PEDOT:PSS is the conducting polymer poly(3,4-ethylenedioxythiophene):polystyrene sulphonate): in this report, modelling of the P3HT/(ZnPc)/ZnO interface was undertaken, calculating that the presence of the ZnPc layer reduces the electronic overlap between separated hole and electrons pairs by around three times (from 12 % to 4 %), thus acting as a 'spacing' layer.[160] Devices fabricated with a 4 nm layer of ZnPc showed modest improvements in device performance with a ~52 % increase in J_{sc} and a reduced rate of electron–hole recombination as measured by transient open circuit voltage decay (TOCVD). Lastly, non-metal dyes such as indolines, also used in DSSCs [161], and the near-IR-absorbing

squaraines[162] have been used as modifiers. Indoline dye modification has been carried out using the structurally similar D149[163] and D205[164] species (shown in Figure 8), both of which were shown to improve device performance; however, in both cases the improvements in device performance changed significantly for differently processed ZnO layers. In the study by Ruankham *et al.* both ZnO NR arrays and sintered ZnO NP substrates were modified with D205, 5-[[4-[4-(2,2-diphenylethenyl)phenyl]-1,2,3,3a,4,8b-hexahydrocyclopent[*b*]indol-7-yl]methylene]-2-(3-octyl-4-oxo-2-thioxo-5-thiazolidinylidene)-4-oxo-3-thiazolidineacetic acid.[164] On the NR arrays, D205 improved all the solar cell characteristics: a 23 % improvement in J_{sc} (to 1.75 mA cm^{-2}), a 42 % increase in V_{oc} (to 0.505 V), a 20 % increase in *FF*, and an improvement in *PCE* from 0.259 % to 0.546 %. On NP arrays however, the J_{sc} was observed to decrease from 1.10 mA cm^{-2} to 0.45 mA cm^{-2}; however, the V_{oc} increased from 0.437 V to 0.761 V and a larger *FF* increase of 47 % (to 0.625) was observed. The origin of this J_{sc} decrease on the NP layers was attributed to incomplete infiltration of the layers by P3HT, despite the higher hydrophobicity of the modified oxide. Chen *et al.* used D149 (related to D205, carrying an ethyl group on the thiazolidinylidene unit) to modify two substrates: ZnO NR arrays, and ZnO NR arrays with epitaxially grown ZnO shells (hereafter referred to as NR-S), made using a two-step solution process. Modification of the bare NR arrays with D149 led to a 24 % reduction in J_{sc} (from 3.20 mA cm^{-2} to 2.45 mA cm^{-2}) but a V_{oc} increase from 0.32 V to 0.43 V, leaving the overall *PCE* relatively unchanged. However, dye modification of NR-S arrays yielded more substantial device performance improvements: J_{sc} increased by 22 % from 2.55 mA cm^{-2} to 3.11 mA cm^{-2} and V_{oc} from 0.43 V to 0.60 V, giving an overall *PCE* increase from 0.55 % to 1.16 %. This is reflected in the *EQE* measurements, with the modified NR-S arrays exhibiting higher values in the range 375–600 nm. The authors attributed this to the NR-S array being a 'more fitting' surface for D149 modification as similar results had previously been reported in ZnO/D149-based DSSCs;[165] however, whether this arises due to changes in ZnO binding, dye loading, or other effects was not studied in detail. Measures of capacitance suggest that the surface dipole induced by D149 adsorption raises the CB edge of the ZnO surface, leading to the observed

increase in V_{oc}: in the case of the NR-S arrays, the outer ZnO shell was also posited to provide an additional energetic recombination barrier. Squaraine modification has been shown to improve J_{sc} in various ZnO/P3HT systems:[164,166] for NR arrays, a ~3.5-fold increase (1.53 mA cm^{-2} to 5.53 mA cm^{-2}); for NP-coated NRs, ~3 fold improvement (2.07 mA cm^{-2} to 6.04 mA cm^{-2}); for sintered NP layers, a 33 % increase (1.10 mA cm^{-2} to 1.47 mA cm^{-2}), the relatively small gains attributed to poor infiltration of the ZnO array. Whilst the dye has been shown to yield slight decreases in V_{oc} in all cases, the modification leads to improvements in *FF* and, in the case of NRs, the overall maximum *IQE* measured at ~520 nm was shown to double, attributed to increased light harvesting by the dye.

Polymer morphology plays an important role in device performance, particularly at the D–A interface: more ordered polymers tend to have better charge transport characteristics which may aid in separation of charge. To improve the interaction between the oxide and polymer, molecules with alkyl chains may be used: these bond to the ZnO surface through a head group (such as thiol or silane), leaving the organic chains pointing away from the substrate. These apolar groups may interact more favourably with the polymer and promote a greater degree of crystallisation than the bare oxide surface. Alkanethiol modification has been shown to improve hPV performance, whereas the analogous use of alkylethoxysilanes such as octadecyltriethoxysilane (OTES) has been found to decrease device performance due to the formation charge-inhibiting multilayers.[93] In one study, SAMs of alkanethiols ($C_nH_{2n+1}SH$) with chain lengths of C_6, C_{10}, C_{14}, and C_{18} were inserted at the ZnO/P3HT interface: the resulting UV-vis spectra suggesting an increasing degree of polymer ordering with increasing alkyl chain length.[167] The R_s of the resulting hPV devices was observed to increase with increasing chain length, expected due to the insulating nature of the alkanethiols; despite this, the J_{sc} increased from 0.28 mA cm^{-2} to 0.42 mA cm^{-2} for the C_{18} modifier leading to an overall *PCE* increase from 0.037 % to 0.053 % (the V_{oc} remained at ~0.31 V). A later study investigated this system using GI-XRD and TAS and attributed the observed photocurrent increases to the changes in polymer morphology on alkanethiol-modified ZnO: the higher polymer ordering was thought to reduce the defect density in P3HT leading to an overall decrease in early-stage

charge recombination: this was reflected in the enhanced lifetimes for transient species in these films compared to both unmodified ZnO and glass substrates.[168] Dominguez *et al.* noted in their computational study on modified ZnO NWs that this thiol derivatives introduced intra-gap electronic states at the interface, arising from hybridisation of the modifier orbitals with those in the valence band; however, the impact that this would have on device performance has not been studied.[90]

Fullerenes and their derivatives have become an important class of compounds in organic photovoltaics due to their effectiveness as acceptor molecules, one common example being PCBM. The carboxylic acid derivative of this species, phenyl-C_{61}-butyric acid (PCBA) has been investigated as an IM in hPV devices, first reported by Vaynzof *et al.*: PCBA forms a SAM on ZnO[169] and in this first study was reported to triple the external quantum efficiency (from 3 % to 9 %) and improve the four main *J–V* parameters, notably through significant increases in J_{sc} (0.47 mA cm^{-2} to 1.1 mA cm^{-2}) as well as an increase in V_{oc} from 0.21 V to 0.32 V. This was attributed to several effects: the work function was observed to increase by 0.5 eV (from 3.6 eV to 4.1 eV), interpreted as the formation of a dipole at the surface. This was thought to increase the magnitude of the electric field at the ZnO surface, thereby reducing charge recombination. In a later report, PCBA was calculated to not only contribute to improvements in exciton harvesting (by 45 % *cf.* unmodified ZnO), but also to reduce the probability of BCP formation, (28 %, as opposed to 52 % in unmodified ZnO).[126] PCBA modification of ZnSrO layers was shown to be more effective than for undoped ZnO: it was posited that the increased surface –OH coverage in ZnSrO allows for the more complete formation of a PCBA monolayer, accounting for the differences in *PCE* (~0.14 % for ZnO/PCBA, ~0.33 % for ZnSrO/PCBA).[138] Lastly, Zhong *et al.* reported the use of a different fullerene acceptor, C_{60} pyrrolidine tris-acid (C60-PTA), which induces a smaller $\Delta\phi$ on modification than PCBA (0.15 eV *cf.* 0.50 eV for ZnO/PCBA): given that the *EQE* improvements in this work were almost identical to those in the PCBA modification studies above, the authors concluded that the device performance improvements were attributable not only to the changes in

the ZnO electronic properties, but also to the changes in polymer morphology brought on by fullerene modification.[170] XRD measurements of the ZnO/C60-PTA/P3HT films exhibited enhanced crystallinity for the P3HT (*100*) orientation which would be expected to contribute to the enhanced photocurrent observed in these devices.

Molecules specifically designed for IM of hPVs were reported by Yu *et al.* for TiO_2/P3HT devices, consisting of species with cyanoacrylic acid groups to anchor to the oxide (creating a dipole pointing away from the acceptor) and conjugated thiophene tails; additionally, the energy levels of these modifiers were tuned by changing the molecular structure of the tail section. These modifiers proved to be effective in raising both photocurrent and voltage, leading to *EQE* enhancement from ~3 % in the unmodified devices to a maximum value of ~34 %.[171] The most successful modifier (containing a thiadiazole group) from this study was incorporated into ZnO/P3HT devices in the study by Eom *et al.*, as well as a second modifier with a higher-lying LUMO closer to that of P3HT (containing triphenylamine, naphthalene, and thiophene groups).[172] The thiadiazole-containing modifier was found to be more effective: whilst device performance improvements were not as striking as for the TiO_2 based hPV devices in [171], the J_{sc} (0.27 mA cm^{-2} to 0.91 mA cm^{-2}), V_{oc} (0.57 V to 0.78 V) and *PCE* (0.09 % to 0.42 %) were all observe to improve. The second triphenylamine-based modifier was less successful: it was noted that the energy of this molecule's LUMO was very close to the LUMO of P3HT which may lower the driving force for exciton dissociation; additionally, molecular geometry calculations showed that this molecule possessed a lesser degree of conjugation over the structure, leading to a wider energy gap. However, both modifiers were shown to greatly improve the diode characteristics of the hPV devices, reflected in the ~10-fold improvement in R_{sh}; in general, both these studies have shown how effective tailored interfacial modification approaches can be in oxide-based devices.

3.6. ZnO Nanoparticle Modification for Bulk Heterojunction hPVs

Bulk-heterojunction hPVs based on blended NP-ZnO:P3HT active layers have generally outperformed devices based on solid ZnO arrays: a comprehensive review of this device type has been written by Li & Chen.[173] As with solid array acceptor hPVs, the local polymer:oxide interaction has a substantial effect on photocurrent generation. The morphology of these devices is also of great importance in terms of charge transport, and is affected by the dispersion of NPs within the polymer matrix.[118] Typically, ZnO:polymer blend devices have been produced either by: *i)* dispersing NPs in a mixed solvent medium (typically methanol/chlorobenzene which allows NP dispersion without the need for capping ligands often used in other applications),[174] adding polymer and spin-casting,[147] or *ii)* forming a mixture of dissolved polymer with the ZnO precursor diethylzinc (DEZ) which crystallises within the polymer matrix on contact with residual H_2O.[175] IM of the ZnO may be undertaken through the addition of molecular species to the NP suspension. Moulé *et al.* note that the choice of NP ligand may affect four main contributions to photocurrent generation: *i)* the proportion of excitons which may undergo dissociation; *ii)* the efficiency of exciton dissociation as the ligand can affect the D–A separation; *iii)* efficiency of charge transport as the ligands influence charge-hopping probabilities between particles; *iv)* efficiency of charge collection as the ligands affect hopping probabilities between NPs and the electrodes.[174]

Dithiol-based liquid crystal ligand modification of ZnO NPs has been reported in ZnO:P3HT blends: the rationale behind these studies is that, on heating, the modified NPs may self-assemble to form 1-D structures, potentially leading to improved charge transport through the active layer.[176,177] Li *et al.* used the ligand 4-(5-(1,2-dithiolan-3-yl)pentanoate)-4'-(hexyloxy)-terphenyl (HTph-S, **Figure 11**), yielding *PCE* increases from 0.47 % to 0.81 %, predominantly through J_{sc} enhancement (2.01 mA cm^{-2} to 2.94 mA cm^{-2}).[176] Annealing for 20 minutes at 120 °C increased the J_{sc} by a further 28 % (as well as an *FF* increase from 0.45 to 0.51) for a *PCE* of 1.23 % (a 51 % increase) and an *EQE* of ~32 %. It should be noted that these improvements were more substantial than those achieved for annealing control devices without the ligand (a 17 % increase in J_{sc} and a

19 % increase in *PCE*). After annealing, the modified layers exhibited strong absorption at ~620 nm: this is generally assigned to inter-chain interaction in P3HT, suggesting that the ligand improves the crystallinity of the polymer which would facilitate hole transport; additionally, transmission electron microscopy (TEM) images provided evidence for suppression of NP aggregation in the polymer matrix. Similar device performance improvements were measured for the ligand 2-[(5-(1,2-dithiolan-3-yl)-pentanoate)]-3,6,7,10,11-pentakis(butoxy) triphenylene (TP-S, **Figure 11**) by Chen *et al.*:[177] in particular, X-ray diffraction measurements showed a substantial increase in intensity of the P3HT (*100*) reflection, indicative of increased lamellar ordering of the polymers.[178] **Figure 11** (a)–(d) presents the TEM data from this study, showing the changes in the distribution of NPs in the polymer matrix on modification with TP-S.

Several of the molecular species used in the modification of planar ZnO-based hPV devices discussed above have been transferred to NP-ZnO:P3HT systems. PCBA modification of NP-ZnO was undertaken by Yao *et al.*: in this study, the modification was observed to hinder aggregation of the NPs in solution and promote formation of crystalline P3HT fibres in the ZnO:P3HT layer.[179] As with PCBA modification of solid ZnO films, substantial gains in J_{sc} — a 55 % increase from 3.47 mA cm^{-2} to 5.39 mA cm^{-2} — were recorded (*PCE* increased from 0.59 % to 1.20 %). Although the gains in J_{sc} were not as pronounced as for the bilayer ZnO–PCBA:P3HT devices, the *EQE* was measured to be above 30 % over the range 400–650 nm - expected due to the greater surface area and reduced average D–A distance in the BHJ devices. Dye modification with squaraine (SQ36, **Figure 9**),[180] Z907,[181] N3, and α-sexithiophen-2-yl-phosphonic acid (6-TP)[182] has also been reported. Squaraine modification was undertaken using a one-pot synthesis method (precursor containing DEZ, P3HT, and the dye). Although hPV devices were not fabricated in this study, characterisation of the charge generation and recombination dynamics was carried out using TAS: here, charge separation was observed to be slightly slower for SQ36-modified NPs (< 1 ps for unmodified NPs, 3.3 ps for SQ-modification); however, charge recombination was found to be over

five times slower at the interface (*i.e.* between electrons in the ZnO CB and holes in P3HT) and much slower for trap-assisted recombination.

In summary, despite the perceived shortcomings of metal oxide:polymer hPV systems in terms of absolute performance, a variety of IMs have been shown to be successful in improving the heterointerface and the resulting improvements in device performance have similarly been observed to arise from a range of pathways.

4. Organic Solar Cells

OPV devices based on all-organic, distributed D–A bulk heterojunctions have received widespread attention and have been earmarked as a potentially commercially viable technology. Whilst a multitude of different D and A species have been synthesised, blended active layers consisting of a photoactive polymer and fullerene-based acceptors have been the most commonly reported, particularly the P3HT/PC$_x$BM combination. ZnO has been incorporated into these devices as an electron transport/hole-blocking layer (ETL) aiming to improve R_{sh} and electrode charge selectivity. In devices with a normal architecture, **Figure 5 (b)**, the ZnO ETL is deposited onto the active layer, sitting between the polymer and the metal contact: as such, it requires low-temperature processing with orthogonal solvents (in the case of solution processing) to avoid damaging the organic layer.[183,184] As discussed previously, inverted devices have become more popular in recent years as the use of higher work-function metals as top contacts tends to confer a greater degree of stability to the devices.[185] In such cells, ZnO ETLs are inserted between the bottom contact (usually ITO) and the active layer, similar to most of the ZnO array-based hPV devices discussed in the previous section. Huang *et al.* provide an excellent review of ZnO-containing OPVs, covering its incorporation into both normal and inverted devices, as well as the use of nanostructured ZnO layers.[1]

Although ZnO interlayers have been shown to be effective in improving device performance, large variations in leakage current and 'S-shaped' *J–V* behaviour have been reported by several groups.[186–189] It has been proposed that the formation of leakage current pathways in the ETL, indicated by severe reductions in R_{sh}, leads to increasing non-selective behaviour thus giving rise to the observed performance anomalies. Many groups have attributed this to the interaction between ZnO and adsorbed O_2: these impurities may trap electrons, creating negative depletion regions in ZnO and also creating a barrier to charge transfer from PCBM to ZnO; under UV-irradiation and forward biasing, desorption of O_2 from the ZnO can change the electronic structure and properties of the surface. Whilst these anomalous characteristics may be removed using short reverse bias pulses,[187] Wilken *et al.* reported that gas-permeable, *i.e.* non-encapsulated devices, exhibited only partial recovery of device characteristics.[189] The study by Cowan *et al.* of phosphonic acid-modified ZnO ETLs noted that these 'S-shaped' *J–V* characteristics may be reversible or irreversible, depending on the nature of the ZnO interface. The authors note that, in both of these cases, this device behaviour arises from low conductivity of the ETL leading to a slower rate of charge extraction than charge generation.[190] The O_2 absorption mechanism, for example, is an example of reversible change in *J–V* behaviour in which little change in the V_{oc} is observed; however, in the case where unfavourable band alignment hinders charge extraction, this behaviour is irreversible, leading to a decrease in V_{oc}.

As discussed in Section 2.1, both experimental and computational studies have established that defect species in ZnO may strongly influence the measured work functions.[54,56] In the work by Schulz *et al.*, the interaction between C_{60} (chosen over functionalised fullerenes due to its symmetry: as such, orientation effects could be ignored) and differently processed ZnO layers was examined: in this work, changes in the predominant defect type and density were effected by post-processing using controlled sputtering processes — work function data from this study is presented in **Table 1**. The ultraviolet photoelectron spectroscopy (UPS) results of this study suggest that interaction between ZnO and C_{60} is governed by the dominant population of oxide defects, leading

to different degrees of hybridisation between the oxide and polymer: whilst significant electron transfer (0.24 e^- per molecule) was measured between the fullerene and ZnO with large Zn_i populations, little transfer was observed for surfaces containing large numbers of deep level donors (V_O), nor for the stoichiometric surface. Whilst greater degrees of hybridisation (*i.e.* where more electron transfer was observed) was associated with greater electron injection efficiency, for the V_O-dominant surface, a ~0.4 eV barrier to charge extraction was observed: this is shown in the energy level diagrams presented in **Figure 12 (a)**. As such, despite the efficacy of ZnO layers in improving OPV performance, the surface chemistry of the material needs to be carefully controlled in order to produce repeatable device performance. Although the use of ZnO in OPVs has been well-established in the literature for some years, widespread research into modification of these ETLs is a more recent development: the following sections review the different strategies used for improving the functional properties of the ZnO layers.

4.1 Doping of ZnO Electron Transport Layers

Doping of ZnO ETLs has been carried out with a variety of different elements, predominantly to improve the conductivity, allowing for the use of thicker interlayers which may be produced in fast production techniques such as roll-to-roll processing. Al-doped ZnO (AZO) has been used primarily as a TCO electrode material in optoelectronic devices as a substitute for ITO: the Al^{3+} ion acts as a donor, increasing the conductivity of ZnO. A number of recent studies have employed these layers as ETLs:[191–193] Li *et al.* noted that doping of Al into the ZnO surface would firstly lower the work function by increasing the carrier concentration in the film, as well as potentially improving electron injection into ZnO by removing the electron-acceptor states associated with the V_{Zn} defect.[54] Stubhan *et al.* have incorporated sol-gel-derived AZO layers (containing an Al atomic fraction of 1 %) into inverted P3HT:PCBM-based OPVs using low temperature processing (140 °C).[192,193] Whilst little difference in device performance between thin ETLs (~30 nm) of pristine and AZO was observed, increasing thickness (~120 nm) led to substantial declines in the *PCE* of the former (2.56 % to 1.54 %), whilst not substantially affecting AZO-based devices: this

was attributed to the improved conductivity of the doped ETL and may be of particular interest in the context of nanostructured ZnO ETLs in which the conduction path lengths are typically much longer than for 'flat' interlayers. The study by Jagadamma *et al.* presents data from OPV devices using a range of ZnO and AZO ETLs, showing that optimisation of both the morphology and the surface chemistry of these interlayers may produce significant gains in device performance.[194] For thermally evaporated AZO layers, only small gains in performance were recorded for devices with a $PC_{70}BM$ and PTB-7 (poly({4,8-bis[(2-ethylhexyl)oxy]benzo[1,2-b:4,5-b']dithiophene-2,6-diyl}{3-fluoro-2-[(2-ethylhexyl)carbonyl]thieno[3,4-b]thiophenediyl}), **Figure 6**) active layer; however, the incorporation of ETLs derived from AZO NPs yielded substantial increases in J_{sc}, V_{oc}, and *FF*, and an overall *PCE* increase from 4.90 % to 7.66 % (taking thermally evaporated pristine ZnO ETLs as a reference). Adding NH_3 to the pre-deposition AZO NP suspension was found to alter the morphology of the resulting ETL substantially, decreasing the size of the NPs through etching (from 40–100 nm to *ca.* 5–10 nm); consequently, the roughness of the resulting ETL was much lower for the NH_3-treated NPs, with RMS (root mean square) roughness values of 3.6 nm, compared to 20.3 nm for the untreated NPs. Secondly, as was reported for NH_3-treated NRs,[150] XPS measurements showed that N was incorporated into the AZO surface with an estimated concentration of ~0.9 at. %. OPV devices with these interlayers improved device performances over the untreated AZO NP ETLs through slight increases in J_{sc} and an increase in *FF* from 0.62 to 0.71 (R_{sh} increased from 7 kΩ·cm^2 to 10 kΩ·cm^2, whereas R_s decreased from 2.3 Ω·cm^2 to 0.6 Ω·cm^2); moreover, the *EQE* was measured to fall > 80 % in the range 390–510 nm. Notably, further ETL modification with species such as PEIE and C_{60} SAMs (discussed later in this review) did not lead to *PCE* improvements, revealing the effectiveness of the NH_3 treatment. Lastly, increasing ETL thickness from 22 nm to 75 nm led to only a 9 % reduction in *PCE* (8.9 % to 8.1 %). Two studies by Shin *et al.* found similar effects for Ga-doped ZnO (GZO):[195,196] for 50 nm thick GZO interlayers, an optimal composition of x_{Ga} = 0.02 was determined, yielding a 12.5 % improvement in J_{sc} from 10.28 mA cm^{-2} to 11.56 mA cm^{-2} for a P3HT:PCBM active layer. Whilst

the changes in J_{sc} correlated well with decreasing series R_s, the XPS data suggested that Ga acted to fill V_O defects in ZnO. In-doped[197] and Cs-doped ZnO[198] also appear to improve performance by lowering R_s: in the IZO devices, degradation of devices stored in ambient conditions was observed, consistent with the studies into ZnO ETL oxygen adsorption;[188] however, full restoration of device performance was observed after a few minutes of UV illumination.

Y-doping of ZnO has been carried out on ZnO NW arrays (around 500 nm in length) grown by electrodeposition: ETLs with optimal performance were obtained from growth solutions containing 0.02 mM of the precursor YCl_3.[199] Introduction of Y predominantly affected the *FF* through increases in R_{sh} for the doped NWs (R_s values were not derived in this study, however), yielding a *PCE* increase from 1.5 % to 2.3 %. MgZnO layers, also employed as acceptors in hPVs as discussed in Section 3.3[132] have been used in P3HT:PCBM and P3HT:ICBA (indene C_{60}-bis-adduct, **Figure 7**) active layer OPVs with the expectation that these would effect gains in V_{oc}.[133] Whilst in previous studies it had been assumed that Mg incorporation would increase the V_{oc} through increasing the offset between the donor HOMO and acceptor CB (by pushing the CB level towards vacuum), in this study no evidence of a CB shift was observed with Mg-doping: as previously mentioned, the authors note that the role of Mg in band-gap tuning in ZnO is currently disputed. In this study, improvements in *PCE* were observed, mainly through improvements in V_{oc} and *FF*. The composition $x_{Mg} = 0.10$ was found to be the optimal doping level for both PCBM and ICBA acceptors, yielding V_{oc} improvements of 12 % (to 0.577 V) and 14 % (to 0.828 V) respectively, and *FF* improvements from 44.9 to 56.8 for PCBM, and 55.5 to 67.0 for ICBA. At higher doping levels, J_{sc} was observed to fall, as was previously observed in the MgZnO hPV devices. Whilst no solid conclusion was drawn as to the precise origin of these device improvements, the authors posit that the fullerenes interact differently with the doped and undoped surfaces: this may affect the magnitude of the interfacial dipoles which form as a result, thereby altering barriers to charge extraction. Lastly, ZnO composites with other oxide materials have been investigated for ETLs: Gadisa *et al.* mixed AZO NPs in a TiO_x matrix, creating low work-function

films (~3.0 to 3.3 eV depending on annealing temperature) with high surface Ti content (Ti/Zn ~0.8 at the surface, *cf.* ~0.4 in the bulk region of the interlayer).[200] These films were found to be effective interlayers in P3HT:PCBM devices despite the high resistivity of TiO_x, and were measured to possess high *FF* values (> 0.60); however comparisons with pristine ZnO reference devices were not cited in this report. Ta_2O_5, a high-*k* dielectric, was mixed with ZnO in an attempt to control ZnO defect formation.[201] From structural data, the films were found to consist of crystalline ZnO mixed with amorphous Ta_2O_5; additionally, from the XPS data, a shift in the Zn 2*p* binding energy suggests that some chemical interaction occurs between Ta and Zn in these films, giving rise to a slight increase in the Zn oxidation state (nominally +2). From this, the authors propose that some amorphous regions of ZnO exist in these films. The optimal composition for ETLs was found to contain 18 % Ta_2O_5 — the resulting OPV devices exhibited *PCE* increases from 3.70 % to 4.12 %, predominantly accounted for by increases in *FF*. The R_s was observed to decrease (although at higher Ta_2O_5 content, the R_s was observed to increase which is expected given its insulating characteristics) and the R_{sh} was observed to improve almost 5-fold. Moreover, the performance of these ETLs was fairly insensitive to processing conditions, *i.e.* preparation in N_2 or O_2 atmospheres. A similar study was carried out using $SrTiO_3$, yielding similar results and trends to the Ta_2O_5 study.[202] $SrTiO_3$ was chosen due to its [TiO_6] octahedra which may exhibit polarisation under an electric field; however, as no evidence of crystalline $SrTiO_3$ was found in these films, further work is required to verify whether such functional properties do have a meaningful effect on OPV devices. Lastly, 10–15 nm films of amorphous zinc tin oxide (ZTO) films were found to be an effective ETL as compared to amorphous TiO_x interlayers, although no comparison to devices with pristine ZnO ETLs was made.[203]

4.2 Molecular Modification of ZnO Electron Transport Layers

In addition to the junction between the active layer and ETL, the electrode interfaces play a key role in charge collection in OPV devices. Yip *et al.* investigated modification of normal architecture OPV devices with the layer structure ITO/PEDOT:PSS/P3HT:PCBM/ZnO/(SAM)/M (M = Al, Ag,

Au), aiming to form an Ohmic contact between the oxide and the metal and thereby preventing the formation of an energy barrier to charge extraction. This was undertaken using a series of *para*-substituted benzoic acids[204] (similar to those used by Goh *et al.* in modification of hPV devices,[148] with the magnitude and direction of the molecular dipole governed by the electron-donating or withdrawing nature of the *para*-substituent) and saturated alkyl chains with carboxyl head groups.[205] In these studies, the efficacy of these SAMs was determined both by the surface dipole of these species, as well as the work function of the metal contact. A comprehensive summary of these results in provided by Tada *et al.*.[206]

Modification of the ZnO:organic interface with fullerenes and fullerene derivatives — as has also been undertaken for hPV devices, detailed in Section 3.5 — has been shown to be effective in improving the performance of ZnO ETLs. A number of different strategies have been devised for this type of IM: synthesis of functionalised fullerene species for oxide modification by SAM formation; impregnation of ZnO with C_{60}-derivatives using co-deposition techniques; and formation of polymerised fullerene interlayers on the ZnO surface. Hau *et al.* conducted two studies into SAM-modification with a variety of fullerene derivatives, studying the changes in device performance on modification,[207] the effect of using different binding groups (BAs, phosphonates, catechols) as well as the effect of different processing methods (spin-coating *vs.* substrate immersion).[208] Spin-coating a layer of C_{60}-substituted BA on ZnO ETLs was found to improve the *PCE* of P3HT/PCBM devices by ~35 % (3.32 % to 4.45 %) when processed in ambient conditions, primarily through gains in J_{sc} (10.5 mA cm^{-2} to 12.0 mA cm^{-2}) and *FF* (50.8 to 59.5); on top of this, the *EQE* at 500 nm was shown to increase from 44 % to 70 %. Out of the SAMs used in these studies, the largest gains in performance were achieved by spin-coating a layer of C_{60}-substituted BA on ZnO, in part due to the high surface coverage of this SAM as shown by contact angle measurements — in contrast, the more acidic phosphonic acid derivative was shown to etch the ZnO layer. The observed performance enhancements were attributed to improvements in charge transfer from the active layer to the ETL *via* the fullerene modifiers. Liao *et al.* synthesised

ZnO:PCBM composite ETLs from a sol-gel containing a PCBM precursor weight fraction of 0.5 %, in which the fullerene species is thought to form a complex with the Zn acetate precursor.[209] Subsequently, active layers consisting of PTB-7 or thiophene-modified PTB-7 (PTB7-Th, **Figure 6**) donor polymers and $PC_{71}BM$ acceptors were incorporated into these devices. The modified interlayers were shown to possess a fullerene-rich surface and a narrower band gap than undoped ZnO, with the ETL CB calculated to shift away from vacuum by around 0.4 eV. The electron mobility of these modified layers was found to be around 50 times greater than for pristine ZnO, and their surface conductivity was observed to increase dramatically from 0.015 S cm^{-1} to 1.09 S cm^{-1}. Consequently, the R_s of the resulting OPV devices was found to be reduced by ~73 % (15.13 $\Omega \cdot cm^2$ to 4.16 $\Omega \cdot cm^2$), contributing to an overall *PCE* increase from 6.65 % to 8.21 %. ETL modification with polymeric interlayers (~10 nm thick) containing fullerene units have been reported to improve both P3HT:PCBM[210] and P3HT:ICBA[211] devices. In these studies, the interlayers were synthesised by thermal cross-linking of phenyl-C_{61}-butyric styryl denrdron ester; consequently, 26 % and 29 % increases in *PCE* were recorded for PCBM and ICBA acceptor devices respectively. These modifiers were shown to reduce the surface roughness of the ETL (referred to as planarisation), reduce leakage current, and double the R_{sh} whilst simultaneously reducing R_s.

The surface energy and wetting properties of inorganic ETLs may influence the morphology of the organic layer and conformation of polymer close to the oxide surface (as well as the bulk crystallisation of the active layer), as was the case for alkanethiol modification of ZnO acceptor layers in hPVs previously discussed in Section 3.5.[167] Bulliard *et al.* employed a mixed monolayer modification to investigate the influence of surface energy on P3HT:PCBM devices. The mixed monolayer consisted of two species, polar aminopropyltrimethoxysilane and apolar octyltrimethoxysilane: by changing the ratio between these two species, the ETL surface energy could be tuned systematically.[212] Moreover, all of these mixed monolayers possessed similar work function values (~4.3 eV), thus strengthening any correlations between surface energy and device

performance. **Figure 13** presents both TEM, (a)–(d), and device performance data, (*i*)–(*v*): SAM-modified films possessed surface energies in the range 36–61 mN m^{-1} *cf.* a value of 71 mN m^{-1} for pristine ZnO. Over this range, J_{sc} appeared to make the biggest contributions to variation in *PCE*, reaching a maximum value at a surface energy of 51 mN m^{-1}. Variation in the active layer topography was compared with the device performance, showing that the best-performing films contained well-defined fibrils and fine phase domain separation: although these IM species did not substantially improve the overall device performance, such effects should be taken into account when choosing or designing molecular IMs. This strategy has also been employed by Brenner *et al.* in order to investigate the effect of changing work function on ETL performance: here, a mixture of phenyltriethoxysilane and *p*-chlorophenyltriethoxysilane was used (the two species possessing opposing dipoles), allowing tuning of the work function over a ~0.6 eV range.[94] Whilst V_{oc} was shown to increase with decreasing work-function, the authors noted that pinholes and sub-monolayer coverage by the SAM may have influenced these observed device characteristics. BPA and phenylphosphonic (PPA) derivatives have also been used to study the effect of work function on ETL performance.[84,190] A computational and experimental study by Li *et al.* investigated the effects of these modifiers on the electronic structure of GZO surfaces using fluoro-substituted BPA and PPA species: each modifier was shown to increase the GZO work function (~3.30 eV for the unmodified layer) with values between +0.48 eV (*o*-2FBPA) and +1.57 eV (pentafluoro-PPA) through introduction of surface dipoles.[97] In this study, these modifiers were shown to anchor to ZnO through the Zn–O and bridging Zn–OH surface species (whilst populations of hydroxyl groups near V_O were shown to be unaffected by the modification). For BPA, the benzene ring was found to carry a neutral charge, whereas 5FBPA was calculated to possess a net positive charge of +3.22 electrons per molecule using Bader analysis, indicating stronger coupling with the oxide surface and leading to a greater work function shift (+1.13 eV). Cowan *et al.* used *p*-trifluoromethyl-BPA (*p*-F_3CBPA) and *o*-2FBPA modification of ZnO in OPV devices with PCDTBT:PC_{71}BM active layers:

here, work function shifts of +0.9 eV (*p*-F_3CBPA) and –0.2 eV (*o*-2FBPA) were recorded[3], as well as an apparent narrowing of the surface band gap with both BPA species.[190] The resulting device performance was shown to be strongly affected by these changes in surface electronic properties: energy barriers for electron transfer from active layer to ETL were calculated finding values of 0.4 eV (unmodified ZnO), 0.6 eV (*p*-F_3CBPA), and 0.3 eV (*o*-2FBPA), the lower barrier associated with enhanced J_{sc} and V_{oc}, and the higher barrier with substantially reduced values. Although the species used in these fundamental studies do not provide large gains in device performance by themselves, they provide an excellent set of guidelines which may be used in the choice and design of interface modifiers.

Conjugated thiol species such as 2-napthalenethiol and phenylthiol derivatives have been shown to improve ZnO NR ETL performance through defect passivation and by inducing changes in its transport properties.[213,214] Although these modifiers have not been seen to increase free charge yield, it was found that their presence affected both hole and electron mobilities (μ_h and μ_e respectively), as measured using admittance spectroscopy. 4-terphenylthiol (4-TPT) modification was found to produce the most efficient devices, were measured to possess the lowest ratio μ_e/μ_h, *i.e.* the most balanced charge transport out of the devices measured (around half that of unmodified ZnO), leading to a 40 % improvement in J_{sc} values (8.84 mA cm^{-2} to 12.40 mA cm^{-2}) and a *PCE* improvement from 1.71 % to 3.01 %. These improvements in hole mobility were attributed to changes in polymer phase domain structure induced by the increasing length of the modifier chain (from phenylthiol to 4-TPT). Eom *et al.* also investigated modifiers containing aromatic chains, employing these in both OPV and hPV devices (as described previously in Section 3.5): here, a modifier based on a cyanoacrylic oxide linking group and a chain consisting of two thiophene units flanking a benzothiodiazole group was used. Despite a decrease in J_{sc} (probably accounted for by the observed doubling of R_s — it was proposed that the modifier may introduce a small barrier to

[3] *N.B.* this study was carried out on undoped ZnO layers, as opposed to the GZO layers in Ref. [97], hence the difference in work function shifts between the two studies.

charge transfer to the ETL), improvements in R_{sh} (around 2.25-fold) and increased *FF* led to a modest gain in *PCE* from 4.12 % to 4.69 %.[172] Wang *et al.* used ZnO ETLs modified with Cs-stearate (which contain long hydrocarbon tails, similar to the aforementioned alkanethiol species) in PTB-7:$PC_{71}BM$ devices, finding a reduction in PL emission intensity (indicative of a reduced defect population), lower leakage current, and a slightly higher rate of exciton generation.[215] The Cs-stearate was shown to decrease the surface roughness of the ZnO and conductive AFM sweeps of the modified films exhibited a much reduced variation in local conductivity over the surface compared to the pristine ZnO. The modified devices exhibited a 21 % increase in *PCE* (6.97 % to 8.46 %), and ~8 % and ~10 % improvements in J_{sc} and *FF* respectively, as well as improved stability over a 25 day period in an inert atmosphere. The role of changes in morphology were not discussed in depth in this study, although it would be expected that the change in ZnO surface energy on modification with Cs-stearate would also affect the transport properties of the active layer as was discussed earlier in this section with reference to the work by Bulliard *et al.*.[212] Diethanolamine (DEA) was used as a both an additive for ZnO NP growth and as a surface modifier in the study by Lee *et al.*.[216] Increasing the concentration of the DEA additive (from 0.001 M to 0.01 M) led to successive gains in *PCE*: although modification slightly lowered J_{sc}, the V_{oc} values for these devices were observed to increase by ~11 %. DEA-modification led to a decrease in observed work function from 4.40 eV to 4.00 eV, and the authors concluded that E_F pinning was occurring between the acceptor molecules and the ETL, thus the overall V_{oc} was determined by the energy levels of the active layer components rather than the energy levels of the ZnO. The R_{sh} was also observed to improve, coinciding with an increase in *FF*. Cheng *et al.* employed a novel modification approach using the small molecule tetrafluoroteraphthalate, a tetrafluorophenyl ring with two *para*-substituted carboxyl groups. This molecule is expected to lie parallel to the ZnO surface (anchoring through the carboxyl groups) and form strong interactions with the fullerene acceptors through a δ^+ charge on the benzene ring induced by presence of the fluorine substituent, thereby reducing contact between the donor and the ZnO.[217] The best-performing devices were

made by depositing the modifier on ZnO, coating with a PCBM solution to form an acceptor layer, then putting down the active layer. J_{sc} was seen to improve by ~15 % for P3HT:PC_{61}BM, ~19 % for P3HT:PC_{71}BM, and ~14 % for PTB-7:PC_{71}BM relative to unmodified reference cells, whereas V_{oc} was not measured to vary substantially between devices. The authors attributed the improvements in J_{sc} to the removal of –OH groups by the modifiers, and it was concluded from PES measurements that the modifier introduces a cascading energy level structure into the ETL leading to improved charge transport. Lastly, the Ru-based dye N719 (previously reported in IM of hPV devices) has been incorporated into OPVs in two studies, one using ZnO NR arrays,[218] the other on AZO ETLs.[191] Whilst both studies reported improved device performance (~72 % and ~37 % increases in *PCE* respectively), the *EQE* was only observed to increase for the NR arrays (34 % increase in J_{sc}, albeit with a reduction in *FF*); for AZO–N719, the *EQE* did not change on modification, but a *PCE* increase from 2.79 % to 3.83 % was measured, predominantly accounted for by the change in FF from 0.49 to 0.60 (accompanied by a ~50 % in R_s and an almost three-fold improvement in R_{sh}), as well as substantially reduced dark current. These discrepancies may arise firstly due to the difference in the electronic properties between AZO and undoped ZnO; additionally, it is possible that the dye affects wetting properties of the NR array leading to improved filling and/or morphology of the active layer which would contribute to the improved *EQE* of the modified devices — however, these effects were not studied.

4.3 ZnO–Polymer Bilayer and Composite Electron Transport Layers

Polymer modification of ZnO ETLs has been shown to be an immensely effective route for improving charge extraction in OPVs. Bilayer structures in which a thin film of polymer (< 10 nm) is applied to the ZnO surface, have been reported;[219] additionally, ETLs of composite interlayers consisting of ZnO and the modifying polymer have been fabricated by co-deposition, either by dispersing ZnO NPs in a precursor solution containing the polymer,[220] or by adding the polymer to a ZnO precursor sol-gel and processing the films at low temperature.[221] ETLs modified with poly(vinylpyrrolidone), PVP (**Figure 15**), were initially reported by Small *et al.*.[221] PVP

modification of ZnO may improve the ETL performance on several counts: *i)* the polymer acts as a void-filling agent and can reduce the surface roughness of the interlayer, which improves the R_{sh} by reducing contact between the D and the bottom electrode; *ii)* PVP lowers the work function of ZnO (Lee *et al.* reported a change from 4.4 eV to ~4.0 eV on PVP modification)[216] leading to reduced contact resistance between ZnO and acceptor molecules, reflected in the lower R_s values measured for these devices;[216,222] and *iii)* reduced dark current has been observed in PVP-modified OPVs suggesting that the polymer plays a role in passivating ZnO surface defects. As such, for a PTB-7/$PC_{70}BM$ active layer device using a ZnO interlayer modified with a ~6 nm of PVP, Lampande *et al.* recorded an 18 % increase in *PCE* from 6.18 % to 7.30 %, owing improvements in J_{sc} (14.00 mA cm^{-2} to 15.17 mA cm^{-2}), *FF* (62.5 to 66.7), and a 20 % decrease in R_s.[222] It was noted by Small *et al.* that the PVP-modified ETLs required light soaking to achieve their maximum performance; however, it was found that layers exposed to a 10 minute UV–ozone treatment did not require light-soaking and, moreover, exhibited enhanced *EQE* (from ~66.0 % to 73.6 %) which was attributed to reducing the thickness of PVP covering the ZnO clusters and thereby improving contact between ZnO and the active layer. Poly(ethylene oxide) (PEO), also referred to as poly(ethylene glycol),[220,223] and polyethylenimine 80 % ethoxylated (PEIE)[219] have produced similar improvements in device performance. Hu *et al.* demonstrated the effect of PEO M_w (*i.e.* polymer chain length) on the effectiveness of modified ZnO NP composite ETLs, finding that short chain polymers (PEO M_w = 400 g mol^{-1}) were less effective in eliminating defect emission, whilst larger chains (PEO M_w = 20,000 g mol^{-1}) were thought to block charge transfer; consequently, PEO M_w = 6,000 g mol^{-1} was found to be the most effective species, with a composite containing a weight fraction of 5 % PEO yielding roughly a 10 % improvement in *IQE*, reflected in significant improvements in *FF* (0.35 to 0.51) and J_{sc} (6.27 mA cm^{-2} to 8.19 mA cm^{-2}). Additionally, the *PCE* reductions on increasing the active device area from 4 mm^2 to 12 mm^2 were much less pronounced for the modified ETLs (a reduction of 33 %, compared with 57 % for pristine ZnO). Shao *et al.* also modified ZnO NP layers: in this study, much heavier PEO was used (M_w = 100,000 g mol^{-1})

with a much lower composite weight fraction, 0.05 %. Despite the weight of the modifying polymer (which could have been a hindrance to charge transfer), the resulting devices exhibited substantially reduced defect emission in photoluminescence measurements and measured to provide both a higher J_{sc} (8.69 mA cm^{-2} to 9.60 mA cm^{-2}) and greatly reduced R_s (22 $\Omega \cdot cm^2$ down to 8.1 $\Omega \cdot cm^2$).[223] The study by Kyaw into ZnO/PEIE bilayers (~10 nm layer of PEIE on ZnO) likewise suggested that the polymer modification greatly reduced the degree of trap-assisted recombination, consistent with the observation that these species passivate ZnO defects.[219]

Amphiphilic conjugated polyelectrolytes (CPEs) are extremely well suited to modification of metal oxide–organic interfaces. CPEs feature an organic backbone with ionic sidegroups which may interact favourably with the ZnO surface. Xie *et al.* tested three different CPE species on P3HT:PCBM-based OPVs with ZnO ETLs: anionic poly[(3-(4'-sulfonatobutyl)oxymethyl-2,5-thiophene)-alt-2,5-thiophene] sodium, PTSO-Na; neutral HT-(poly[3-(6'-diethanolamino)-hexylthiophene]), PTNOH; and cationic HT-poly[3-(6'-N,N,N-trimethylammonium)-hexylthiophene, PTN-Br,[224] all presented in **Figure 15**. Thin layers (6–8 nm) of each of these CPEs improved device performance in the order PTSO-Na < PTNOH < PTN-Br, predominantly through increases in J_{sc} (10.2 mA cm^{-2} to 11.5 mA cm^{-2} for PTN-Br) and a ~10 % increase in *FF*. In terms of the surface electronic properties, modification was observed to induce a shift in the ZnO CB towards vacuum, the biggest shift being recorded for PTN-Br (from –4.40 eV to –3.93 eV) which was interpreted as the formation of a dipole pointing away from the oxide. Due to the less favourable interaction of the anionic PTSO-Na with ZnO, this modifier was observed to exhibit a substantial degree of disorder on the oxide surface, in contrast with the more ordered PTNOH and PTN-Br. Subsequent AFM phase measurements suggested that the latter two modifiers reduced the degree of active layer phase separation between polymer and fullerene. All modifiers, including PTSO-Na, were shown to improve device performance with PTN-Br yielding the most efficient cells (*PCE* 4.08 %, *cf.* 2.99 % for the unmodified ETL). Further increases in device performance were achieved with a 20 minute UV–ozone treatment, thought to improve electrostatic interaction

between ZnO surface O and the N^+ cations on the CPE through generation of O^{2-} species (whilst also partially degrading some of the CPE, as evidenced by the reduced C 1*s* signal in XPS measurements). For PTN-Br, this processing step further raised the *PCE* from 4.05 % to 4.45 %, predominantly accounted for by improvements in *FF* (0.57 to 0.61). Yang *et al.* found similar device improvements for modification of ETLs with a ~5 nm layer of poly[(9,9-bis(3'-((N,N -dimethyl)-N-ethylammonium)-propyl)-2,7-fluorene)-*alt*-2,7-(9,9-dioctylfluorene)], PFN-Br, in PBDT-DTNT:$PC_{71}BM$ OPVs with gains in V_{oc} (8.5 %), J_{sc} (14 %), *FF* (11 %), leading to an overall *PCE* increase from 6.1 % to 8.4 % (~38 % gain).[225] Other CPEs tested include PDADMAC (poly(diallyldimethylammonium chloride) and PTMAHT (poly(3-(6-trimethylammoniumhexyl)thiophene).[226,227]

5 Conclusions

Whilst ZnO has attracted substantial interest as an n-type semiconductor in numerous optoelectronic platforms it is apparent that the surface electronic properties are highly sensitive to processing conditions and post-deposition treatments owing to the rich defect chemistry that exists in this material. Recently there has been a tremendous activity focussed on regulating, stabilising and tuning this surface to ensure continued device improvement and surface stabilisation. Through experimental and theoretical investigations it has become apparent that the influence of defects and surface states can significantly influence the inherent electronic properties of ZnO and consequently how the heterointerface between ZnO and other active materials in devices is impacted. Consequently, surface and interfacial modification of ZnO using both organic and inorganic species has been investigated not only to improve device performance characteristics but to fundamentally study the surface properties of this fascinating material. In particular, efforts to improve the energetic alignment and charge transfer between ZnO and organic/molecular semiconductors have intensified in recent years. The smorgasbord of materials systems investigated to achieve these goals and their impact on modifying and regulating electronic properties highlight the importance of

such steps in the long-term implementation of ZnO in optoelectronic platforms and emphasise the toolbox of materials that can be accessed to give tailored properties.

Acknowledgements

The authors gratefully acknowledge J.C.D. Faria for the SEM image in Figure 2 (b) and for numerous fruitful discussions; Dr N. Treat and Dr C. Small obtaining the PV device data in Figure 4 (b); and to Dr C. McGilvery and C. Burgess for imaging and preparation of the micrograph in Figure 7 (a).

Received: ((will be filled in by the editorial staff))
Revised: ((will be filled in by the editorial staff))
Published online: ((will be filled in by the editorial staff))

References

[1] J. Huang, Z. Yin, Q. Zheng, *Energy Environ. Sci.* **2011**, *4*, 3861.

[2] W. J. E. Beek, M. M. Wienk, R. A. J. Janssen, *Adv. Funct. Mater.* **2006**, *16*, 1112.

[3] T.-H. Lai, S.-W. Tsang, J. R. Manders, S. Chen, F. So, *Mater. Today* **2013**, *16*, 424.

[4] M. J. Tan, S. Zhong, J. Li, Z. Chen, W. Chen, *ACS Appl. Mater. Interfaces* **2013**, *5*, 4696.

[5] Q. Zhang, C. S. Dandeneau, X. Zhou, G. Cao, *Adv. Mater.* **2009**, *21*, 4087.

[6] C.-Y. Lin, Y.-H. Lai, H.-W. Chen, J.-G. Chen, C.-W. Kung, R. Vittal, K.-C. Ho, *Energy Environ. Sci.* **2011**, *4*, 3448.

[7] M. Sessolo, H. J. Bolink, *Adv. Mater.* **2011**, *23*, 1829.

[8] J. C. D. Faria, A. J. Campbell, M. A. McLachlan, *Adv. Funct. Mater.* **2015**, DOI 10.1002/adfm.201501411.

[9] E. Fortunato, P. Barquinha, A. Pimentel, A. Gon{\c c}alves, A. Marques, L. Pereira, R. Martins, *Thin Solid Films* **2005**, *487*, 205.

[10] A. Bashir, P. H. Wobkenberg, J. Smith, J. M. Ball, G. Adamopoulos, D. D. C. Bradley, T. D. Anthopoulos, *Adv. Mater.* **2009**, *21*, 2226.

[11] G. Adamopoulos, S. Thomas, D. D. C. Bradley, M. A. McLachlan, T. D. Anthopoulos, *Appl. Phys. Lett.* **2011**, *98*, 3503.

[12] U. Özgür, Y. I. Alivov, C. Liu, A. Teke, M. A. Reshchikov, S. Doğan, V. Avrutin, S.-J. Cho, H. Morkoç, *J. Appl. Phys.* **2005**, *98*, 1301.

[13] A. Janotti, C. G. Van de Walle, *Reports Prog. Phys.* **2009**, *72*, 6501.

[14] E. A. Meulenkamp, *J. Phys. Chem. B* **1998**, *102*, 5566.

[15] M. Monge, M. L. Kahn, A. Maisonnat, B. Chaudret, *Angew. Chemie Int. Ed.* **2003**, *42*, 5321.

[16] I. Gonzalez-Valls, M. Lira-Cantu, *Energy Environ. Sci.* **2009**, *2*, 19.

[17] J. M. Downing, M. P. Ryan, M. A. McLachlan, Thin Solid Films 2013, 539, 18.

[18] P. D. Yang, H. Q. Yan, S. Mao, R. Russo, J. Johnson, R. Saykally, N. Morris, J. Pham, R. R. He, H. J. Choi, *Adv. Funct. Mater.* **2002**, *12*, 323.

[19] T. Sumida, Y. Wada, T. Kitamura, S. Yanagida, *Chem. Lett.* **2001**, 38.

[20] B. N. Illy, A. C. Cruickshank, S. Schumann, R. Da Campo, T. S. Jones, S. Heutz, M. a. McLachlan, D. W. McComb, D. J. Riley, M. P. Ryan, *J. Mater. Chem.* **2011**, *21*, 12949.

[21] Y. Yang, H. Yan, Z. Fu, B. Yang, J. Zuo, S. Fu, *Solid State Commun.* **2006**, *139*, 218.

[22] Y. Tong, Y. Liu, C. Shao, Y. Liu, C. Xu, J. Zhang, Y. Lu, D. Shen, X. Fan, *J. Phys. Chem. B* **2006**, *110*, 14714.

[23] P. X. Gao, Y. Ding, W. J. Mai, W. L. Hughes, C. S. Lao, Z. L. Wang, *Science (80-.).* **2005**, *309*, 1700.

[24] J. K. Park, Y. J. Kim, J. Yeom, J. H. Jeon, G. C. Yi, J. H. Je, S. K. Hahn, *Adv. Mater.* **2010**, *22*, 4857.

[25] C. Y. Jiang, X. W. Sun, G. Q. Lo, D. L. Kwong, J. X. Wang, *Appl. Phys. Lett.* **2007**, *90*, 263501.

[26] Y. Qiu, S. Yang, *Adv. Funct. Mater.* **2007**, *17*, 1345.

[27] M. C. Newton, S. Firth, T. Matsuura, P. A. Warburton, *Emag-Nano 2005 Imaging, Anal. Fabr. Nanoscale* **2006**, *26*, 251.

[28] T. Taniguchi, K. Yamaguchi, A. Shigeta, Y. Matsuda, S. Hayami, T. Shimizu, T. Matsui, T. Yamazaki, A. Funatstu, Y. Makinose, N. Matsushita, M. Koinuma, Y. Matsumoto, *Adv. Funct. Mater.* **2013**, *23*, 3140.

[29] Y. Y. Lin, C. W. Chen, T. H. Chu, W. F. Su, C. C. Lin, C. H. Ku, J. J. Wu, C. H. Chen, *J. Mater. Chem.* **2007**, *17*, 4571.

[30] G. Eranna, B. C. Joshi, D. P. Runthala, R. P. Gupta, *Crit. Rev. Solid State Mater. Sci.* **2004**, *29*, 111.

[31] V. E. Ferry, A. Polman, H. A. Atwater, *ACS Nano* **2011**, *5*, 10055.

[32] C.-P. Liu, J. Xin, L. Wang, J. Song, A. Y. S. Lee, P. Ho, *RSC Adv.* **2014**, *4*, 34669.

[33] J. Weickert, R. B. Dunbar, H. C. Hesse, W. Wiedemann, L. Schmidt-Mende, *Adv. Mater.* **2011**, *23*, 1810.

[34] D. C. Look, D. C. Reynolds, J. R. Sizelove, R. L. Jones, C. W. Litton, G. Cantwell, W. C. Harsch, *Solid State Commun.* **1998**, *105*, 399.

[35] A. Kohan, G. Ceder, D. Morgan, C. Van de Walle, *Phys. Rev. B* **2000**, *61*, 15019.

[36] A. Janotti, C. G. Van de Walle, *Phys. Rev. B* **2007**, *76*, 5202.

[37] C. G. Van de Walle, *Phys. Rev. Lett.* **2000**, *85*, 1012.

[38] D. C. Look, G. C. Farlow, P. Reunchan, S. Limpijumnong, S. B. Zhang, K. Nordlund, *Phys. Rev. Lett.* **2005**, *95*, 5502.

[39] J. Koßmann, C. Hättig, *Phys. Chem. Chem. Phys.* **2012**, *14*, 16392.

[40] C. Wöll, *Prog. Surf. Sci.* **2007**, *82*, 55.

[41] S. Torbrügge, F. Ostendorf, M. Reichling, *J. Phys. Chem. C* **2009**, *113*, 4909.

[42] R. Heinhold, G. T. Williams, S. P. Cooil, D. A. Evans, M. W. Allen, *Phys. Rev. B* **2013**, *88*, 235315.

[43] M. Losurdo, M. M. Giangregorio, *Appl. Phys. Lett.* **2005**, *86*, 091901.

[44] S. Hövel, C. Kolczewski, M. Wühn, J. Albers, K. Weiss, V. Staemmler, C. Wöll, *J. Chem. Phys.* **2000**, *112*, 3909.

[45] J. H. Lee, J.-H. Shin, J. Y. Song, W. Wang, R. Schlaf, K. J. Kim, Y. Yi, *J. Phys. Chem. C* **2012**, *116*, 26342.

[46] M. W. Allen, C. H. Swartz, T. H. Myers, T. D. Veal, C. F. McConville, S. M. Durbin, *Phys. Rev. B* **2010**, *81*, 5211.

[47] C. H. Swartz, *J. Mater. Res.* **2012**, *27*, 2205.

[48] B. J. Coppa, *J. Appl. Phys.* **2004**, *95*, 5856.

[49] K. Ozawa, K. Mase, *Phys. Rev. B* **2011**, *83*, 125406.

[50] M. Ali, M. Winterer, *Chem. Mater.* **2010**, *22*, 85.

[51] M. Kunat, S. Gil Girol, T. Becker, U. Burghaus, C. Wöll, *Phys. Rev. B* **2002**, *66*, 081402.

[52] D. C. Look, H. L. Mosbacker, Y. M. Strzhemechny, L. J. Brillson, *Superlattices Microstruct.* **2005**, *38*, 406.

[53] O. Schmidt, P. Kiesel, C. G. Van de Walle, N. M. Johnson, J. Nause, G. H. Döhler, *Jpn. J. Appl. Phys.* **2005**, *44*, 7271.

[54] H. Li, L. K. Schirra, J. Shim, H. Cheun, B. Kippelen, O. L. A. Monti, J.-L. Bredas, *Chem. Mater.* **2012**, *24*, 3044.

[55] H. Noei, H. Qiu, Y. Wang, E. Löffler, C. Wöll, M. Muhler, *Phys. Chem. Chem. Phys.* **2008**, *10*, 7092.

[56] P. Schulz, L. L. Kelly, P. Winget, H. Li, H. Kim, P. F. Ndione, A. K. Sigdel, J. J. Berry, S. Graham, J.-L. Brédas, A. Kahn, O. L. A. Monti, *Adv. Funct. Mater.* **2014**, *24*, 7381.

[57] H. Ma, H.-L. Yip, F. Huang, A. K.-Y. Jen, *Adv. Funct. Mater.* **2010**, *20*, 1371.

[58] R.-D. Sun, A. Nakajima, A. Fujishima, T. Watanabe, K. Hashimoto, *J. Phys. Chem. B* **2001**, *105*, 1984.

[59] S. Oh, T. Nagata, J. Volk, Y. Wakayama, *J. Appl. Phys.* **2013**, *113*, 083708.

[60] T. Makino, Y. Segawa, M. Kawasaki, A. Ohtomo, R. Shiroki, K. Tamura, T. Yasuda, H. Koinuma, *Appl. Phys. Lett.* **2001**, *78*, 1237.

[61] H. Ishizakiz, N. Yamada, *Electrochem. Solid State Lett.* **2006**, *9*, C178.

[62] D. Zhao, X. Zhang, H. Dong, L. Yang, Q. Zeng, J. Li, L. Cai, P. Luan, Q. Zhang, M. Tu, S. Wang, W. Zhou, S. Xie, *Nanoscale* **2013**, *5*, 4443.

[63] L. E. Greene, M. Law, B. D. Yuhas, P. Yang, *J. Phys. Chem. C* **2007**, *111*, 18451.

[64] N. O. V Plank, I. Howard, A. Rao, M. W. B. Wilson, C. Ducati, R. S. Mane, J. S. Bendall, R. R. M. Louca, N. C. Greenham, H. Miura, R. H. Friend, H. J. Snaith, M. E. Welland, *J. Phys. Chem. C* **2009**, *113*, 18515.

[65] H. Fujisawa, Y. Iwamoto, S. Nakashima, M. Shimizu, in *2012 Fifth Int. Conf. Emerg. Trends Eng. Technol.*, IEEE, **2012**, pp. 57–60.

[66] C.-Y. Hsieh, M.-L. Lu, J.-Y. Chen, Y.-T. Chen, Y.-F. Chen, W. Y. Shih, W.-H. Shih, *Nanotechnology* **2012**, *23*, 5201.

[67] K. Kim, D. C. Lim, J. Hu, J. Kwon, M.-G. Jeong, H. O. Seo, J. Y. Lee, K.-Y. Jang, J. Lim, K. H. Lee, Y. Jeong, Y. D. Kim, S. Cho, *ACS Appl. Mater. Interfaces* **2013**, *5*, 8718.

[68] K. Keis, J. Lindgren, S.-E. Lindquist, A. Hagfeldt, *Langmuir* **2000**, *16*, 4688.

[69] B. Zhang, T. Kong, W. Xu, R. Su, Y. Gao, G. Cheng, *Langmuir* **2010**, *26*, 4514.

[70] N. S. Norberg, D. R. Gamelin, *J. Phys. Chem. B* **2005**, *109*, 20810.

[71] K. Ogata, T. Hama, K. Hama, K. Koike, S. Sasa, M. Inoue, M. Yano, *Appl. Surf. Sci.* **2005**, *241*, 146.

[72] P. W. Sadik, S. J. Pearton, D. P. Norton, E. Lambers, F. Ren, *J. Appl. Phys.* **2007**, *101*, 104514.

[73] N. H. Moreira, A. Domıinguez, T. Frauenheim, A. L. da Rosa, *Phys. Chem. Chem. Phys.* **2012**, *14*, 15445.

[74] M. Niskanen, M. Kuisma, O. Cramariuc, V. Golovanov, T. I. Hukka, N. Tkachenko, T. T. Rantala, *Phys. Chem. Chem. Phys.* **2013**, *15*, 17408.

[75] L. Shi, A. J. T. Naik, J. B. M. Goodall, C. Tighe, R. Gruar, R. Binions, I. Parkin, J. Darr, *Langmuir* **2013**, *29*, 10603.

[76] S. Akhter, K. Lui, H. H. Kung, *J. Phys. Chem.* **1985**, *89*, 1958.

[77] O. Taratula, E. Galoppini, D. Wang, D. Chu, Z. Zhang, H. Chen, G. Saraf, Y. Lu, *J. Phys. Chem. B* **2006**, *110*, 6506.

[78] C. L. Perkins, *J. Phys. Chem. C* **2009**, *113*, 18276.

[79] C. L. Rhodes, S. Lappi, D. Fischer, S. Sambasivan, J. Genzer, S. Franzen, *Langmuir* **2008**, *24*, 433.

[80] X. Tian, J. Xu, W. Xie, *J. Phys. Chem. C* **2010**, *114*, 3973.

[81] D. Cornil, T. Van Regemorter, D. Beljonne, J. Cornil, *Phys. Chem. Chem. Phys.* **2014**, *16*, 20887.

[82] N. H. Moreira, A. L. da Rosa, T. Frauenheim, *Appl. Phys. Lett.* **2009**, *94*, 193109.

[83] H. Kung, A. Teplyakov, *J. Phys. Condens. Matter* **2015**, *27*, 054007.

[84] A. Bulusu, S. A. Paniagua, B. A. MacLeod, A. K. Sigdel, J. J. Berry, D. C. Olson, S. R. Marder, S. Graham, *Langmuir* **2013**, *29*, 3935.

[85] I. Lange, S. Reiter, M. Pätzel, A. Zykov, A. Nefedov, J. Hildebrandt, S. Hecht, S. Kowarik, C. Wöll, G. Heimel, D. Neher, *Adv. Funct. Mater.* **2014**, *24*, 7014.

[86] C. Wood, H. Li, P. Winget, J.-L. Brédas, *J. Phys. Chem. C* **2012**, *116*, 19125.

[87] M. Timpel, M. V. Nardi, S. Krause, G. Ligorio, C. Christodoulou, L. Pasquali, A. Giglia, J. Frisch, B. Wegner, P. Moras, N. Koch, *Chem. Mater.* **2014**, *26*, 5042.

[88] Y. Zhou, C. Fuentes-Hernandez, J. Shim, J. Meyer, A. J. Giordano, H. Li, P. Winget, T. Papadopoulos, H. Cheun, J. Kim, M. Fenoll, A. Dindar, W. Haske, E. Najafabadi, T. M. Khan, H. Sojoudi, S. Barlow, S. Graham, J.-L. Brédas, S. R. Marder, A. Kahn, B. Kippelen, *Science (80-.).* **2012**, *336*, 327.

[89] H. Li, P. Winget, J.-L. Brédas, *Chem. Mater.* **2014**, *26*, 631.

[90] A. Dominguez, M. Lorke, A. L. Schoenhalz, A. L. Rosa, T. Frauenheim, A. R. Rocha, G. M. Dalpian, *J. Appl. Phys.* **2014**, *115*, 203720.

[91] T. Le Bahers, T. Pauporté, F. Labat, G. Lefèvre, I. Ciofini, *Langmuir* **2011**, *27*, 3442.

[92] J. W. Soares, J. E. Whitten, D. W. Oblas, D. M. Steeves, *Langmuir* **2008**, *24*, 371.

[93] D. J. Baker, C. G. Allen, T. D. Berman, M. R. Bergren, J. M. Albin, D. C. Olson, E. C. Przekwas, M. S. White, D. S. Ginley, R. T. Collins, T. E. Furtak, *Phys. Technol. Org. Semicond. Devices* **2010**, *1115*, 143.

[94] T. M. Brenner, G. Chen, E. P. Meinig, D. J. Baker, D. C. Olson, R. T. Collins, T. E. Furtak, *J. Mater. Chem. C* **2013**, *1*, 5935.

[95] M. T. Greiner, M. G. Helander, W.-M. Tang, Z.-B. Wang, J. Qiu, Z.-H. Lu, *Nat. Mater.* **2011**, *11*, 76.

[96] H. Li, P. Paramonov, J.-L. Bredas, *J. Mater. Chem.* **2010**, *20*, 2630.

[97] H. Li, E. L. Ratcliff, A. K. Sigdel, A. J. Giordano, S. R. Marder, J. J. Berry, J.-L. Brédas, *Adv. Funct. Mater.* **2014**, *24*, 3593.

[98] O. T. Hofmann, J.-C. Deinert, Y. Xu, P. Rinke, J. Stähler, M. Wolf, M. Scheffler, *J. Chem. Phys.* **2013**, *139*, 174701.

[99] P. Winget, L. K. Schirra, D. Cornil, H. Li, V. Coropceanu, P. F. Ndione, A. K. Sigdel, D. S. Ginley, J. J. Berry, J. Shim, H. Kim, B. Kippelen, J.-L. Brédas, O. L. A. Monti, *Adv. Mater.* **2014**, *26*, 4711.

[100] R. Schlesinger, Y. Xu, O. T. Hofmann, S. Winkler, J. Frisch, J. Niederhausen, A. Vollmer, S. Blumstengel, F. Henneberger, P. Rinke, M. Scheffler, N. Koch, *Phys. Rev. B* **2013**, *87*, 5311.

[101] Y. Xu, O. T. Hofmann, R. Schlesinger, S. Winkler, J. Frisch, J. Niederhausen, A. Vollmer, S. Blumstengel, F. Henneberger, N. Koch, P. Rinke, M. Scheffler, *Phys. Rev. Lett.* **2013**, *111*, 6802.

[102] N. Kedem, S. Blumstengel, F. Henneberger, H. Cohen, G. Hodes, D. Cahen, *Phys. Chem. Chem. Phys.* **2014**, *16*, 8310.

[103] B. R. Lee, E. D. Jung, J. S. Park, Y. S. Nam, S. H. Min, B.-S. Kim, K.-M. Lee, J.-R. Jeong, R. H. Friend, J.-S. Kim, S. O. Kim, M. H. Song, *Nat. Commun.* **2014**, *5*, 4840.

[104] S. Höfle, A. Schienle, M. Bruns, U. Lemmer, A. Colsmann, *Adv. Mater.* **2014**, *26*, 2750.

[105] D. Kälblein, H. Ryu, F. Ante, B. Fenk, K. Hahn, K. Kern, H. Klauk, *ACS Nano* **2014**, *8*, 6840.

[106] P. E. Shaw, A. Ruseckas, I. D. W. Samuel, *Adv. Mater.* **2008**, *20*, 3516.

[107] N. Greenham, X. Peng, A. Alivisatos, *Phys. Rev. B* **1996**, *54*, 17628.

[108] D. Ginger, N. Greenham, *Phys. Rev. B* **1999**, *59*, 10622.

[109] W. U. Huynh, J. J. Dittmer, A. P. Alivisatos, *Science (80-.).* **2002**, *295*, 2425.

[110] S. Dayal, N. Kopidakis, D. C. Olson, D. S. Ginley, G. Rumbles, *Nano Lett.* **2010**, *10*, 239.

[111] D. Verma, A. Ranga Rao, V. Dutta, *Sol. Energy Mater. Sol. Cells* **2009**, *93*, 1482.

[112] S. Günes, K. P. Fritz, H. Neugebauer, N. S. Sariciftci, S. Kumar, G. D. Scholes, *Sol. Energy Mater. Sol. Cells* **2007**, *91*, 420.

[113] E. Arici, N. S. Sariciftci, D. Meissner, *Adv. Funct. Mater.* **2003**, *13*, 165.

[114] M. S. White, D. C. Olson, S. E. Shaheen, N. Kopidakis, D. S. Ginley, *Appl. Phys. Lett.* **2006**, *89*, 3517.

[115] S. K. Hau, H.-L. Yip, N. S. Baek, J. Zou, K. O'Malley, A. K.-Y. Jen, *Appl. Phys. Lett.* **2008**, *92*, 3301.

[116] S. Sanchez, S. Berson, S. Guillerez, C. Lévy-Clément, V. Ivanova, *Adv. Energy Mater.* **2012**, *2*, 541.

[117] Y.-H. Sung, W.-P. Liao, D.-W. Chen, C.-T. Wu, G.-J. Chang, J.-J. Wu, *Adv. Funct. Mater.* **2012**, *22*, 3808.

[118] S. D. Oosterhout, M. M. Wienk, S. S. van Bavel, R. Thiedmann, L. Jan Anton Koster, J. Gilot, J. Loos, V. Schmidt, R. A. J. Janssen, *Nat. Mater.* **2009**, *8*, 818.

[119] M. T. Dang, L. Hirsch, G. Wantz, *Adv. Mater.* **2011**, *23*, 3597.

[120] K. Noori, F. Giustino, *Adv. Funct. Mater.* **2012**, *22*, 5089.

[121] T. Nagata, S. Oh, Y. Yamashita, H. Yoshikawa, R. Hayakawa, K. Kobayashi, T. Chikyow, Y. Wakayama, *Appl. Phys. Lett.* **2012**, *101*, 173303.

[122] P. Tiwana, P. Docampo, M. B. Johnston, H. J. Snaith, L. M. Herz, *ACS Nano* **2011**, *5*, 5158.

[123] A. Furube, R. Katoh, T. Yoshihara, K. Hara, S. Murata, H. Arakawa, M. Tachiya, *J. Phys. Chem. B* **2004**, *108*, 12583.

[124] J. Piris, N. Kopidakis, D. C. Olson, S. E. Shaheen, D. S. Ginley, G. Rumbles, *Adv. Funct. Mater.* **2007**, *17*, 3849.

[125] T. M. Clarke, J. R. Durrant, *Chem. Rev.* **2010**, *110*, 6736.

[126] Y. Vaynzof, A. A. Bakulin, S. Gélinas, R. H. Friend, *Phys. Rev. Lett.* **2012**, *108*, 6605.

[127] G. Wu, Z. Li, X. Zhang, G. Lu, *J. Phys. Chem. Lett.* **2014**, *5*, 2649.

[128] J. Weickert, F. Auras, T. Bein, L. Schmidt-Mende, *J. Phys. Chem. C* **2011**, *115*, 15081.

[129] C. P. Liu, H. E. Wang, T. W. Ng, Z. H. Chen, W. F. Zhang, C. Yan, Y. B. Tang, I. Bello, L. Martinu, W. J. Zhang, S. K. Jha, *Phys. status solidi* **2011**, n/a.

[130] G. V. Rao, F. Säuberlich, A. Klein, *Appl. Phys. Lett.* **2005**, *87*, 2101.

[131] M. Wang, J.-P. Sun, S. Suei, I. G. Hill, *J. Appl. Phys.* **2012**, *112*, 044511.

[132] D. C. Olson, S. E. Shaheen, M. S. White, W. J. Mitchell, M. F. A. M. van Hest, R. T. Collins, D. S. Ginley, *Adv. Funct. Mater.* **2007**, *17*, 264.

[133] B. A. MacLeod, P. Schulz, S. R. Cowan, A. Garcia, D. S. Ginley, A. Kahn, D. C. Olson, *Adv. Energy Mater.* **2014**, *4*, 1400073.

[134] M. D. McCluskey, S. J. Jokela, *J. Appl. Phys.* **2009**, *106*, 071101.

[135] M. T. Lloyd, Y.-J. Lee, R. J. Davis, E. Fang, R. M. Fleming, J. W. P. Hsu, R. J. Kline, M. F. Toney, *J. Phys. Chem. C* **2009**, *113*, 17608.

[136] P. Ruankham, T. Sagawa, H. Sakaguchi, S. Yoshikawa, *J. Mater. Chem.* **2011**, *21*, 9710.

[137] R. T. Ginting, C. C. Yap, M. Yahaya, M. M. Salleh, *ACS Appl. Mater. Interfaces* **2014**, *6*, 5308.

[138] O. Pachoumi, A. A. Bakulin, A. Sadhanala, H. Sirringhaus, R. H. Friend, Y. Vaynzof, *J. Phys. Chem. C* **2014**, *118*, 18945.

[139] D. C. Olson, Y. J. Lee, M. S. White, N. Kopidakis, S. E. Shaheen, D. S. Ginley, J. A. Voigt, J. W. P. Hsu, *J. Phys. Chem. C* **2008**, *112*, 9544.

[140] J. J. Uhlrich, D. C. Olson, J. W. P. Hsu, T. F. Kuech, *J. Vac. Sci. Technol. A* **2009**, *27*, 328.

[141] K. P. Musselman, S. Albert-Seifried, R. L. Z. Hoye, A. Sadhanala, D. Munoz-Rojas, J. L. MacManus-Driscoll, R. H. Friend, *Adv. Funct. Mater.* **2014**, *24*, 3562.

[142] M. S. White, D. C. Olson, N. Kopidakis, A. M. Nardes, D. S. Ginley, J. J. Berry, *Phys. Status Solidi a* **2010**, *207*, 1257.

[143] Y.-J. Lee, R. J. Davis, M. T. Lloyd, P. P. Provencio, R. P. Prasankumar, J. W. P. Hsu, *IEEE J. Sel. Top. Quantum Electron.* **2010**, *16*, 1587.

[144] P. Atienzar, T. Ishwara, B. N. Illy, M. P. Ryan, B. C. O'Regan, J. R. Durrant, J. Nelson, *J. Phys. Chem. Lett.* **2010**, *1*, 708.

[145] E. D. Spoerke, M. T. Lloyd, E. M. McCready, D. C. Olson, Y.-J. Lee, J. W. P. Hsu, *Appl. Phys. Lett.* **2009**, *95*, 3506.

[146] R. M. Hewlett, Solution-Processed Lead Zirconate Titanate As An Interfacial Modifier in Hybrid Oxide/Polymer Solar Cells, Imperial College London, **2015**.

[147] W. J. E. Beek, M. M. Wienk, M. Kemerink, X. N. Yang, R. A. J. Janssen, *J. Phys. Chem. B* **2005**, *109*, 9505.

[148] C. Goh, S. R. Scully, M. D. McGehee, *J. Appl. Phys.* **2007**, *101*, 114503.

[149] P. Ruankham, S. Yoshikawa, T. Sagawa, *Mater. Chem. Phys.* **2013**, *141*, 278.

[150] S. Pradhan, S. Karak, A. Dhar, *J. Phys. D. Appl. Phys.* **2012**, *45*, 235104.

[151] B. Song, C. Rolin, J. D. Zimmerman, S. R. Forrest, *Adv. Mater.* **2014**, *26*, 2914.

[152] P. Peumans, A. Yakimov, S. R. Forrest, *J. Appl. Phys.* **2003**, *93*, 3693.

[153] S. Chang, H. Park, J. J. Cheng, P. H. Rekemeyer, S. Gradečak, *J. Phys. D. Appl. Phys.* **2014**, *47*, 394016.

[154] P. Ravirajan, A. M. Peiro, M. K. Nazeeruddin, M. Graetzel, D. D. C. Bradley, J. R. Durrant, J. Nelson, *J. Phys. Chem. B* **2006**, *110*, 7635.

[155] S. Sista, Y. Yao, Y. Yang, M. L. Tang, Z. Bao, *Appl. Phys. Lett.* **2007**, *91*, 223508.

[156] A. Barito, M. E. Sykes, B. Huang, D. Bilby, B. Frieberg, J. Kim, P. F. Green, M. Shtein, *Adv. Energy Mater.* **2014**, *4*, 1400216.

[157] Y. Y. Lin, Y. Y. Lee, L. W. Chang, J. J. Wu, C. W. Chen, *Appl. Phys. Lett.* **2009**, *94*, 3308.

[158] P. Peumans, S. R. Forrest, *Appl. Phys. Lett.* **2001**, *79*, 126.

[159] G. D. Sharma, R. Kumar, S. K. Sharma, M. S. Roy, *Sol. Energy Mater. Sol. Cells* **2006**, *90*, 933.

[160] G. Mattioli, S. Ben Dkhil, M. I. Saba, G. Malloci, C. Melis, P. Alippi, F. Filippone, P. Giannozzi, A. K. Thakur, M. Gaceur, O. Margeat, A. K. Diallo, C. Videlot-Ackermann, J. Ackermann, A. A. Bonapasta, A. Mattoni, *Adv. Energy Mater.* **2014**, *4*, n/a.

[161] S. Ito, H. Miura, S. Uchida, M. Takata, K. Sumioka, P. Liska, P. Comte, P. Pechy, M. Grätzel, *Chem. Commun.* **2008**, 5194.

[162] L. Hu, Z. Yan, H. Xu, *RSC Adv.* **2013**, *3*, 7667.

[163] D.-W. Chen, T.-C. Wang, W.-P. Liao, J.-J. Wu, *ACS Appl. Mater. Interfaces* **2013**, *5*, 8359.

[164] P. Ruankham, S. Yoshikawa, T. Sagawa, *Phys. Chem. Chem. Phys.* **2013**, *15*, 9516.

[165] C.-T. Wu, J.-J. Wu, *J. Mater. Chem.* **2011**, *21*, 13605.

[166] P. Ruankham, S. Yoshikawa, T. Sagawa, *Jpn. J. Appl. Phys.* **2014**, *53*, 01AB14.

[167] T. C. Monson, M. T. Lloyd, D. C. Olson, Y.-J. Lee, J. W. P. Hsu, *Adv. Mater.* **2008**, *20*, 4755.

[168] M. T. Lloyd, R. P. Prasankumar, M. B. Sinclair, A. C. Mayer, D. C. Olson, J. W. P. Hsu, *J. Mater. Chem.* **2009**, *19*, 4609.

[169] Y. Vaynzof, D. Kabra, L. Zhao, P. K. H. Ho, A. T.-S. Wee, R. H. Friend, *Appl. Phys. Lett.* **2010**, *97*, 3309.

[170] P. Zhong, W. Que, Y. N. Liang, X. Yin, Y. Liao, L. B. Kong, X. Hu, *RSC Adv.* **2013**, *3*, 17904.

[171] J. Yu, T.-L. Shen, W.-H. Weng, Y.-C. Huang, C.-I. Huang, W.-F. Su, S.-P. Rwei, K.-C. Ho, L. Wang, *Adv. Energy Mater.* **2011**, *2*, 245.

[172] S. H. Eom, M.-J. Baek, H. Park, L. Yan, S. Liu, W. You, S.-H. Lee, *ACS Appl. Mater. Interfaces* **2014**, *6*, 803.

[173] S.-S. Li, C.-W. Chen, *J. Mater. Chem. A* **2013**, *1*, 10574.

[174] A. J. Moulé, L. Chang, C. Thambidurai, R. Vidu, P. Stroeve, *J. Mater. Chem.* **2012**, *22*, 2351.

[175] D. J. D. Moet, L. J. A. Koster, B. de Boer, P. W. M. Blom, *Chem. Mater.* **2007**, *19*, 5856.

[176] F. Li, W. Chen, K. Yuan, Y. Chen, *Org. Electron.* **2012**, *13*, 2757.

[177] X. Chen, L. Chen, Y. Chen, *RSC Adv.* **2014**, *4*, 3627.

[178] H. Sirringhaus, P. J. Brown, R. H. Friend, M. M. Nielsen, K. Bechgaard, B. M. W. Langeveld-Voss, A. J. H. Spiering, R. A. J. Janssen, E. W. Meijer, P. Herwig, D. M. de Leeuw, *Nature* **1999**, *401*, 685.

[179] K. Yao, L. Chen, Y. Chen, F. Li, P. Wang, *J. Phys. Chem. C* **2012**, *116*, 3486.

[180] Q. Shen, Y. Ogomi, S. K. Das, S. S. Pandey, K. Yoshino, K. Katayama, H. Momose, T. Toyoda, S. Hayase, *Phys. Chem. Chem. Phys.* **2013**, *15*, 14370.

[181] M. Zhong, D. Sheng, C. Li, S. Xu, X. Wei, *Sol. Energy Mater. Sol. Cells* **2014**, *121*, 22.

[182] E. Rezasoltani, M. Wang, I. G. Hill, C. Silva, *J. Appl. Phys.* **2014**, *116*, 074502.

[183] J. B. Franklin, J. M. Downing, F. Giuliani, M. P. Ryan, M. A. McLachlan, *Adv. Energy Mater.* **2012**, *2*, 528.

[184] S. B. Jo, J. H. Lee, M. Sim, M. Kim, J. H. Park, Y. S. Choi, Y. Kim, S.-G. Ihn, K. Cho, *Adv. Energy Mater.* **2011**, *1*, 690.

[185] C. J. Brabec, S. Gowrisanker, J. J. M. Halls, D. Laird, S. Jia, S. P. Williams, *Adv. Mater.* **2010**, *22*, 3839.

[186] A. Wagenpfahl, D. Rauh, M. Binder, C. Deibel, V. Dyakonov, *Phys. Rev. B* **2010**, *82*, 115306.

[187] A. Manor, E. A. Katz, T. Tromholt, F. C. Krebs, *Adv. Energy Mater.* **2011**, *1*, 836.

[188] A. Manor, E. A. Katz, T. Tromholt, F. C. Krebs, *Sol. Energy Mater. Sol. Cells* **2012**, *98*, 491.

[189] S. Wilken, J. Parisi, H. Borchert, *J. Phys. Chem. C* **2014**, *118*, 19672.

[190] S. R. Cowan, P. Schulz, A. J. Giordano, A. Garcia, B. A. MacLeod, S. R. Marder, A. Kahn, D. S. Ginley, E. L. Ratcliff, D. C. Olson, *Adv. Funct. Mater.* **2014**, *24*, 4671.

[191] A. Gadisa, Y. Liu, E. T. Samulski, R. Lopez, *Appl. Phys. Lett.* **2012**, *100*, 253903.

[192] T. Stubhan, H. Oh, L. Pinna, J. Krantz, I. Litzov, C. J. Brabec, *Org. Electron.* **2011**, *12*, 1539.

[193] T. Stubhan, I. Litzov, N. Li, M. Salinas, M. Steidl, G. Sauer, K. Forberich, G. J. Matt, M. Halik, C. J. Brabec, *J. Mater. Chem. A* **2013**, *1*, 6004.

[194] L. K. Jagadamma, M. Al-Senani, A. El-Labban, I. Gereige, G. O. Ngongang Ndjawa, J. C. D. Faria, T. Kim, K. Zhao, F. Cruciani, D. H. Anjum, M. a. McLachlan, P. M. Beaujuge, A. Amassian, *Adv. Energy Mater.* **2015**, *5*, 15000204.

[195] K.-S. Shin, K.-H. Lee, H. H. Lee, D. Choi, S.-W. Kim, *J. Phys. Chem. C* **2010**, *114*, 15782.

[196] K.-S. Shin, H.-J. Park, G. C. Yoon, S.-W. Jeong, B. Kumar, S.-W. Kim, *J. Phys. Chem. C* **2013**, *117*, 24692.

[197] A. Puetz, T. Stubhan, M. Reinhard, O. Loesch, E. Hammarberg, S. Wolf, C. Feldmann, H. Kalt, A. Colsmann, U. Lemmer, *Sol. Energy Mater. Sol. Cells* **2011**, *95*, 579.

[198] A. Savva, S. A. Choulis, *Appl. Phys. Lett.* **2013**, *102*, 233301.

[199] H. Woo Choi, K.-S. Lee, N. David Theodore, T. L. Alford, *Sol. Energy Mater. Sol. Cells* **2013**, *117*, 273.

[200] A. Gadisa, T. Hairfield, L. Alibabaei, C. L. Donley, E. T. Samulski, R. Lopez, *ACS Appl. Mater. Interfaces* **2013**, *5*, 8440.

[201] J.-L. Lan, S.-J. Cherng, Y.-H. Yang, Q. Zhang, S. Subramaniyan, F. S. Ohuchi, S. A. Jenekhe, G. Cao, *J. Mater. Chem. A* **2014**, *2*, 9361.

[202] J.-L. Lan, Z. Liang, Y.-H. Yang, F. S. Ohuchi, S. A. Jenekhe, G. Cao, *Nano Energy* **2014**, *4*, 140.

[203] T. Z. Oo, R. Devi Chandra, N. Yantara, R. R. Prabhakar, L. H. Wong, N. Mathews, S. G. Mhaisalkar, *Org. Electron.* **2012**, *13*, 870.

[204] H. L. Yip, S. K. Hau, N. S. Baek, H. Ma, A. K. Y. Jen, *Adv. Mater.* **2008**, *20*, 2376.

[205] H.-L. Yip, S. K. Hau, N. S. Baek, A. K.-Y. Jen, *Appl. Phys. Lett.* **2008**, *92*, 193313.

[206] A. Tada, Y. Geng, M. Nakamura, Q. Wei, K. Hashimoto, K. Tajima, *Phys. Chem. Chem. Phys.* **2012**, *14*, 3713.

[207] S. K. Hau, H.-L. Yip, H. Ma, A. K.-Y. Jen, *Appl. Phys. Lett.* **2008**, *93*, 3304.

[208] S. K. Hau, Y.-J. Cheng, H.-L. Yip, Y. Zhang, H. Ma, A. K.-Y. Jen, *ACS Appl. Mater. Interfaces* **2010**, *2*, 1892.

[209] S.-H. Liao, H.-J. Jhuo, Y.-S. Cheng, S.-A. Chen, *Adv. Mater.* **2013**, *25*, 4766.

[210] C.-H. Hsieh, Y.-J. Cheng, P.-J. Li, C.-H. Chen, M. Dubosc, R.-M. Liang, C.-S. Hsu, *J. Am. Chem. Soc.* **2010**, *132*, 4887.

[211] Y.-J. Cheng, C.-H. Hsieh, Y. He, C.-S. Hsu, Y. Li, *J. Am. Chem. Soc.* **2010**, *132*, 17381.

[212] X. Bulliard, S.-G. Ihn, S. Yun, Y. Kim, D. Choi, J.-Y. Choi, M. Kim, M. Sim, J.-H. Park, W. Choi, K. Cho, *Adv. Funct. Mater.* **2010**, *20*, 4381.

[213] J.-Y. Chen, F.-C. Hsu, Y.-M. Sung, Y.-F. Chen, *J. Mater. Chem.* **2012**, *22*, 15726.

[214] Y.-M. Sung, F.-C. Hsu, Y.-F. Chen, *Sol. Energy Mater. Sol. Cells* **2014**, *125*, 239.

[215] G. Wang, T. Jiu, G. Tang, J. Li, P. Li, X. Song, F. Lu, J. Fang, *ACS Sustain. Chem. Eng.* **2014**, *2*, 1331.

[216] Y.-J. Lee, J. Wang, S. R. Cheng, J. W. P. Hsu, *ACS Appl. Mater. Interfaces* **2013**, *5*, 9128.

[217] Y.-S. Cheng, S.-H. Liao, Y.-L. Li, S.-A. Chen, *ACS Appl. Mater. Interfaces* **2013**, *5*, 6665.

[218] R. Thitima, C. Patcharee, S. Takashi, Y. Susumu, *Solid. State. Electron.* **2009**, *53*, 176.

[219] A. K. K. Kyaw, D. H. Wang, V. Gupta, J. Zhang, S. Chand, G. C. Bazan, A. J. Heeger, *Adv. Mater.* **2013**, *25*, 2397.

[220] T. Hu, F. Li, K. Yuan, Y. Chen, *ACS Appl. Mater. Interfaces* **2013**, *5*, 5763.

[221] C. E. Small, S. Chen, J. Subbiah, C. M. Amb, S.-W. Tsang, T.-H. Lai, J. R. Reynolds, F. So, *Nat. Photonics* **2012**, *6*, 115.

[222] R. Lampande, G. W. Kim, R. Pode, J. H. Kwon, *RSC Adv.* **2014**, *4*, 49855.

[223] S. Shao, K. Zheng, T. Pullerits, F. Zhang, *ACS Appl. Mater. Interfaces* **2013**, *5*, 380.

[224] C. Xie, L. Chen, Y. Chen, *J. Phys. Chem. C* **2013**, *117*, 24804.

[225] T. Yang, M. Wang, C. Duan, X. Hu, L. Huang, J. Peng, F. Huang, X. Gong, *Energy Environ. Sci.* **2012**, *5*, 8208.

[226] J. P. Tiwari, S. Pillai, S. Parakh, F. Ali, A. Sharma, S. Chand, *Appl. Phys. Lett.* **2014**, *104*, 041114.

[227] Y.-M. Chang, C.-Y. Leu, *J. Mater. Chem. A* **2013**, *1*, 6446.

[228] K. Momma, F. Izumi, *J. Appl. Crystallogr.* **2011**, *44*, 1272.

[229] T. Yamashita, R. Hansson, P. C. Hayes, *J. Mater. Sci.* **2006**, *41*, 5559.

[230] H.-J. Yang, S.-C. Lim, S.-Y. He, H.-Y. Tuan, *RSC Adv.* **2015**, *5*, 33392.

[231] M. Wang, X. Hu, P. Liu, W. Li, X. Gong, F. Huang, Y. Cao, *J. Am. Chem. Soc.* **2011**, *133*, 9638.

[232] R. González-Moreno, P. L. Cook, I. Zegkinoglou, X. Liu, P. S. Johnson, W. Yang, R. E. Ruther, R. J. Hamers, R. Tena-Zaera, F. J. Himpsel, J. E. Ortega, C. Rogero, *J. Phys. Chem. C* **2011**, *115*, 18195.

Tables

Table 1. ZnO work functions from the study by Schulz *et al.*: for the experimentally measured values, polycrystalline ZnO films were grown by atomic layer deposition, and the post-treated films were sputtered using Ar^+; subsequently, work-function measurements were conducted using photoelectron spectroscopy. For the computational results, the ZnO surfaces were modelled by DFT, incorporating zinc interstitial (Zn_i), oxygen vacancy (V_O), or zinc vacancy (V_{Zn}) defects. Table adapted from [56] with permission.

ZnO Surface	Method	Work Function [eV]
As-deposited	Experimental	3.70
Soft-sputtered	Experimental	4.00
Hard-sputtered	Experimental	4.50
$(10\bar{1}0)$ Stoichiometric	Theory	4.58
$(10\bar{1}0)$ Zn_i	Theory[a)]	3.56
$(10\bar{1}0)$ V_O	Theory[a)]	4.52
(0002) V_{Zn}	Theory[b)]	3.41

a) For Zn_i and V_O, the defects were introduced in the near-surface region in concentrations of 1 defect per 80 Zn or O atoms respectively.

b) For the (0002) surface model, a surface unit cell containing one V_{Zn} and six OH groups to preserve charge neutrality was considered.

Table 2. Data from the study by Wood *et al.* detailing the effect of fluorinated benzyl phosphonic acid (BPA) modification on the surface electronic properties of ZnO, where each BPA species carries a different dipole moment: *o*-2FBPA is *ortho*-difluorobenzylphosphonic acid; *p*-FBPA is *para*-fluorobenzylphosphonic acid; 5FBPA is pentafluorobenzylphosphonic acid. The work function, $\Delta\phi$, is decomposed into individual components using the relation: $\Delta\phi = \Delta V_{SAM} + \Delta V_{ZnO} + \Delta V_{interface}$ (see main text for details of each parameter). Table adapted from [86] with permission, © 2012 American Chemical Society.

Modifier	ΔV_{SAM} [eV]	ΔV_{ZnO} [eV]	$\Delta V_{interface}$ [eV]	$\Delta\phi$ [eV]
		Bidentate		
o-2FBPA	–1.15	–1.48	1.23	–1.38
BPA	–0.75	–1.45	1.20	–1.00
p-FBPA	0.04	–1.46	1.17	–0.24
5FBPA	0.30	–1.42	1.21	0.08
		Tridentate		
o-2FBPA	–0.91	–0.87	2.47	0.69
BPA	–0.46	–0.88	2.40	1.05
p-FBPA	0.36	–0.86	2.12	1.62
5FBPA	0.54	–0.82	2.27	2.00

Table 3. Hybrid photovoltaic performance characteristics for devices using various interface modifiers. The data for the appropriate reference (unmodified) cells used in each study is given beneath in parentheses.

Modifier	Modifier Type	Active Layer Structure	V_{oc} [V]	J_{sc} [mA cm^{-2}]	*FF*	*PCE* [%]	Ref.
Mg (x = 0.25)	Dopant	Bilayer	**~0.82** (~0.50)	**~0.33** (~0.26)	**~0.42** (~0.51)	**~0.12** (~0.06)	[132]
Li (x = 0.15)	Dopant	Bilayer	**~0.47** (~0.22)	**~1.55** (~0.60)	**~0.46** (~0.40)	**~0.34** (~0.06)	[135]
N	Surface Dopant[a)]	Nanorod	**0.71** (0.30)	**0.74** (0.84)	-	-	[59]
TiO_x (~10 nm)	Inorganic Layer	Bilayer	**0.60** (0.22)	**0.23** (0.34)	**0.40** (0.37)	**0.05** (0.03)	[142]
CdS (~20 nm)	Inorganic Layer	Bilayer	**0.60** (0.31)	**0.39** (0.40)	**0.48** (0.44)	**0.11** (0.05)	[145]
PZT (~11 nm)	Inorganic Layer	Bilayer	**0.73**[b)] (0.16)	**0.16** (0.23)	**0.41** (0.30)	**0.05** (0.01)	[146]
NH_3 (5 mins)	Wash Treatment	Nanorod	**0.82** (0.30)	**1.12** (0.11)	**0.32** (0.47)	**0.29** (0.02)	[150]
PTCBI (30 nm)	Evaporated Interlayer	Nanowire	**0.34** (0.40)	**5.52** (2.32)	**0.36** (0.28)	**0.67** (0.26)	[153]
$C_{18}H_{37}SH$	Alkyl SAM	Bilayer	**0.31** (0.30)	**0.42** (0.28)	**0.40** (0.43)	**0.05** (0.04)	[167]
PCBA	Fullerene SAM	Bilayer	**1.10** (0.47)	**0.32** (0.21)	**0.50** (0.42)	**0.18** (0.04)	[169]
ZnPc (4 nm)	Dye	Bilayer (normal cell)	**0.61** (0.71)	**0.26** (0.17)	**0.56** (0.50)	**0.09** (0.06)	[160]
D149	Dye	Nanorod (w/ ZnO shell)	**0.60** (0.43)	**3.11** (2.55)	**0.62** (0.50)	**1.16** (0.55)	[163]
IM-2	Custom Modifier[c)]	Bilayer	**0.79** (0.57)	**0.91** (0.20)	**0.59** (0.57)	**0.42** (0.09)	[172]
TP-S	Liquid Crystal Ligand	BHJ (NP-ZnO)	**0.60** (0.63)	**4.52** (2.47)	**0.35** (0.33)	**0.95** (0.51)	[177]
HTph-S	Liquid Crystal Ligand	BHJ (NP-ZnO)	**0.64** (0.57)	**3.77** (2.35)	**0.51** (0.42)	**1.23** (0.56)	[176]

a) Doping using near-atmospheric nitrogen plasma treatment.
b) V_{oc} observed to increase with prolonged illumination, reaching ~0.95 V for one device.
c) See text for details of the molecular structure.

Table 4. Device performance characteristics for organic photovoltaic devices with different ZnO modifiers. Data for reference (unmodified) cells used in each study are given in beneath parentheses.

Modifier	Modifier Type	V_{oc} [V]	J_{sc} [mA cm^{-2}]	*FF*	*PCE* [%]	R_s [Ω·cm^{-2}]	R_{sh} [kΩ·cm^{-2}]	Ref.
Al (2 %wt, NH_3-treated NPs)	Dopant (22 nm ETL)	**0.74** (0.68)[a)]	**17.10** (13.80)[a)]	**0.71** (0.57)[a)]	**8.90** (4.90)[a)]	**0.55** (3.50)[a)]	**10.00** (3.70)[a)]	[194]
Al (2 %wt NH_3-treated NPs)	Dopant (75 nm ETL)	**0.74** (0.68)[a)]	**16.30** (13.80)[a)]	**0.68** (0.57)[a)]	**8.10** (4.90)[a)]	**0.80** (3.50)[a)]	**7.20** (3.70)[a)]	[194]
Ga (2 %at)	Dopant	**0.87** (0.89)	**9.93** (9.29)	**0.62** (0.59)	**5.43** (4.90)	**1.06** (1.36)	-	[196]
Y (0.02 mM)	Dopant	**0.57** (0.51)	**9.90** (9.50)	**0.40** (0.30)	**2.30** (1.50)	**10.40** (10.30)	**0.25** (0.15)	[199]
Ta_2O_5 (18 %)	Composite	**0.64** (0.64)	9.64 (9.49)	**0.67** (0.61)	**4.12** (3.70)	**7.28** (8.72)	**3.30** (0.67)	[201]
C_{60}-Benzoic Acid	SAM (spin-coated)	**0.62** (0.60)	**11.17** (10.07)	**0.64** (0.58)	**4.40** (3.47)	-	-	[208]
PCBM[b)]	Composite	**0.80** (0.79)	**15.73** (14.02)	**0.74** (0.69)	**9.35** (7.64)	**2.78** (13.46)	**1.38** (0.96)	[209]
4-TPT	SAM	**0.57** (0.52)	**12.40** (8.84)	**0.42** (0.37)	**3.01** (1.71)	**13.00** (26.00)	**0.15** (0.14)	[214]
Cs-stearate (1 mg ml^{-1})	SAM (spin-coated)	**0.74** (0.73)	**17.07** (15.88)	**0.69** (0.62)	**8.46** (6.97)	-	-	[215]
TFTPA w/$PC_{71}BM$	SAM	**0.72** (0.72)	**14.30** (12.50)	**0.67** (0.67)	**6.85** (5.98)	**0.28** (0.38)	**8.70** (10.00)	[217]
N719 (15 min)	Dye (soaked)	**0.61** (0.56)	**10.46** (10.22)	**0.60** (0.49)	**3.83** (2.79)	**11.01** (21.03)	**0.83** (0.27)	[191]
PVP (6 nm)	Interlayer	**0.72** (0.71)	**15.17** (14.00)	**0.67** (0.62)	**7.30** (6.18)	**131.20** (160.10)	-	[222]
PVP (0.7 %wt)	Composite	**0.56** (0.51)	**9.74** (9.53)	**0.60** (0.47)	**3.25** (2.27)	**6.00** (6.00)	**0.65** 0.03	[216]
PEO (0.05 %wt, M_w = 100 kg mol^{-1})	Composite	**0.88** (0.86)	**9.60** (8.69)	**0.67** (0.60)	**5.64** (4.50)	**8.10** (22.00)	**2.17** (0.90)	[223]
PEIE (10 nm, M_w = 70 kg mol^{-1})	Interlayer (spin-coated)	**0.77** (0.72)	**15.20** (14.50)	**0.67** (0.60)	**7.88** (6.29)	**1.10** (1.90)	**1.30** (1.10)	[219]
PTSO-Na (~5 nm)	Interlayer (spin-coated)	**0.59** (0.57)	**11.30** (10.50)	**0.52** (0.50)	**3.47** (2.99)	-	-	[224]
PTNOH (~5 nm)	Interlayer (spin-coated)	**0.60** (0.57)	**11.90** (10.50)	**0.57** (0.50)	**3.98** (2.99)	-	-	[224]
PTN-Br (~5 nm)	Interlayer (spin-coated)	**0.60** (0.57)	**12.00** (10.50)	**0.57** (0.50)	**4.08** (2.99)	-	-	[224]

a) Reference cell: ~20 nm thick, thermally evaporated undoped ZnO layer.
b) Co-deposited with ZnO using the water-soluble precursor phenyl-C_{61}-butyric acid-(2-hydroxy)ethyl ester.

Figures

Figure 1. Illustration of different surface modification strategies adopted for ZnO.

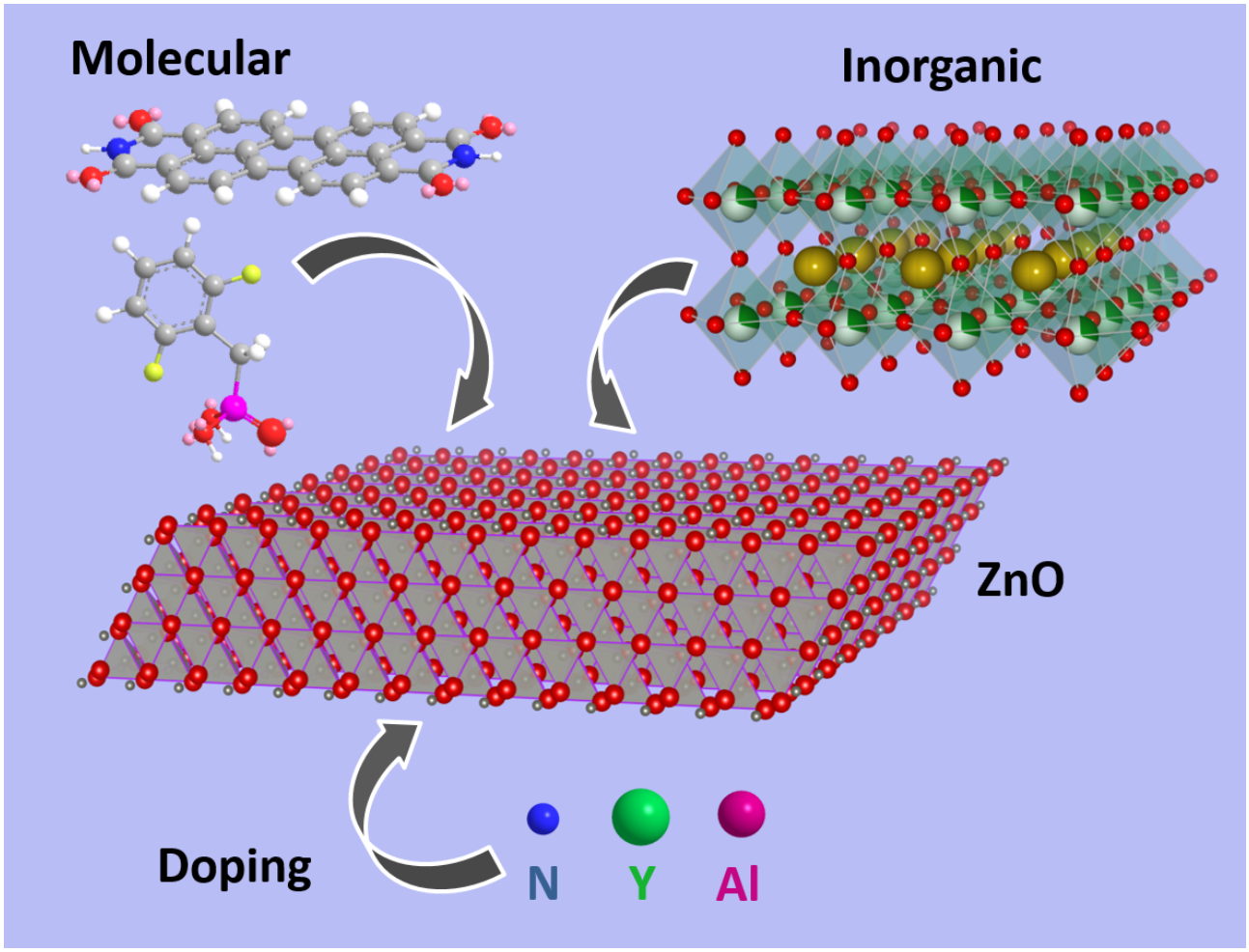

Figure 2. Stick-and-ball representations of the hexagonal wurtzite ZnO structure. The crystal structures were drawn using the VESTA3 programme[228] using ZnO structural data reported by Yamashita *et al.*.[229] The polar Zn- and O-terminated faces shown are ideal structures: these are unstable and are observed to undergo reconstruction as well as forming hydroxyl surface groups to minimise the surface energy.[40]

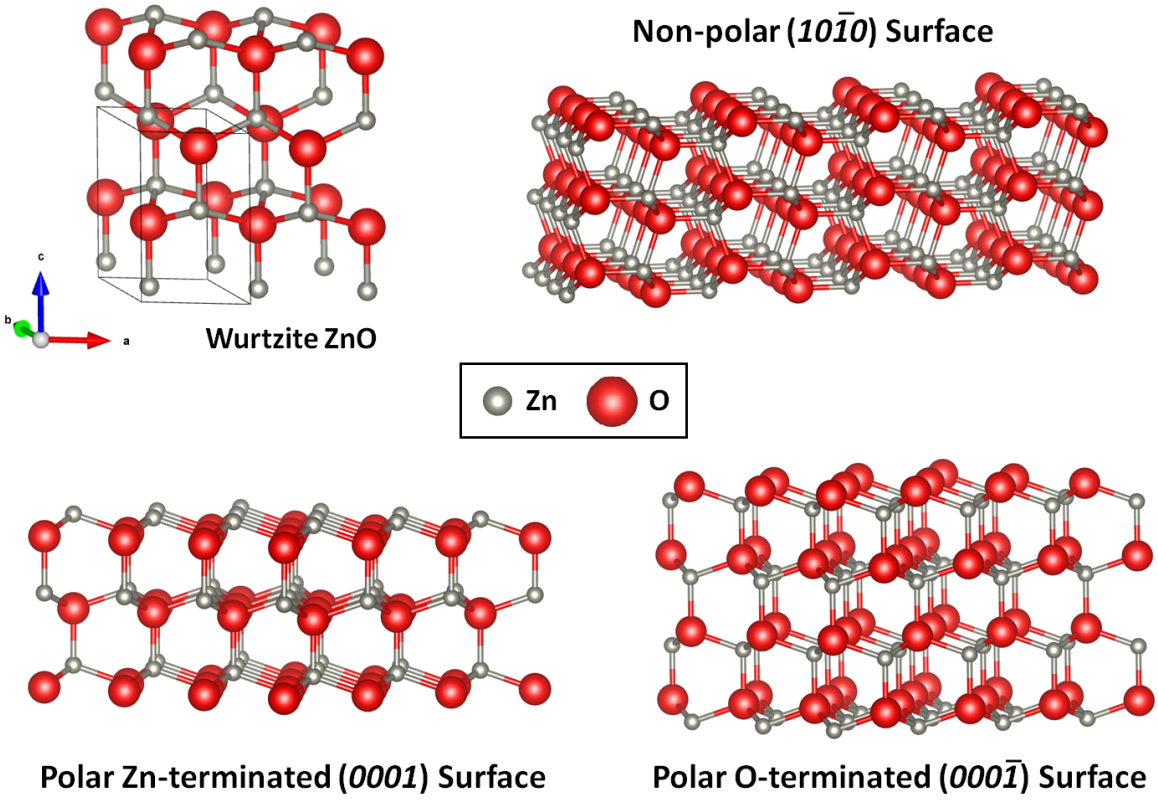

Figure 3. Scanning electron micrographs obtained for different ZnO nanostructures: **(a)** a planar, polycrystalline layer; **(b)** a hydrothermally grown nanorod (NR) array used in fabrication of HyLED devices;[8] **(c)** ZnO nanowires (NW), image adapted from [230] with permission from The Royal Society of Chemistry; **(d)** 3-dimensional ordered macroporous (3DOM) array produced by electrodeposition into a colloidal crystal template; **(e)** ZnO nanohelix reported by Gao *et al.*, adapted from [23]. Reprinted with permission from AAAS.[23]

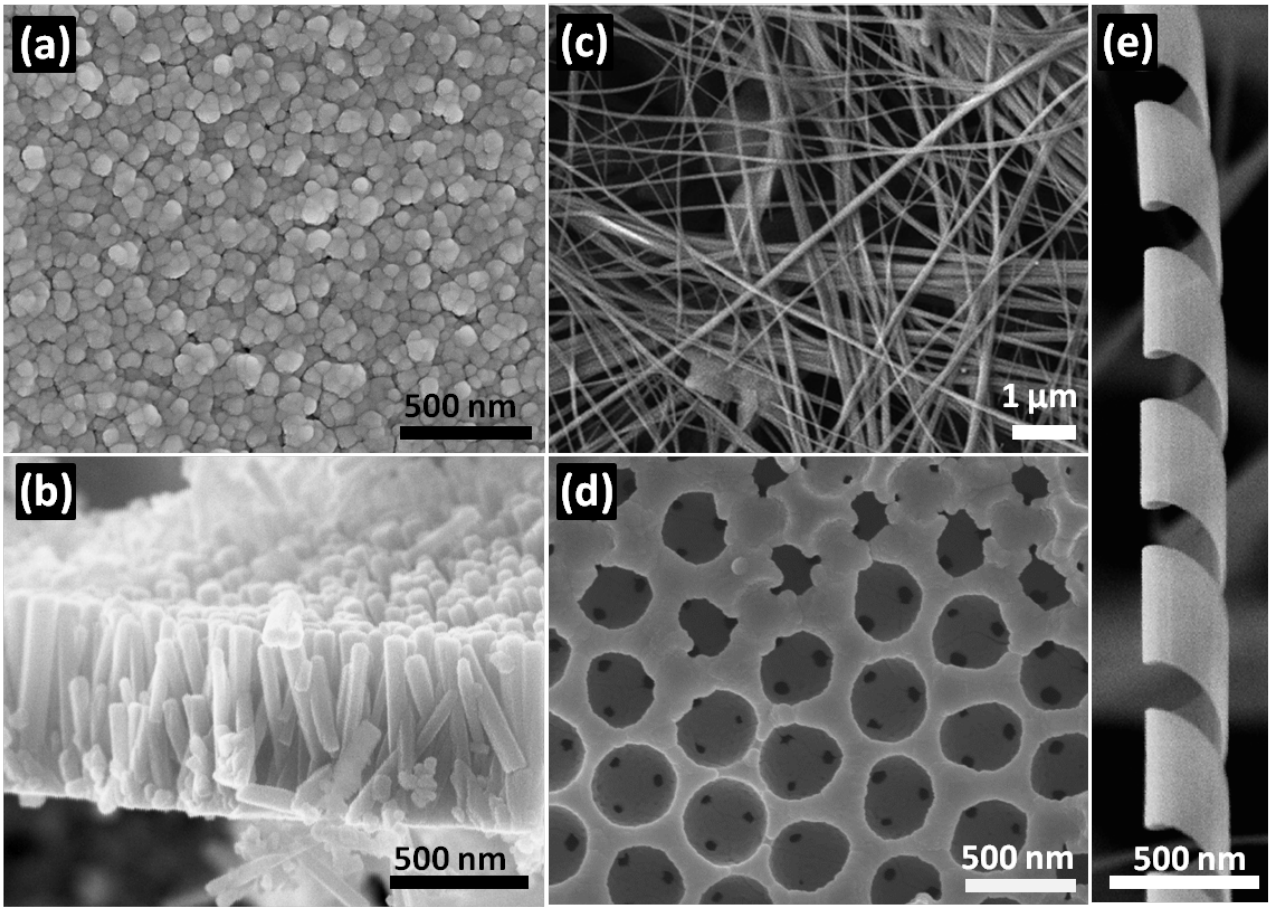

Figure 4. (a) different binding modes for phosphonic acid groups on ZnO. From left to right: monodentate ester, bidentate chelating, bidentate ester, bidentate bridging, tridentate. (b) illustration of bidentate and tridentate bonding modes for phosphonic acid modifiers on ZnO: left, contributions of the bidentate and tridentate bonding modes to the XPS O 1s peak; right, illustration of 3,3,4,4,5,5,6,6,7,7,8,8,8,-tridecafluorooctyl phosphonic acid (tridentate) binding and p-trifluoromethylphenyl phosphonic acid (bidentate) on ZnO. Image reprinted with permission from [87], © 2014 American Chemical Society. (c) Molecular structures for substituted benzylphosphonic acid species used in [86].

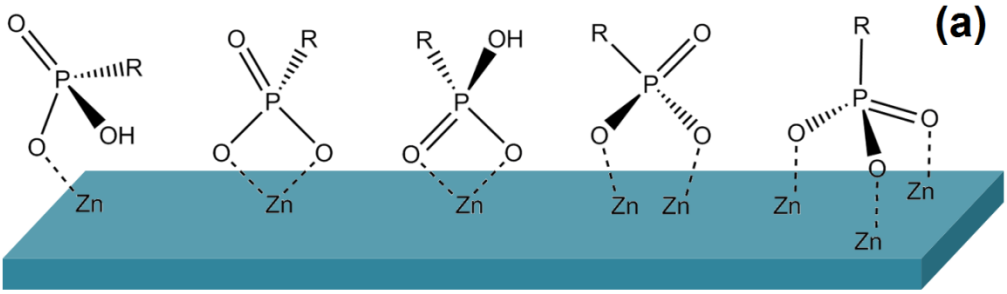
(a)
O
P
R
OH
Zn

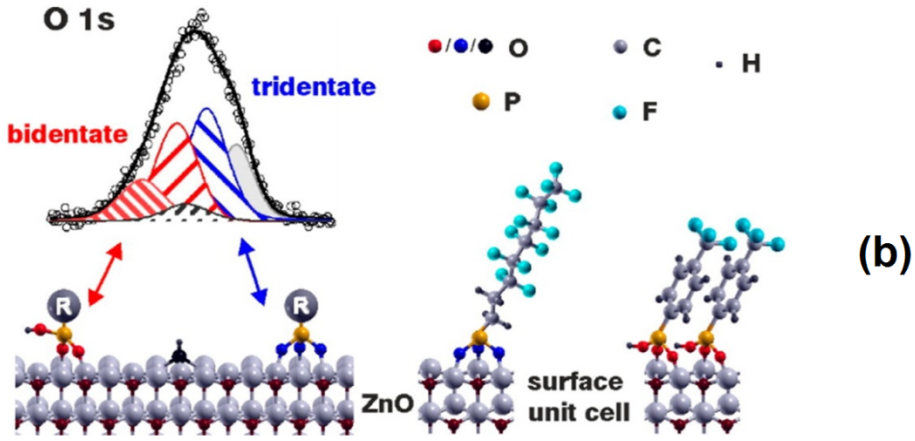
O 1s
tridentate
bidentate
O
C
H
P
F
R
ZnO
surface
unit cell

(b)

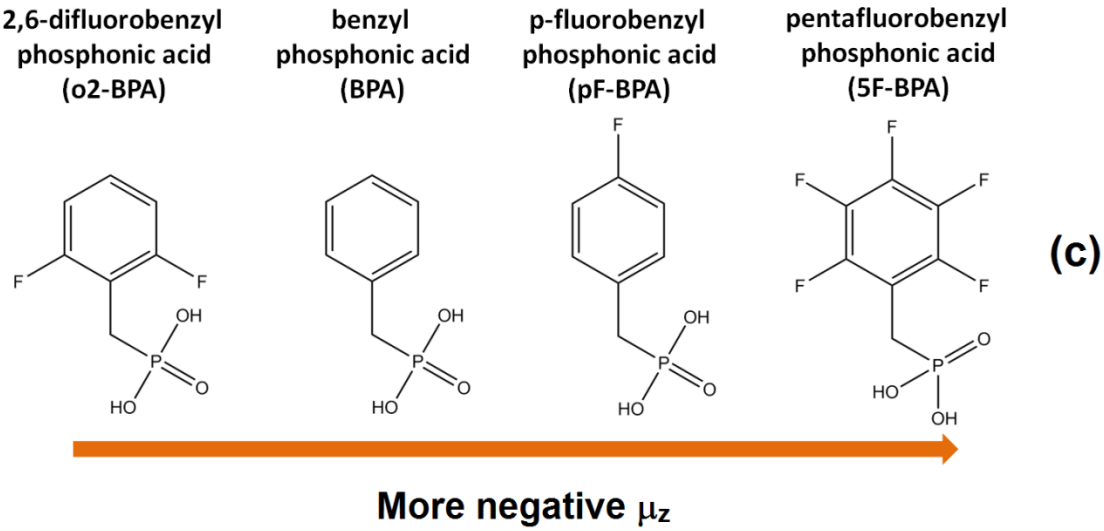
2,6-difluorobenzyl phosphonic acid (o2-BPA)
benzyl phosphonic acid (BPA)
p-fluorobenzyl phosphonic acid (pF-BPA)
pentafluorobenzyl phosphonic acid (5F-BPA)
F
OH
HO
O
P
More negative μz

(c)

Figure 5. (a) sample current density–voltage (*J–V*) curves for an organic photovoltaic device showing characteristics in dark (dashed, blue) and under standard illumination conditions (line-and-circle, blue), as well as a power curve (solid, red). The open-circuit voltage, V_{oc}, and short-circuit current, J_{sc}, are marked, along with the maximum voltage and current points (V_m and I_m respectively), and the maximum power point (P_m). Bottom**:** schematic representations of the device structure for **(b)** normal and **(c)** inverted architecture organic and hybrid photovoltaic devices, along with the location of ZnO surface modification layers; direction of hole (h^+) flow is also given.

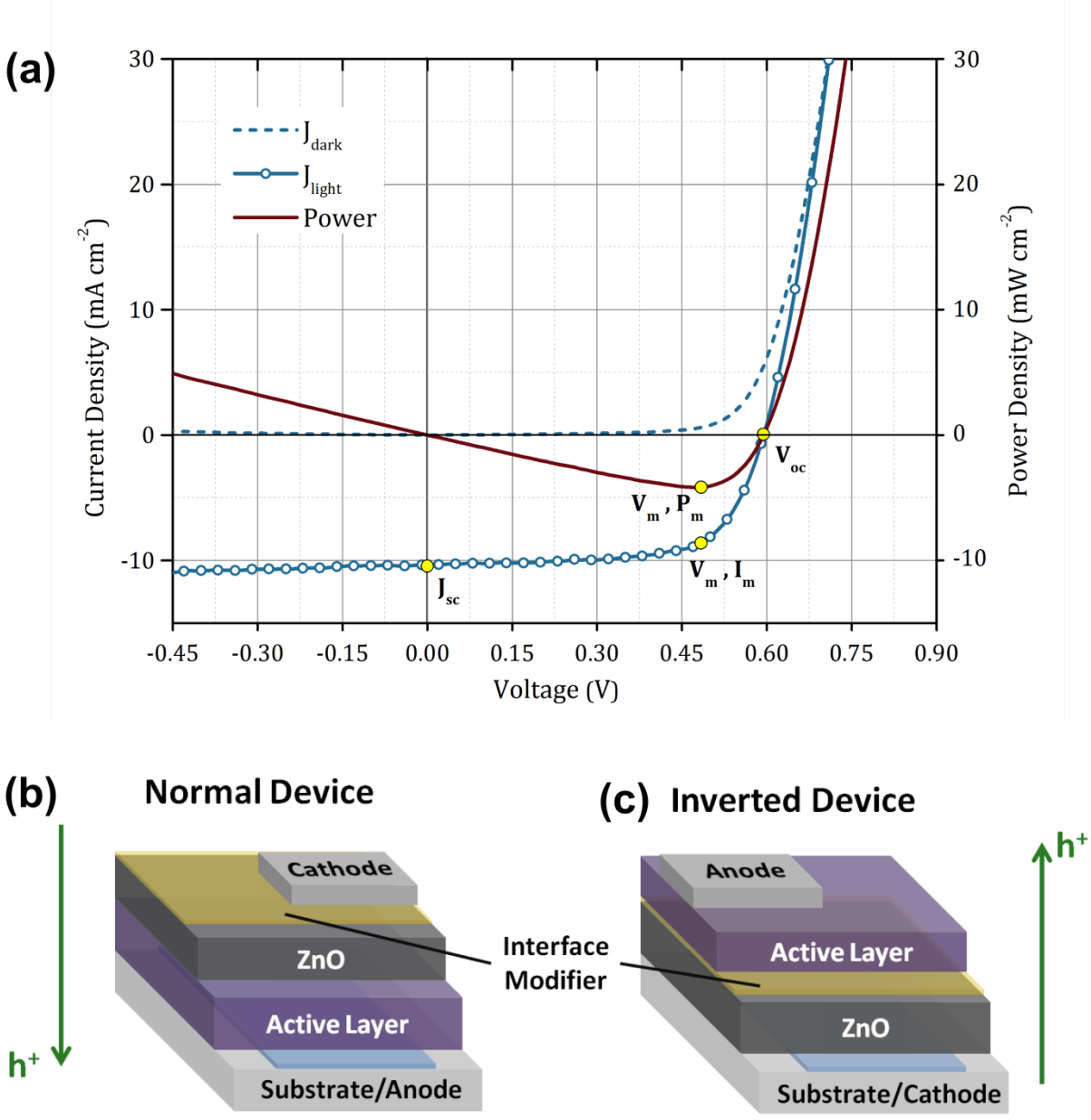

Figure 6. Molecular structures of various donor polymers used in organic and hybrid photovoltaics. **P3HT** is poly(3-hexylthiophene). **PBDT-DTNT** is a D–A polymer based on 2,1,3-benzodithiazole (BT) and naptho[1,2-c:5,6-c]bis[1,2,5]thiadiazole (NT) units.[231] **MDMO-PPV** is poly[2-methoxy-5-(3′,7′-dimethyloctyloxy)-1,4-phenylenevinylene]. **PCDTBT** is poly[N-9'-heptadecanyl-2,7-carbazole-alt-5,5-(4',7'-di-2-thienyl-2',1',3'-benzothiadiazole)]. **PTB7** is poly({4,8-bis[(2-ethylhexyl)oxy]benzo[1,2-b:4,5-b']dithiophene-2,6-diyl}{3-fluoro-2-[(2-ethylhexyl)carbonyl]thieno[3,4-b]thiophenediyl}), whilst use of the thiophene-modified derivative is reported in the work by Liao *et al.*.[209]

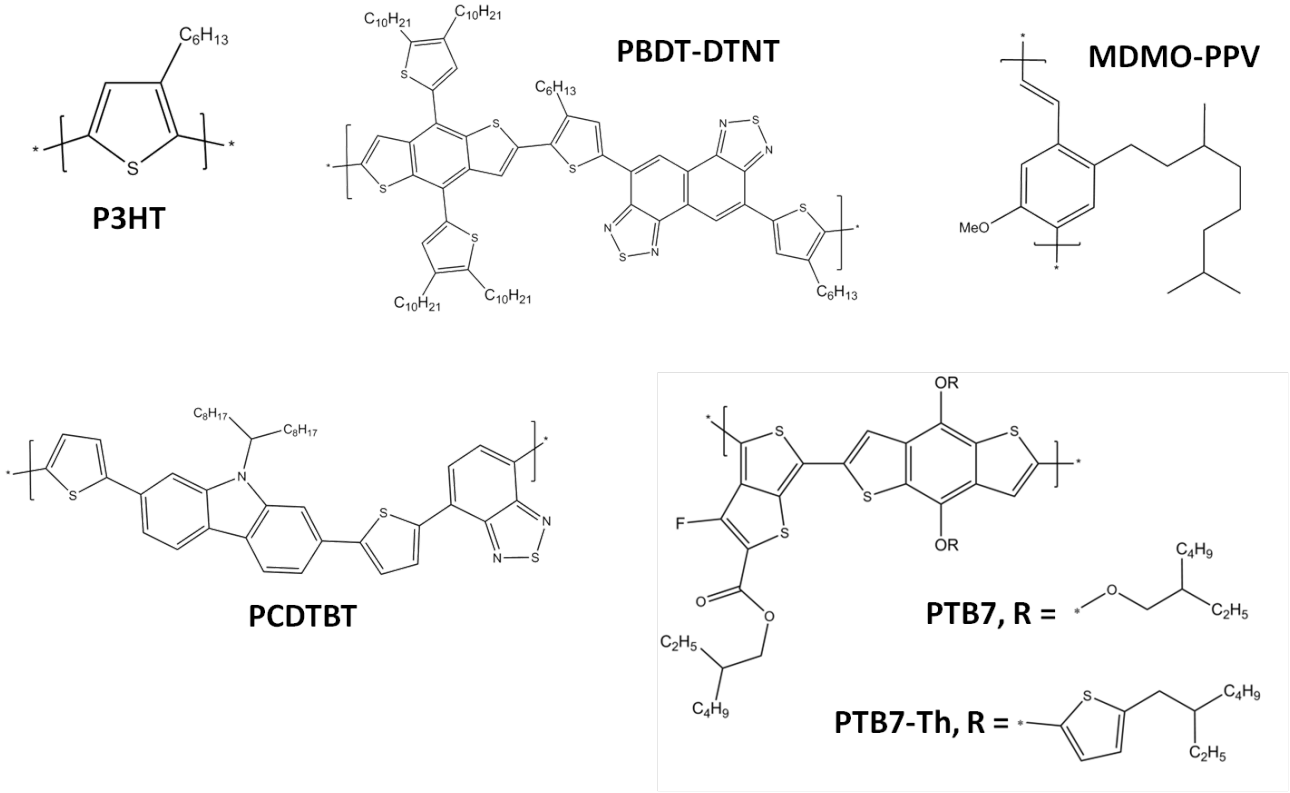

Figure 7. Molecular structures for various electron acceptors: the fullerene derivatives $PC_{61}BM$, phenyl-C_{61}-butyric acid methyl ester (the C_{71} derivative is also commonly used), and ICBA, indene-C_{60} bisadduct, are frequently employed in organic photovoltaic devices. F4TCNQ ([2,3,5,6-tetrafluoro-2,5-cyclohexadiene-1,4-diylidene]dimalononitrile)[100,101] and PTCDI (3,4,9,10-perylenedicarboximide)[99] have been used to study the electronic properties of the ZnO surface.

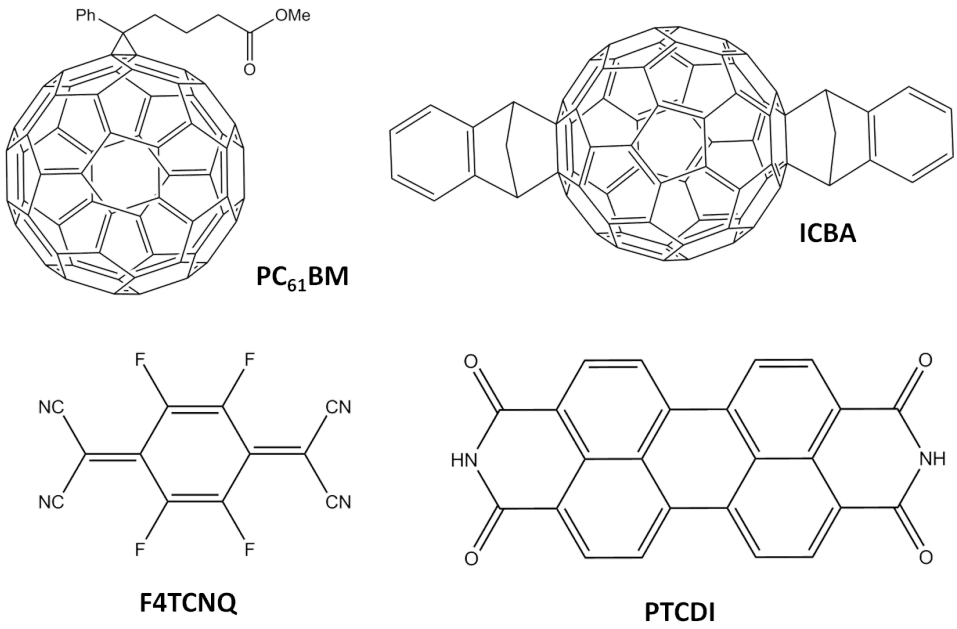

Figure 8. **(a)** Transmission electron micrograph cross-section of an ITO/ZnO/PZT/P3HT film stack (PZT = $PbZr_{0.3}Ti_{0.7}O_3$). The region containing the PZT surface modifier is shaded in yellow. **(b)** Dark (dashed line) and illuminated (line and symbol) current density–voltage (*J–V*) curves showing the effect of PZT modification on the performance of bilayer hPV ZnO:P3HT devices: the reference (unmodified) is presented in black, and the PZT-modified device in green.

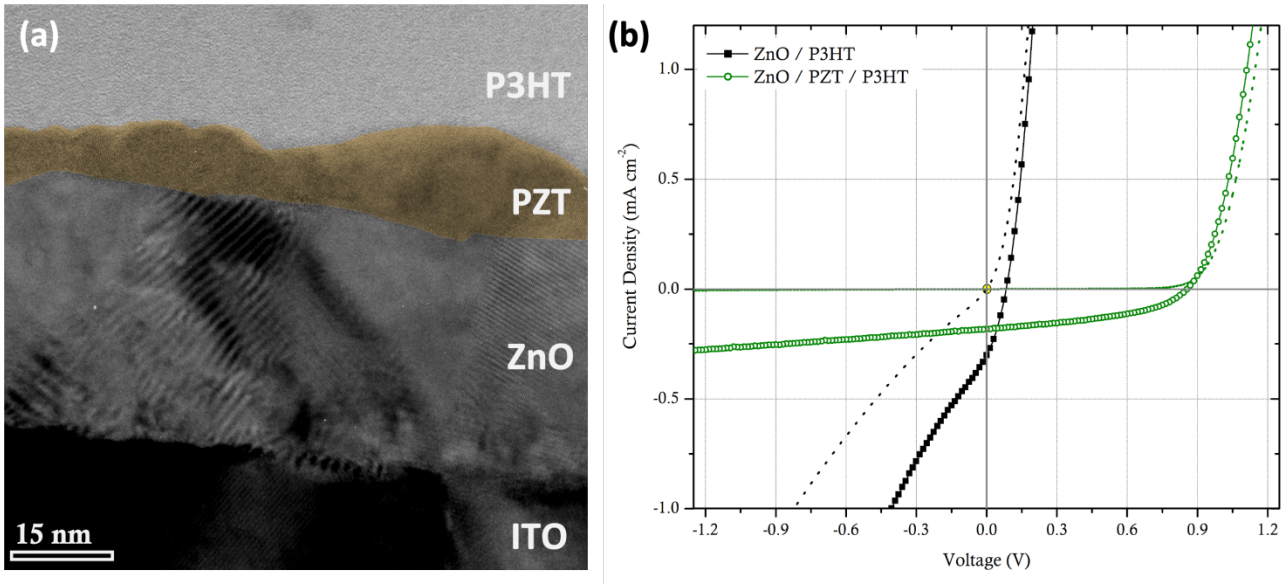

Figure 9. Molecular structures of various dye molecules used as interface modifiers in ZnO-based organic and hybrid photovoltaic devices. The Ru-based **N3** [(cis-bis(isothiocyanato) bis[2,2'-bipyridyl-4,4'-dicarboxylato] ruthenium(II))] dye is closely related to the ditetrabutylammonium derivative, **N719,** and **Z907** [cis-bis(isothiocyanato)(2,2'-bipyridyl-4,4'-dicarboxylato)(4,4'-di-nonyl-2'-bipyridyl)ruthenium(II)], all of which been used extensively in DSSC applications. **SQ-36** is an example of a squaraine dye, as used in [180]. **D149** is 5-[[4-[4-(2,2-Diphenylethenyl)phenyl]-1,2,3-3a,4,8b-hexahydrocyclopent[*b*]indol-7-yl]methylene]-2-(3-ethyl-4-oxo-2-thioxo-5-thiazolidinylidene)-4-oxo-3-thiazolidineacetic acid, whereas in **D205** the underlined ethyl unit is replaced by an octyl group.

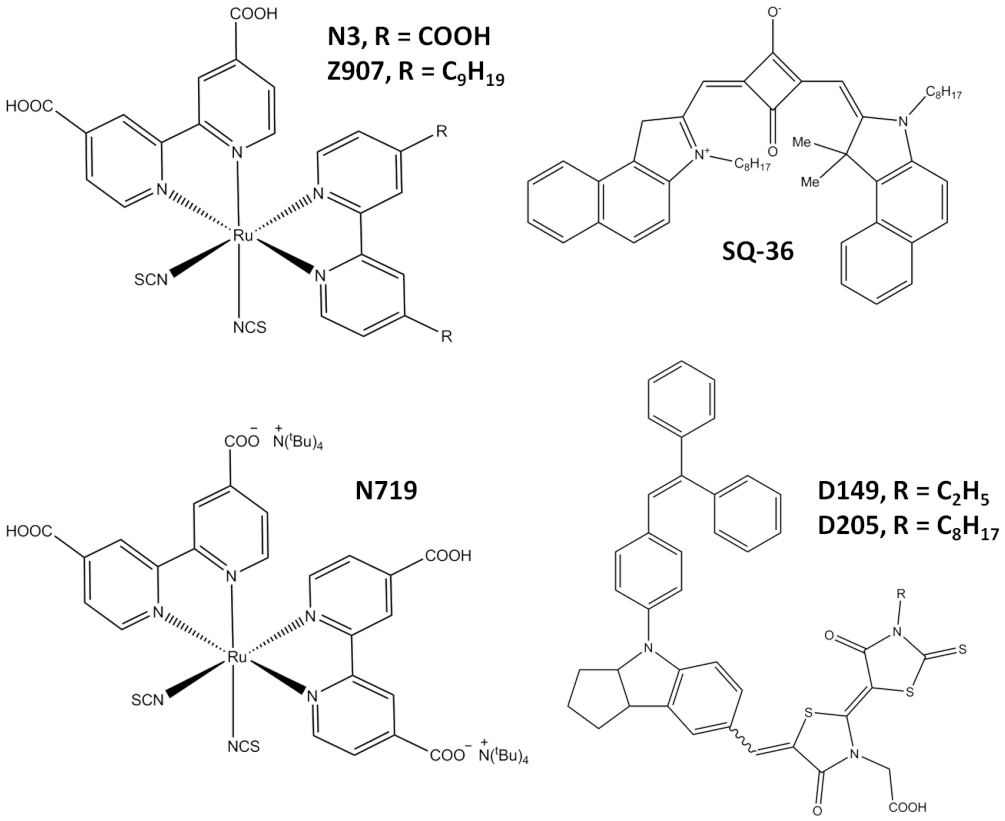

Figure 10. Representation of approximate energy levels for different interface modifiers in ZnO:P3HT-based hybrid photovoltaic devices.

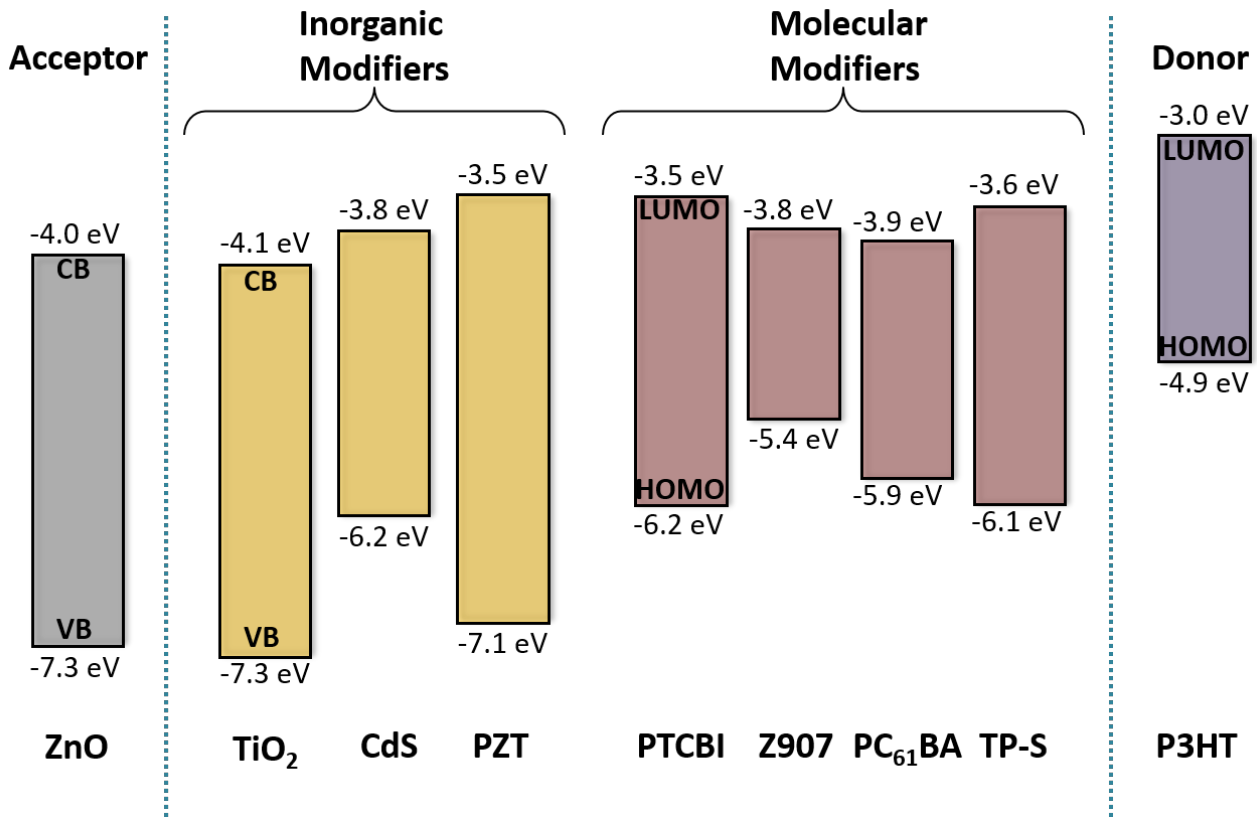

Figure 11. Transmission electron micrographs of the NP-ZnO:P3HT blends showing the effect of both annealing and liquid crystal ligand surface modification using the ligand 2-[(5-(1,2-dithiolan-3-yl)-pentanoate)]-3,6,7,10,11-pentakis(butoxy) triphenylene (TP-S) from the study by Chen *et al.*.[177] **(a)** and **(c)**: micrographs of unmodified NP-ZnO:P3HT blends before and after annealing at 130 °C, respectively; **(b)** and **(d)** micrographs of TP-S-modified NP-ZnO:P3HT blends before and after annealing at 130 °C. Figure reproduced from [177] with permission from The Royal Society of Chemistry. Molecular structures for the ligands TP-S and HTph-S [4-(5-(1,2-dithiolan-3-yl)pentanoate)-4'-(hexyloxy)-terphenyl] (used in [176]) are given.

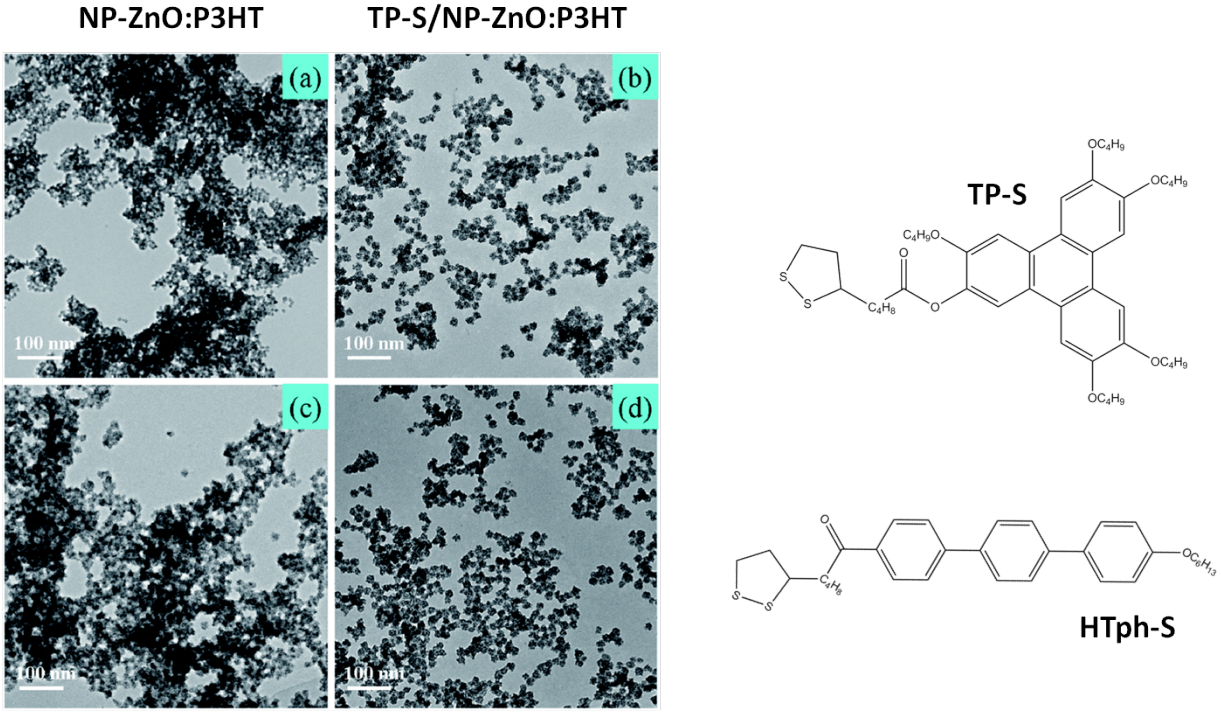

Figure 12. The influence of C_{60} modification on the surface electronic properties of ZnO, as reported in the study by Schulz *et al.*.[56] **(a)** energy level diagrams derived from photoelectron spectroscopy measurements: the oxide:organic interaction was found to vary significantly with the ZnO surface pre-treatment (as deposited/soft-sputtered/hard-sputtered), attributed to the populations of different defects in the ZnO. **(b)** proposed charge transfer mechanisms for C_{60} on ZnO: interaction between the fullerene and shallow donors such as Zn_i are thought to promote substantial electron transfer, whereas deeper level defects, *e.g.* V_O are associated with weaker charge transfer. Figure adapted from [56] with permission.

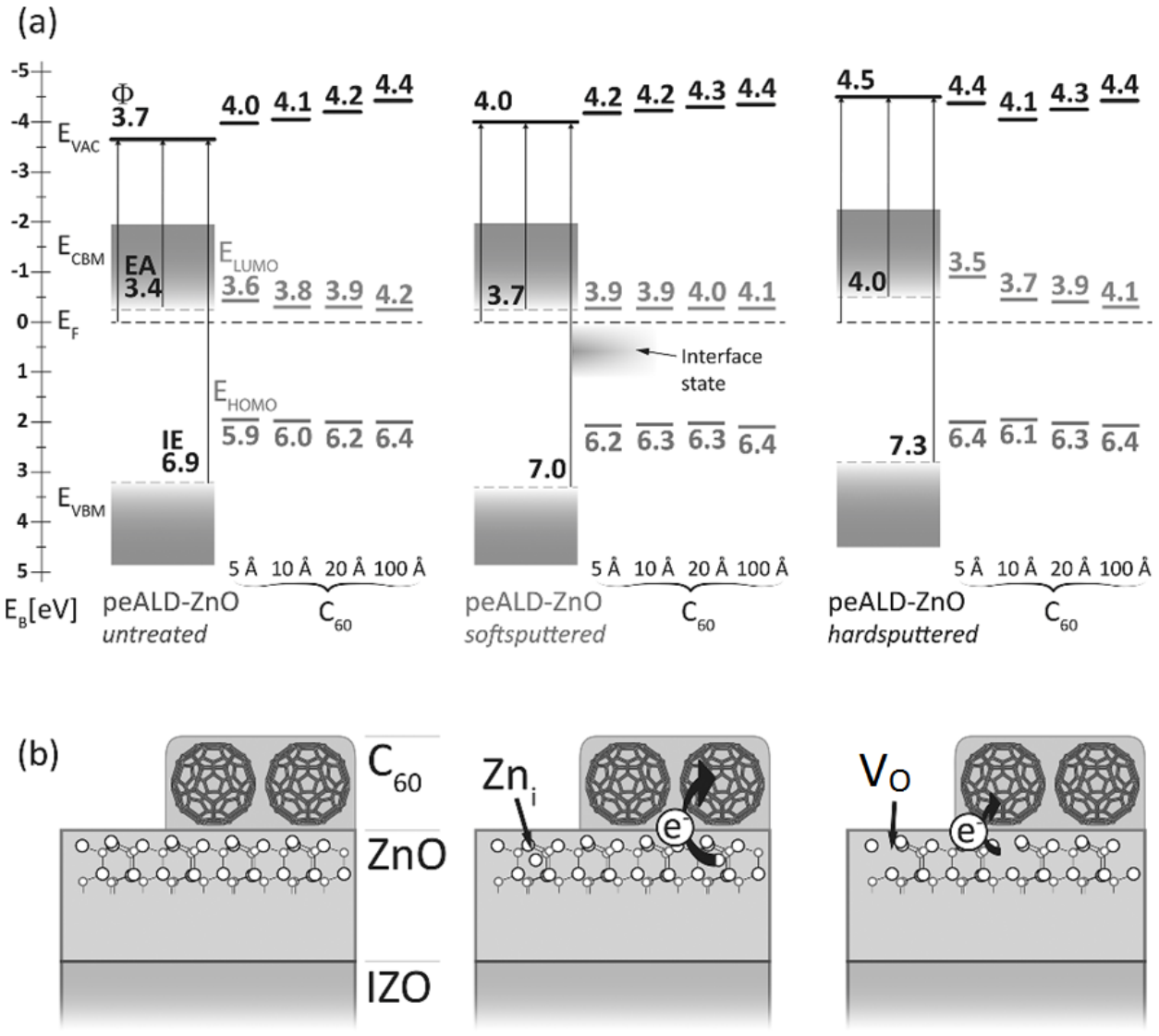

Figure 13. Data from study by Bulliard *et al.* into the effect of ZnO surface energy on organic photovoltaic device performance, studied by using mixed monolayers of aminopropyltrimethoxysilane and octyltrimethoxysilane.[212] **(a)–(d)** transmission electron micrographs of 1:1 P3HT:$PC_{61}BM$ active layers deposited on ZnO surfaces with different surface energies and annealed at 120 °C: **(a)** 71 mN/m, **(b)** 62 mN/m, **(c)** 48 mN/m, **(d)** 42 mN/m. Device performance data for these are given on the right: **(i)** short-circuit current (J_{sc}); **(ii)** power conversion efficiency (*PCE*); **(iii)** open-circuit voltage (V_{oc}); **(iv)** fill-factor (*FF*); **(v)** series resistance (R_s). Images adapted from [212] with permission.

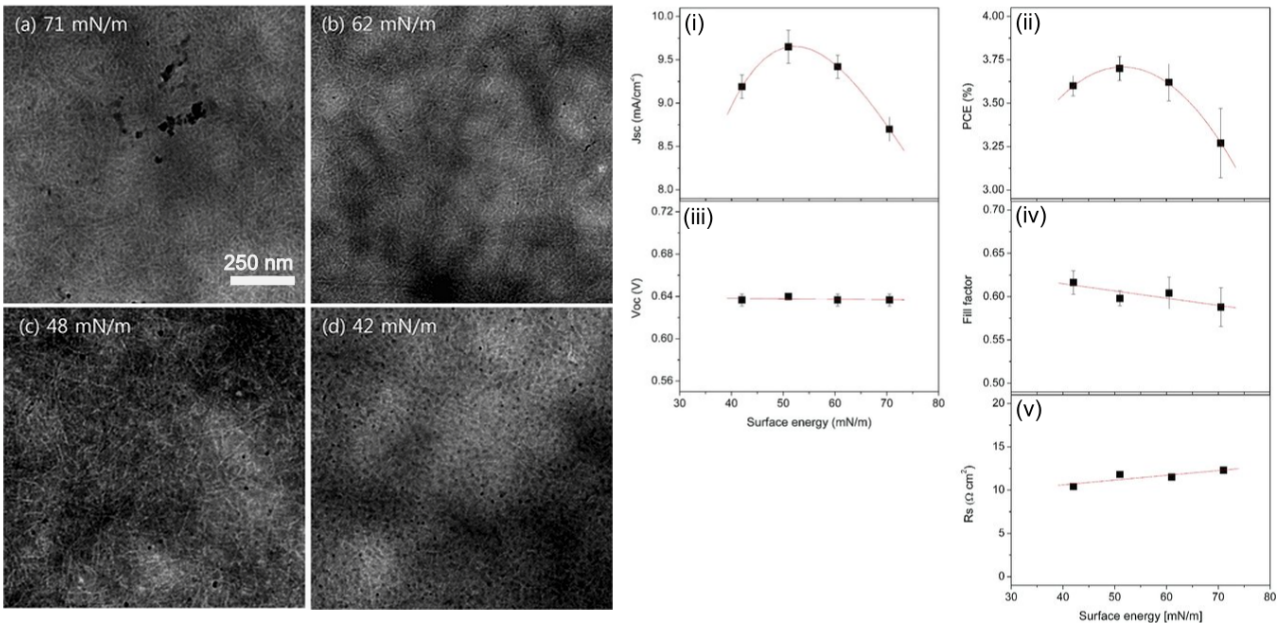

Figure 14. Approximate energy levels for ZnO ETL modifiers used in organic photovoltaic devices: the energy levels for the acceptor $PC_{61}BM$ are included. Note for the modifiers labelled "ZnO+…", the energy levels correspond to those of the modified ZnO, as opposed to the energy levels of the isolated modifiers.

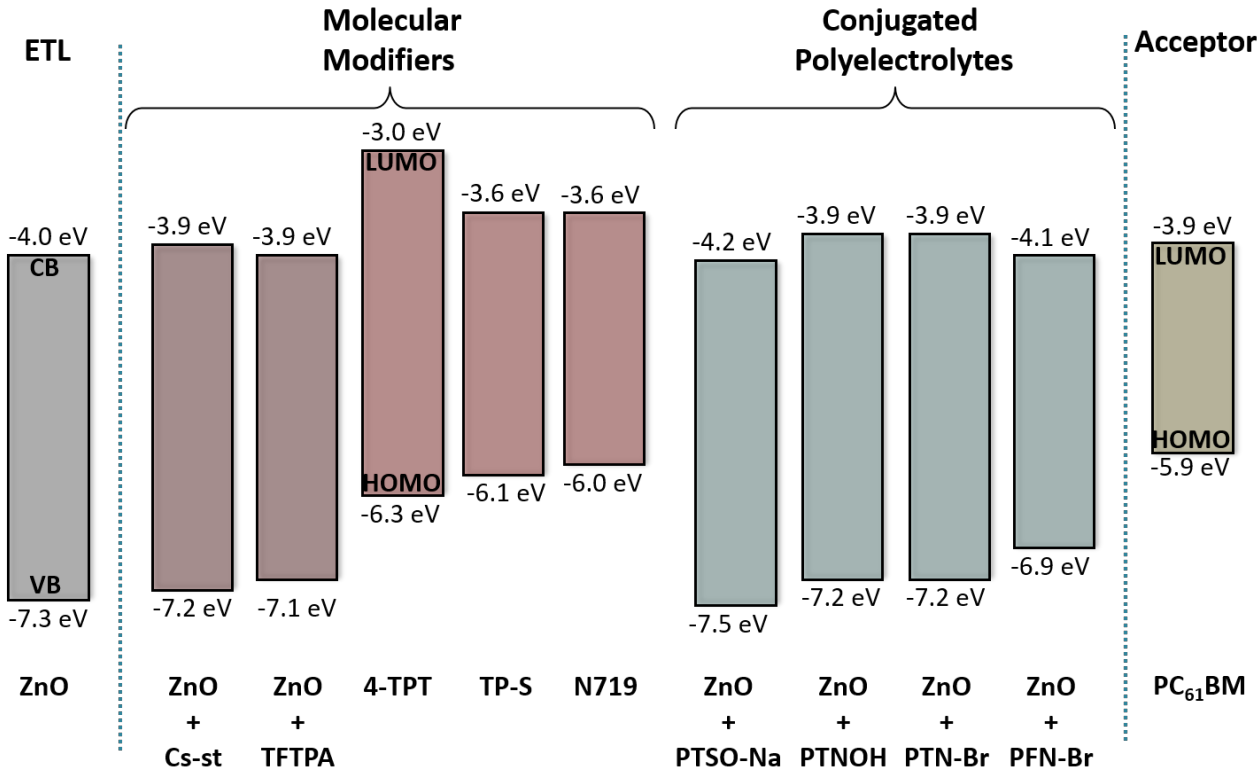

Figure 15. Polymeric species used to modify ZnO ETLs in organic photovoltaic devices. **PVP** (polyvinylpyrrolidone), **PEIE** (polyethylenimine 80 % ethoxylated), and **PEO** (polyethylene oxide) have been used to tune the ZnO work-function. The second group are conjugated polyelectrolytes: anionic **PTSO-Na** (poly[(3-(4′-sulfonatobutyl)oxymethyl-2,5-thiophene)-alt-2,5- thiophene] sodium salt), neutral **PTNOH** (HT-poly[3-(6′-diethano- lamino)-hexylthiophene), cationic **PTN-Br** (HT-poly[3-(6′- N,N,N-trimethylammonium)-hexylthiophene]), and cationic **PFN-Br** (poly[(9,9-bis(3'-((N,N-dimethyl)-N-ethylammonium)-propyl)-2,7-fluorene)-alt-2,7-(9,9-dioctylfluorene)]).

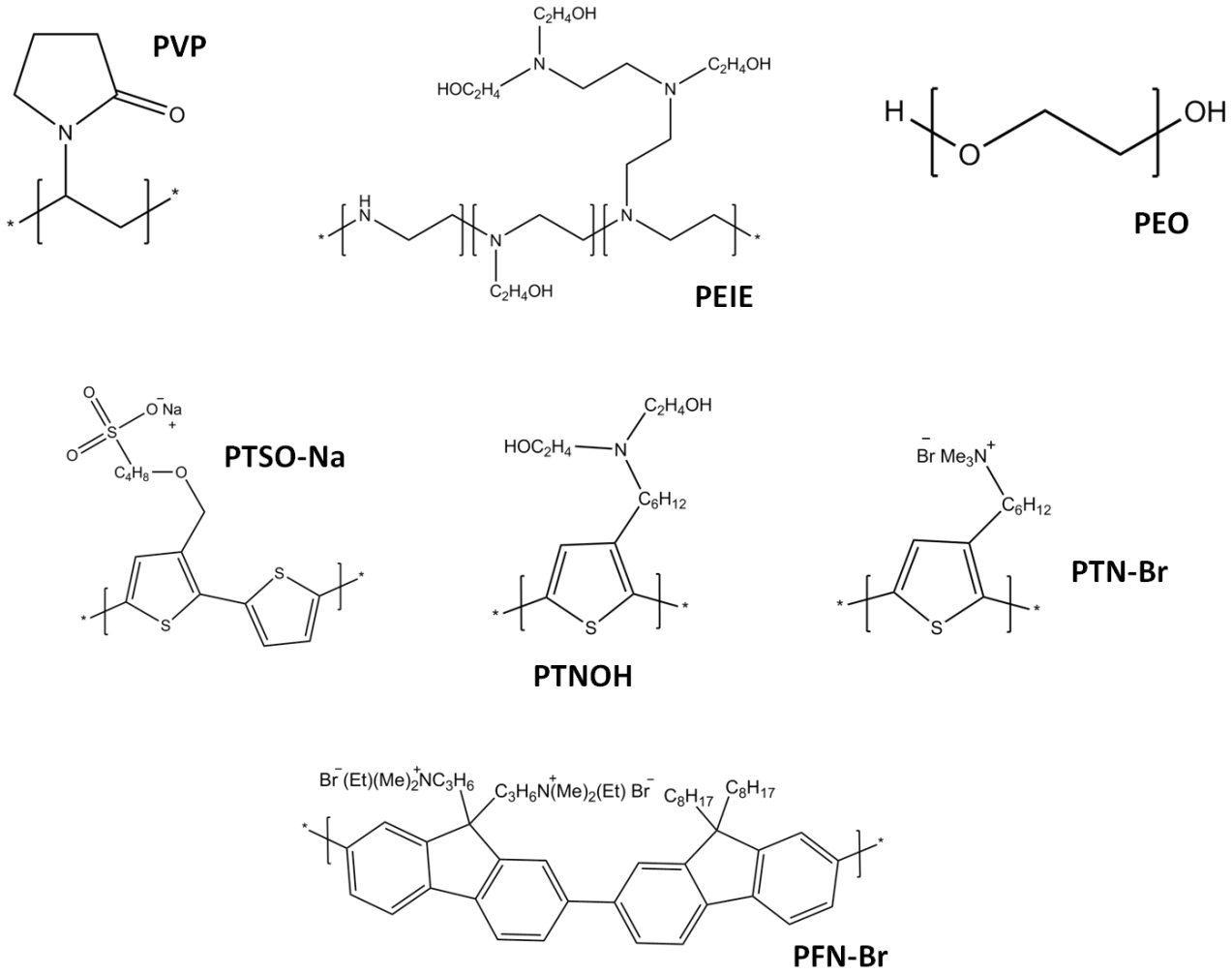

Biographies

Rob Hewlett studied Chemistry at the University of Oxford, completing his research project under Professor P. D. Battle. He recently gained his PhD in Materials Science at Imperial College London under Dr M. A. McLachlan, writing his thesis on oxide interlayers in ZnO:polymer hybrid photovoltaics. His interests include inorganic materials for renewable energy and storage applications and the study of material interfaces, as well as sustainability, responsible innovation, and the relationship between society and technology.

Martyn McLachlan received his Ph.D. in Chemistry from the University of Glasgow in 2005

then joined the Department of Materials, Imperial College London, as a postdoctoral researcher. He was awarded a Royal Academy of Engineering Research Fellowship (2007-2012) followed by his appointment as Lecturer and more recently (2015) as Senior Lecturer. His current research interests are focussed on the growth of metal oxide thin films and their integration into optoelectronic device platforms, with particular emphasis on structural and interfacial characterisation.